Fall 2012

Investigation of geosteering in non-trivial geological settings

Anuroop Pandey

Department:

INVESTIGATION OF GEOSTEERING IN NON-TRIVIAL GEOLOGICAL SETTINGS

by

ANUROOP PANDEY

A THESIS

Presented to the Faculty of the Graduate School of the

MISSOURI UNIVERSITY OF SCIENCE AND TECHNOLOGY

In Partial Fulfillment of the Requirements for the Degree

MASTER OF SCIENCE IN PETROLEUM ENGINEERING

2012

Approved by

Dr. Runar Nygaard, Advisor

Dr. Baojun Bai

Dr. Ralph Flori

ABSTRACT

The well placement technology has advanced to a stage where we can explore small tolerance targets such as thin reservoirs. Well placement with geosteering**,** which is the real time adjustment of the well path based on the geological responses to place and maintain the well within the best part of the reservoir, is the technology that has made this progress possible. Geosteering however can get very complex with the increasing heterogeneities of the formations and there is no fixed methodology to devise a steering strategy in such complex geological settings.

To accommodate this challenge, we investigated three methods to verify their applicability to geosteering. First method was to create a generalized decision matrix which serves as a guideline to select the right tool for a particular well placement challenge. The decision matrix was devised keeping in mind the applications as well as the limitations of each tool with scope limited essentially to well placement. Second method was to analyze the mechanical properties like Mechanical specific energy & Uniaxial compressive strength for their foot printing ability. Third method includes statistical methods like Hierarchal Clustering and Classification tree to identify distinct signatures which could help us differentiate between the reservoir and non-reservoir and hence place the well optimally. All the three methods were applied to the field data from the field of study in Norwegian North Sea and the results indicate that the methods can assist in devising a steering strategy for a highly heterogeneous field with limited uncertainties.

ACKNOWLEDGMENTS

This thesis would not have been possible without help and support of my supervisor Dr. Runar Nygaard. I thank him for accepting me as one of his graduate students, being so patient and pushing me to be a better engineer.

I would like to thank Lundin, Norway especially Svein Hellvik and Espen Hoel for the financial and technical support throughout the course of the research.

I would like to acknowledge the invaluable contributions that my committee members Dr. Bai and Dr. Flori have made to my research with their timely guidance.

I am grateful to my team members especially Mohammed Al-Dushaishi for overall help with my research and also Steven, Sudarshan, Ishan and Max for being good friends and team members.

And FINALLY I would like to thank my Parents, my Brother and all my Friends back home in India.

TABLE OF CONTENTS

Page

LIST OF ILLUSTRATIONS

LIST OF TABLES

1. INTRODUCTION

1.1. OVERVIEW OF DIRECTIONAL DRILLING

Directional drilling is the controlled deviation of the wellbore along a predetermined course to a bottom hole target located at a particular distance and direction from the surface location. Some of the reasons for directional drilling are:

- To place a horizontal wellbore accurately within a thin reservoir. For example, placing horizontal injectors and producers in heavy oil sands for steam assisted gravity drainage and very thin reservoirs where a horizontal lateral will offer better reservoir exposure for enhanced production.
- To place the well in the sweet spot i.e. the best part of the reservoir. In several scenarios reservoirs may be characterized with heterogeneities owing to thin laminations and sedimentological variations and hence there may be regions within the reservoir which are not suited or favorable for production.
- To create wells with multiple branches or laterals that can target widely spaced reservoir compartments, multilateral drilling.
- Sidetracking an existing well because of the hole problems or a fish in the hole. Sidetracking may also be done to use an old or existing well to explore new possible oil zones.
- To reach a producing zone that is otherwise inaccessible with normal vertical drilling process. For example,
    i. It is often difficult to drill a vertical well through a steeply inclined fault so the well bore is deflected parallel to or perpendicular to the fault to avoid problems and for better production, this is also known as fault drilling.
    ii. To reach the producing formations under a salt dome as drilling vertically through a salt dome can cause drilling problems like washouts, lost circulation and corrosion.

iii. To control a wild well, a relief well is drilled at some distance and the wild well is intersected near its source.

1.2. TERMINOLOGIES AND WELL PROFILES

This section defines the main terminologies and the directional profiles for the directional wells. The terminologies are as below.

Azimuth of a well bore at any point is defined as the direction of the well bore measured clockwise with respect to a North reference. It is generally expressed in angles 0°-360° measured from the zero North which may be expressed in 0°-90° quadrants measured from North in the northern quadrants and measured from South in the southern quadrants.

The inclination angle of the deviated well bore is the angle that the well bore axis makes with respect to the vertical. It is denoted as ‘i’ in Figure 1.1.

Measured depth (MD) is measured along the well path from one reference point to the survey point. It is also known as along hole depth and is generally measured by the pipe tally.

True vertical depth (TVD) at some particular point is the vertical distance to that point from the surface. TVD is generally referenced to the rotary table but may also be referenced to the mean sea level.

Kick off point (KOP) is the point below the surface location where the well is deviated from the vertical as shown in Figure 3. The position of the kick off depends on several parameters such as geological considerations, geometry of the well and proximity of other wells.

Dogleg severity (DLS) is a measure of the change in inclination of the well bore measured per 100 ft. of the course length.

The directional wells are categorized into profiles based on the trajectory that a particular well follows and the most common directional well profiles. Type I, II, III and IV are shown in Figure 1.1. Figure 1.1 shows the plot of horizontal displacement along the course of the well against the corresponding TVD and is representative of the well trajectory. All the profiles in the figure share the same KOP and a black marker that intersects the well path indicates the end of a particular section of the well.

Type I directional profile, represented by the red line in Figure 1.1, is a build and hold trajectory. The well is drilled vertically to the Kick off point (KOP) and then deviated from the vertical; the deviated section below the KOP consists of a build section, where we build the angle to reach a particular inclination at the end of build (EOB), and a hold section, where the achieved inclination is maintained constant all the way down to the target coordinates.

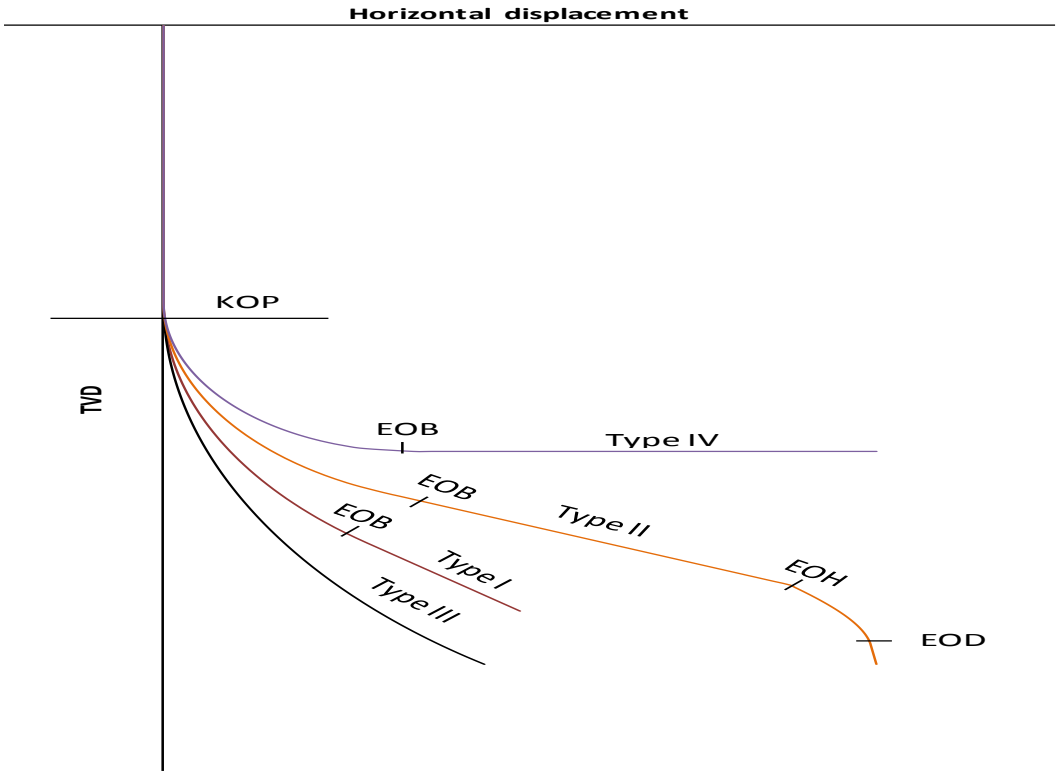

Figure 1.1. Directional well profiles.

Type III directional profile is the continuous build profile as shown in Figure 1.1. Once the well is kicked off from the KOP, inclination is built all the way down to the target co-ordinates. Such a profile generally has a large radius of curvature and the kick off point is generally deeper than the other well types.

Type IV directional profile is also a build and hold trajectory but differs from type I as for this profile, we always build up the angle to achieve an inclination of 90 degrees

at the end of the build section which is then held constant for the remaining course of the well to place a horizontal lateral into the formation of interest.

Type II directional profile is also known as ‘S’ type profile and comprises of three sections, build, hold and drop, below the KOP as shown in Figure 1.1. The well path is deviated at KOP to build a certain inclination angle up to the end of the build section (EOB) which is then held for some distance before dropping the well from the end of hold (EOH) to a particular inclination at the end of drop (EOD) which is then held constant to reach the target co-ordinates. This type of profile is generally used to drill extended reach wells and a modification to this profile, also used for extended reach drilling, is build, hold and build, as shown in Figure 1.2, where instead of dropping the well angle after EOH the angle is built upto 90 degrees and then held constant to place a horizontal lateral.

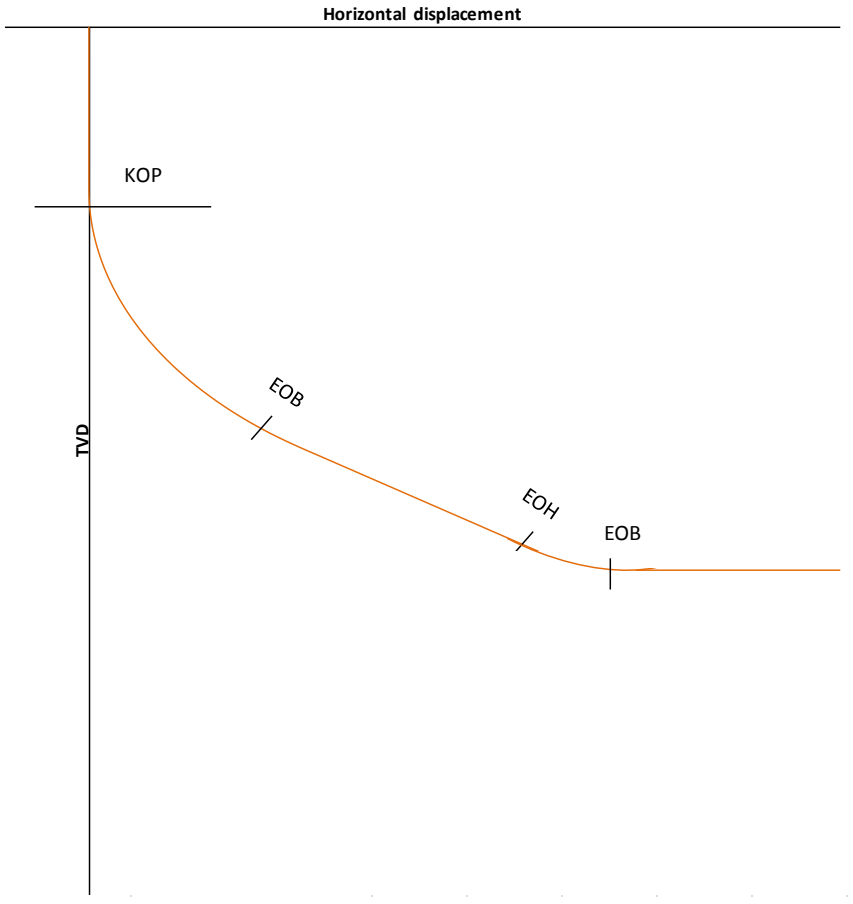

Figure 1.2. Build, hold and build directional profile.

Another type of directional wells, not shown in Figure 1.1 and 1.2, are the designer wells. These types of wells do not follow a specific course or a profile but are deviated to address a particular challenge and the well trajectory is generally adjusted on the fly based on the real time information obtained while drilling the well.

Magnetic tool face (MTF) is the orientation of the BHA relative to the North reference and is measured clockwise. It is generally used for vertical or nearly vertical wells with inclination less than 3°. As the MTF refers to the North, a MTF of 90° means that the well is drilled due East and 0° means that the well is drilled due North.

Gravity tool face is used once the well is kicked off or deviated using the MTF, gravity tool face is mainly used for the deviated portion of the well bore which refers to the high side or the top of the hole as shown in Figure 1.3. The reference is changed because in the deviated course the well might move up or down in inclination or turn left or right which cannot be easily referenced to the north. As the gravity tool face refers to the top of the hole, a gravity tool face of 0° means that the well will increase in inclination and 90° means that the well will decrease in inclination.

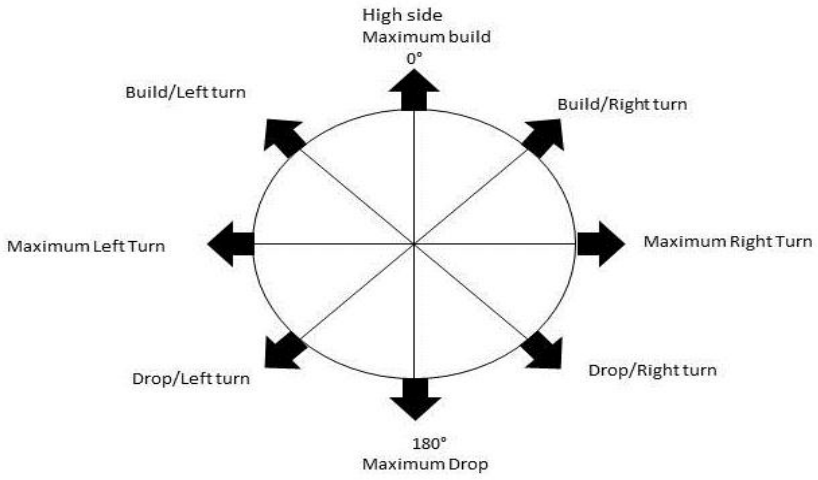

Figure 1.3. Gravity tool face with reference to the high side of the well.

1.3. WELL TRAJECTORY CALCULATIONS

Directional surveys are done to calculate and plot the 3D well path. The coordinates x ,y and z of the well path, which represent the departure of the well bore in North – South, East – west and vertical direction respectively, are determined from azimuth, inclination and MD. The most common method for the well trajectory calculation is the minimum curvature method. The mathematical expressions for the method are presented and discussed in Appendix A (Inglis, 1987).

1.4. MEASUREMENT WHILE DRILLING

As mentioned above, the well path is derived from the MD, inclination and azimuth. MD can be obtained from the drill pipe tally but there is no means to measure the inclination and azimuth from the surface. So a survey instrument is required down hole to keep track of the well path and for this purpose we use MWD which stands for Measurement While Drilling.

MWD measures the physical properties of the bore hole such as temperature, pressure and the trajectory in 3D space and relays the data to the surface using mud pulse telemetry. Real time data transmission varies considerably but generally includes encoding the data and transmitting it to the surface, via mud pressure pulses, where it is decoded. It is to be noted that the pressure pulses can be positive, negative or continuous sine waves.

The electronics of the MWD include triaxial accelerometer and magnetometer housed in a special nonmagnetic collar. The accelerometer measures the component of the earth’s gravitational field where as the magnetometer measures the earth’s magnetic field. The measured forces are used to give inclination, azimuth and the tool face orientation. Batteries are sometimes used to deliver power to the downhole measurement electronics but then the drilling runs would be limited to the life of the batteries. To overcome this limitation, most of the MWD systems incorporate a downhole mud turbine and alternator electrical power generation system. As the mud is pumped through the drilling system, the turbine rotates and drives the attached alternator to generate electrical power. The electrical power thus generated is available to all the MWD subsystems

where an electrical connection is available for power and data connectivity along the BHA (Lyons, 1996).

1.5. ELLIPSOID OF UNCERTAINTY

Every survey measurement has an associated uncertainty. The source of the error or the uncertainty associated with the measurement may be attributed to the equipment error or the assumptions made while calculating the trajectory by a particular method, for example the minimum curvature method assumes a smooth well bore between the two survey points which may not always be practically true. As already discussed that the 3D well path is derived from MD, inclination and azimuth, some of the uncertainties associated with each measurement are listed below:

- Depth – Drill pipe length measurement uncertainty, pipe stretch, thermal expansion and pressure effects
- Inclination and azimuth – Inherent instrument accuracy limitations, instrument alignment errors in the tool, tool misalignments and sag in the borehole, magnetic interference from the drill string or the nearby wells.

Since the well position is described in 3D, the uncertainty of the well position is a 3D problem and is represented by an ellipse at each survey point. This 3D volume of uncertainty is called the ellipsoid of uncertainty, as the well position within the ellipse is not certain and the well could be placed anywhere within the volume of the ellipse. The size of the ellipsoid is specified along the TVD and the semimajor and semiminor axes as shown in Figure 1.4**.**

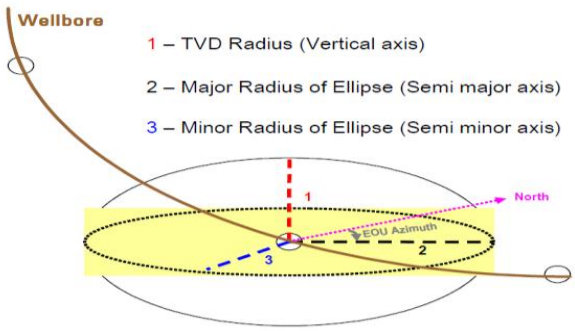

Figure 1.4. 3D representation of the ellipse of uncertainty (Griffiths, 2009)

Each survey point has its own associated uncertainty. As mentioned in the Section 1.3, Δx, Δy and Δz are calculated at each point and summed together with those at all the following points, the uncertainty keeps on mounting with the increasing number of survey points and ellipse gets progressively bigger through the course of the well as shown in Figure 1.5 and eventually forms a cone of uncertainty around the well path.

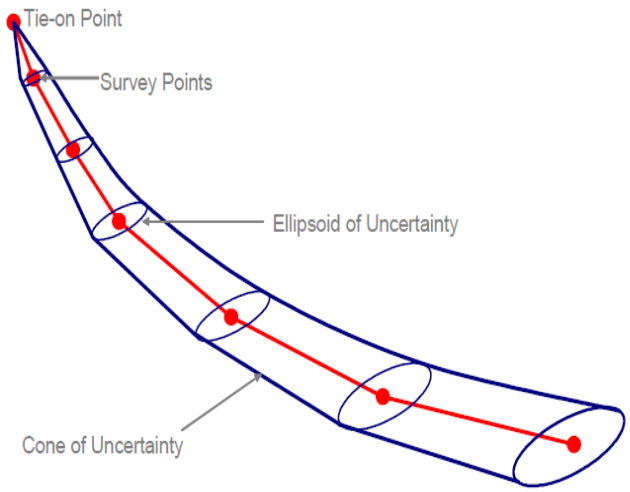

Figure 1.5. Cone of uncertainty around a wellpath (Griffiths, 2009).

The factors that cause uncertainties and affect the size of the ellipse are as below:

- Survey tools used - All the survey instruments have inherent errors. The magnetometers (azimuthal sensors) may read inaccurately owing to the magnetic interference in the bottom hole assembly or the magnetic mud interference and the accelerometers (gravitational or inclination sensors) may be susceptible to errors owing to the BHA sag. Gyroscopic survey systems have a limitation in high angle or horizontal wells; they cannot be used in the wells where the inclination angles are greater than 70°. The magnitude of the error depends on the instruments and the correction applied to them. Certain correction methods can be used such as Multi

station correction (MagCAD) and infield referencing (IFR) (Torkildson et al., 2004).

- Survey frequency - The magnitude of the error or the uncertainty depends on how frequently well is surveyed. As mentioned above in Section 1.3, the methods used for calculating wellbore trajectory include certain assumptions. The radius of curvature method for instance assumes a smooth wellbore path between the two survey stations; however the actual trajectory between the two stations may not be such. Therefore, the less frequently the well is surveyed the farther the survey stations and assumptions are made over a longer course of the trajectory which means a bigger error or uncertainty over the well path. Surveying the well more frequently places the stations close to each other and reduces the uncertainty (Rabia, 2000).
- BHA configuration - Through the course of a directional well the BHA tends to sag or bend causing a misalignment between the hole inclination and the sensors owing to the deflection of the MWD drill collar. The deflection may be under gravity or due to hole curvature. The magnitude of the error depends primarily on the BHA geometry, sensor spacing and the hole size (Studer et al., 2006). The sag correction has to be applied to improve TVD position and improve vertical uncertainty.
- Latitude and longitude - The magnetic measurements used tend to seek magnetic north and the magnetic north and true north of the measurements do not coincide. The angle in degrees between the true north and the magnetic north is called the declination angle which is different for most points on earth and in addition the magnetic north changes its position very slightly each year. Thus the magnetic measurements have an inherent uncertainty in global magnetic models used to determine declination at a specific site and thus the uncertainty may vary based on the position on the earth's surface. True North is however a fixed reference point which does not change, the magnetic surveys are thus corrected to true north (Rabia, 2000). The gyroscopic measures do not suffer from magnetic

interference but are affected by the drift caused by earth's rotation and also by the position of the wellbore on the earth's surface.

1.6. GEOSTEERING

Placing a well and maintaining it within the best part of the reservoir presents multiple and diverse challenges. Traditionally the wells are pre designed based on the target co-ordinates and the well path is controlled by MWD measuring inclination and azimuth at several survey. However MWD surveys are prone to uncertainties or errors, as discussed in Section 1.5, which is represented by the ellipsoid of uncertainty which grows in size progressively leading to a cone of uncertainty. We can never be sure of the actual stratigraphic position of the wellbore within the ellipse as it could be positioned anywhere within the volume of the ellipse. If the thickness of the reservoir interval or the target zone is less than the diameter of the cone at a certain point, there is a possibility that the well may be placed outside the reservoir interval which may affect the well production.

Hence, the geometric steering is not practically feasible in the thin reservoir sections which demand a precise placement and maintaining the well bore in the 'sweet spot' of the reservoir. This is where the LWD comes into play and the steering decisions are made based on the real time LWD response of the geologic formations. The method is known as geologic steering which can be defined as the planned interactive navigation of the well bore based on the geologic criterion. The geosteering methods can be broadly classified into Proactive and Reactive (Chemali et al., 2008).

Proactive geosteering anticipates the geological events before they intersect the wellbore and takes the beforehand appropriate measures to avoid any kind of exit from the reservoir. This method generally employs deep measurements such as deep propagation resistivity which can detect an approaching bed boundary from a sufficient distance to allow evasive action.

As the name suggests, Reactive geosteering is based on reacting in an appropriate manner to a geological event that has already been encountered or traversed by the wellbore. This method is mainly focused on determining the angle of exit of the wellbore through any of the reservoir boundaries and computing the most appropriate corrective

measure to steer the well back into the reservoir. It generally employs the shallow LWD measurements such as gamma ray, micro resistivity and density images which identify an event only when the wellbore has traversed it or is too close for an evasive action, the measurements are then used to calculate the relative dip of the borehole and accordingly steer it back into the reservoir. Thus, the LWD measurements form the core of geo-steering and the selection of an appropriate LWD suite is the key to the success of a geo-steering operation.

1.7. SCOPE OF WORK

The objective of the thesis is to develop well placement methodologies for non-trivial geologic settings i.e. geologic environments characterized by high heterogeneities. The following three methods will be evaluated for their application to geosteering.

The first goal is to develop a decision matrix will to decide on the LWD tools for a particular geosteering challenge. To develop the decision matrix, a case study of several LWD tools will be conducted, which have been utilized for geosteering, to identify their distinct features which may aid in geosteering. This case study will be conducted for several geological settings limiting the scope essentially to geosteering. The identified geosteering applications of the LWD tools will be merged together to create a generalized matrix.

The second goal is to evaluate the application of drilling data to geosteering. The mechanical properties MSE and UCS will be calculated for a set of wells in the field of study from the drilling data and sonic travel time data respectively. The calculated properties will then be statistically analyzed to determine their ability to footprint the formations and hence aid in well placement.

The third goal is to evaluate the application of hierarchal clustering and classification tree to geosteering. The hierarchal clustering method divides a heterogeneous formation into homogeneous sub regions or clusters and the classification tree is used to set quantitative decision criteria for identified clusters in terms of well logs. The two methods are statistical and have been used in the past for characterizing reservoirs by identifying the electrofacies. The methods will be applied to the field of

study using the available wireline well log information as input and verified for their feasibility with respect to the real time geosteering.

2. FIELD DESCRIPTION

2.1. DESCRIPTION OF THE FIELD OF STUDY

The field of study is an offshore field which is located in the southern North Sea. The field is marked by high heterogeneities and the reservoir section is a conglomerate reservoir of Triassic to Cretaceous age. It is comprised of alluvial conglomerates and aeolins sandstone unconformably overlain by sandstone of shallow marine origin. The sandstone is a fragile sandstone with variable grain sizes from very fine to very coarse grained and is occasionally calcite cemented. The conglomerates are very hard to hard, and consist mainly of granitic clasts with varying size and angularity (Hilgedick et al., 2012). Since the reservoir here is a mixture of sandstone and conglomerates, the geological setting is a little more complex than a regular oil sand.

Four wells from the field, well A, B, C and D, will be used for our analysis. The data that will be used is the mud logs and the wireline logs. Tables 2.1 through 2.4 show the geological setting of each well.

Table 2.1. Geological setting for well A

Depth interval (m)	Formation	Group	Lithological description
1913 - 1925	Hod	Shetland	Limestone
1925 - 1964	Jurassic	Jurassic	Sandstone and Conglomerate
1964 -2200	Triassic	Triassic	Conglomerate, sandstone and Claystone

Table 2.1 shows the formations of interest, with respect to geosteering, for well A. The top shoulder bed or the cap here is the Hod formation which consists of Limestone. The reservoir is the Jurassic formation which is a mixture of sandstone and conglomerate and the basement or the lower shoulder bed is the Triassic formation that comprises of conglomerate, sandstone and claystone. Good oil shows were observed in the upper part

of the Jurassic formation which decrease as we move down, becoming negligible in the Triassic sediments. The well placement goal for this scenario is to maintain the well in the upper part of the Jurassic formation and avoid drilling through the roof, into Hod, or into the basement, Triassic.

Table 2.2. Geological setting for well B

Depth interval (m)	Formation	Group	Lithological description
1860 -1889.5	EkofiskFm.	Shetland	Limestone with occasional chert layers
1889.5 - 1898	Undif. Cromer Knoll	Cromer knoll	Marl
1898 - 2151	Undif. Jurassic	Jurassic	Coarsely interbeded conglomeratic and pebbly sandstones

Table 2.2 shows the lithological description for the section of interest for well B. The first hydrocarbon shows were observed in the core chips collected in the Shetland group limestones that overlie the reservoir. The Jurassic reservoir was penetrated at 1898 m and was found to consist of interbedded pebbly sandstones and conglomerates containing granitic boulders. Good shows were observed in the more sandy intervals from 1898 m to 1911 m, which will be the sweet spot for this setting. As we go further down the oil shows become patchier and finally disappear with the oil water contact being at 1965 m. The possible exit through the roof, into the undifferentiated Cromer Knoll or Ekofisk, or drilling through the OWC at 1965 m must be avoided.

Table 2.3 shows the lithological descrition for well C. The oil shows for this well started at 1918.1 m MD RKB in the Asgard sand unit which belongs to Cromer Knoll group, the thickness of the formation is however less than 2m and thus might be a difficult target for well placement. The unit is followed by a thin layer of conglomeratic sandstone column, Draupne sand unit, which belongs to the Viking group followed by the oil bearing Jurassic/Triassic sandstones which belong to the same Group. The oil shows continue upto the undifferentiated Hegre group, which is made up of interbedded sandstones and conglomerates, down to the oil water contact at 1965 m. The goal for this

setting is to maintain the well in the top part of the Jurassic/ Triassic sandstones maintaining a stand off from the oil water contact and exit through the roof into the Marl of the Cromer Knoll group and the Limestone of the Shetland group or an exit through the bottom into undifferentiated Hegre group. Table 2.4 shows the geological setting for well D

Table 2.3. Geological setting for well C

Depth interval (m)	Group	Formation	Lithological description
1888 - 1917	Shetland	Ekofisk	Limestone with occasional chert layers.
1917 - 1917.75	Shetland	Hod formation	ChalkyLimestone
1917.75 - 1918.1	Cromer Knoll	Asgard formation	Upper Asgard is composed of Marl
1918.1 - 1919.46	Cromer Knoll	Asgard sand unit	Thin layer of medium to coarse grained sandstone.
1919.46 - 1920.25	Viking	Draupne sand unit	Conglomeratic sandstones with abundant granitic rock fragments
1920.25 - 19159.8	Viking	Und. Jurassic/Triassic	Cross bedded sandstone sequence of intermediate age
1959.8 -2303	Hegre	Und. Hegre	Conglomerate - sandstone, rounded granitic pebbles and mudstones

Table 2.4. Geological setting for well D

Depth interval (m)	Formation	Group	Lithological description
1892 - 1917	EkofiskFm.	Shetland	Limestone with occasional chert layers.
1917 - 1919	Undif. Cromer Knoll	Cromer Knoll	Marl
1919 -1922	Sandstone	Cromer Knoll	The sandstone member of the Cromer Knoll
1922 -1945	Granite wash	Basement	Weathered or fractured granitic material
1945 -2150	Fractured basement	Basement	Weathered or Fractured granitic material

It can be seen in Table 2.4, the reservoir here is sandstone which belongs to the geological group – Cromer Knoll. The shoulder bed above is undifferentiated Cromer

Knoll which also belongs to the same geological group. However the Ekofisk formation above it will also be considered as a shoulder bed as there is a good chance of exit through the roof into Ekofisk because of the limited thickness of the undifferentiated Cromer Knoll. The top portion of the granite wash immediately below the sandstone is also considered as a reservoir as the core reports indicate fair to medium hydrocarbon shows in the top portion of the formation. The lower shoulder bed here is the fractured basement which comprises of fractured granitic material and is immediately below the Granite wash. Table 2.5 shows a comparison of the geological setting of the four wells.

Table 2.5. Comparison of the geological settings for the wells A, B, C and D

Well	Cap	Reservoir	Basement
A	Hod	Jurassic	Triassic
B	Ekofisk, Undifferentiated Cromer Knoll	Jurassic	Jurassic below OWC
C	Ekofisk, Hod	Undif. Jurassic/ Triassic	Hegre
D	Ekofisk, Undifferentiated Cromer Knoll	Cromer Knoll Sandstone, Granite wash	Fractured basement

As can be seen in Table 2.5, shoulder bed or the cap for some of the wells comprises of more than one formation. This is done to account for the possibility of well exiting the shoulder bed into an adjacent non-reservoir because of the limited thickness of the shoulder bed.

2.2. DATA DESCRIPTION AND UNCERTANITIES IN THE FIELD

The dataset for each of the well, used in the analysis, is represented graphically with respect to depth in Figures 2.1 through 2.4. Each track in the figures represents a well log measurement against the respective formations, in the last track.

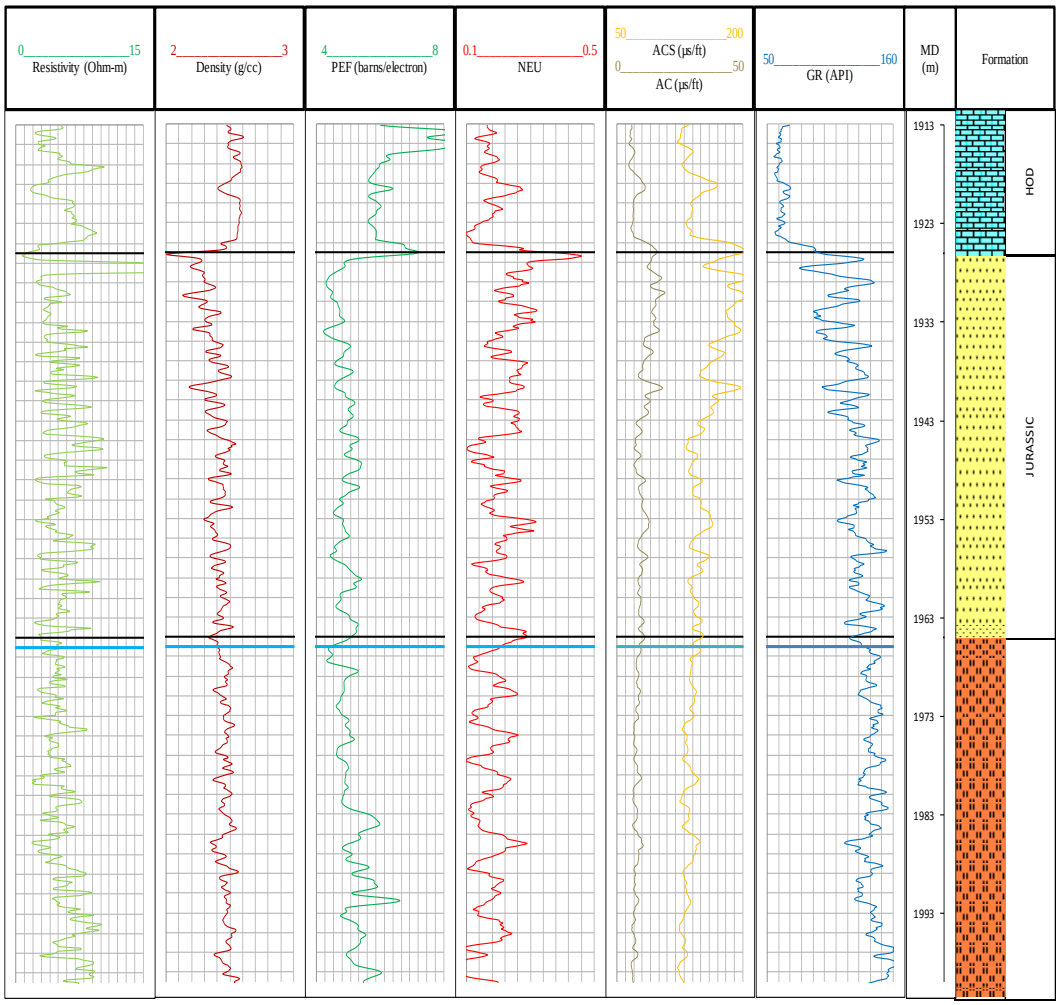

Figure 2.1. Wireline log responses for the formations of interest for well A.

The two black lines in each track of Figure 2.1 mark the upper and lower boundary of the reservoir, Jurassic, whereas the blue line indicates the oil water contact. As can be seen in each track, we observe a distinct log response marking the upper boundary of the reservoir. Resistivity shows a spike, Density, PEF and Sonic travel times show a decrease whereas the neutron porosity increases. All these responses can be used to accurately map the upper boundary of the reservoir and hence avoid an exit through the roof into Hod. However as we move down through each track, we observe that the responses do not change much even when the lower boundary of the reservoir is crossed down into the Triassic formation. Thus, it is very difficult to distinguish between the

Jurassic and Triassic and identify if an exit has been made through the bottom. Figure 2.2 shows the wireline responses for well B.

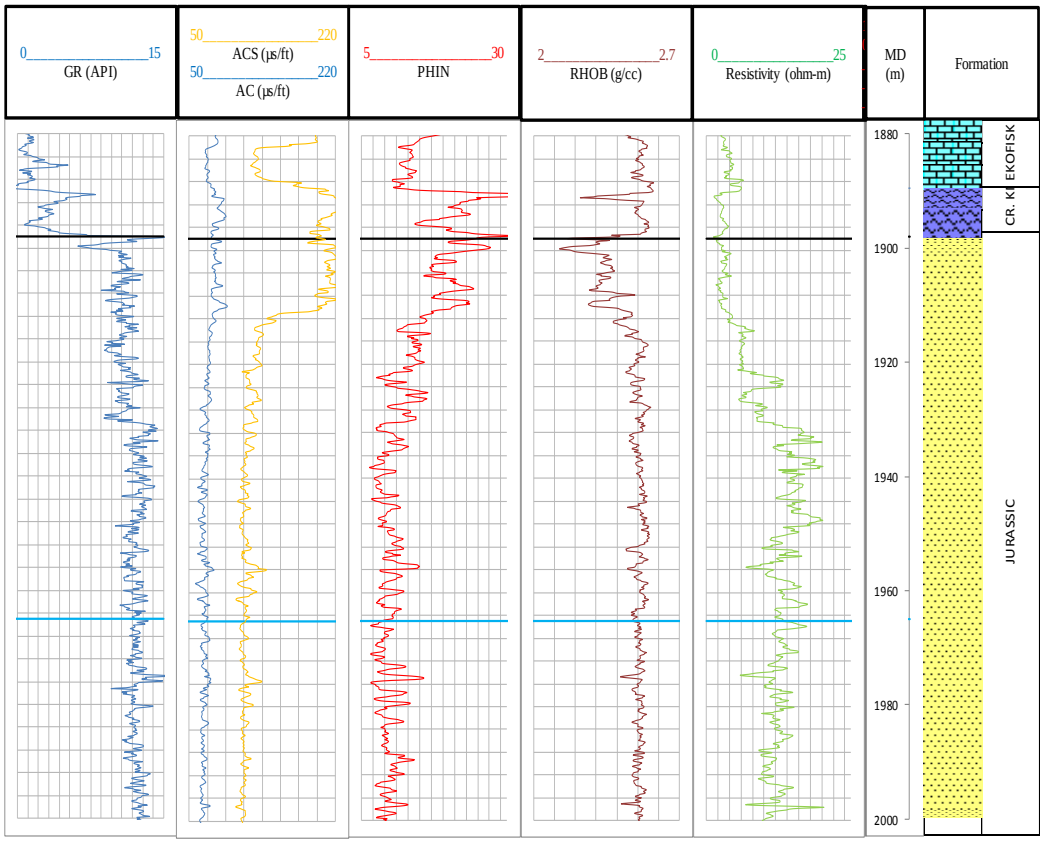

Figure 2.2. Wireline log responses for the formations of interest for well B.

As can be seen in Figure 2.2, the resistivity contrast that we observed at the upper boundary of the reservoir in well A is missing here. However, Gamma ray shows a sharp increase at the upper boundary. Sonic shear travel time shows a sharp increase at the top of Cromer Knoll but does not shows any change at the top Jurassic boundary. Most of the curves remain flat as we move down from the upper boundary except for resistivity which shows some variation within the reservoir and PHIN which shows a steady decrease but none of the curves produce a distinct response at the oil water contact, indicated by a blue line in each track.

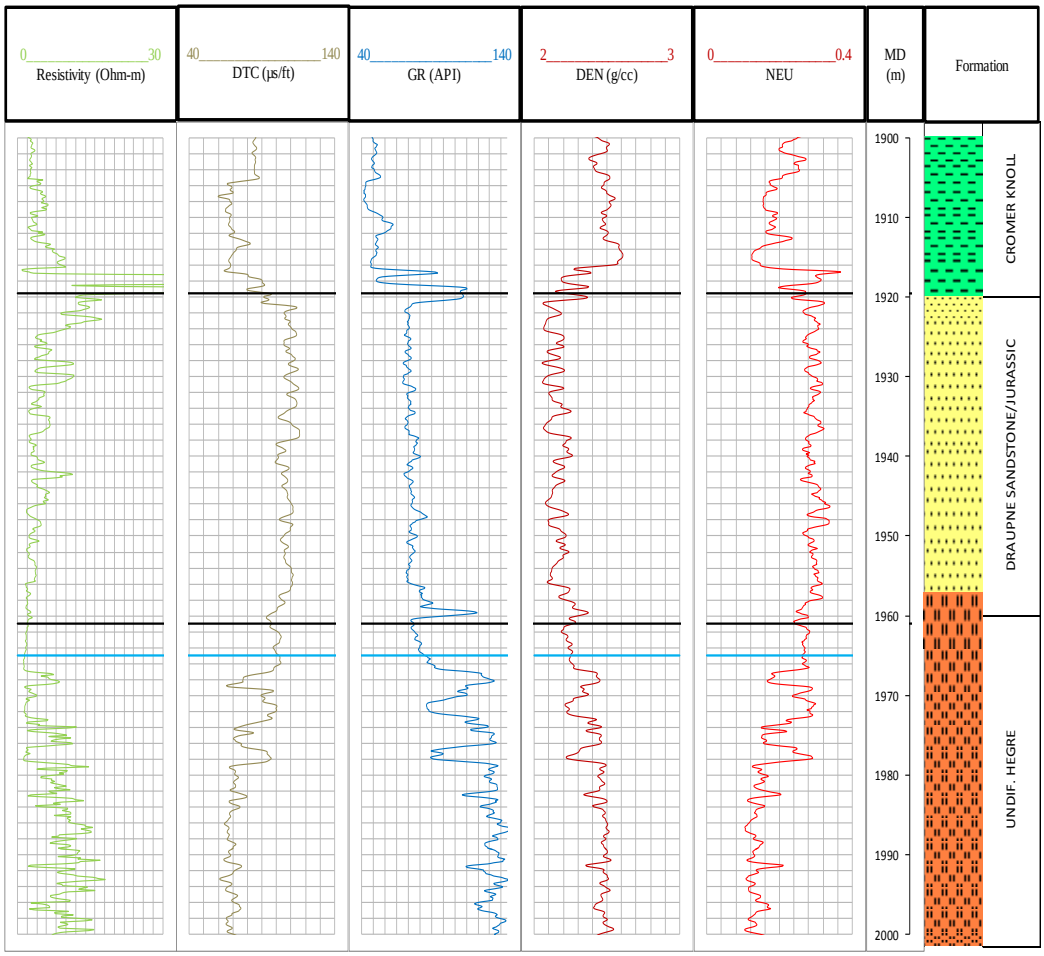

Figure 2.3. Wireline log responses for the formations of interest for well C.

Figure 2.3 shows the wireline log responses for well C, the reservoir is marked by the black lines in each track whereas the blue line indicates the oil water contact. Here again some distinct responses can be seen at the upper boundary of the reservoir. The resistivity shows a spike, DTC increases whereas the density and Gamma Ray decrease. Thus the upper boundary can be marked based on these responses but the responses may not be of much assistance in distinguishing between the formations. The resistivity decreases when in the reservoir and the overall trend of the resistivity curve remains the same in the reservoir and the conglomerates below. DTC shows a higher value for the reservoir but is almost the same for the basement, Undif. Hegre, and the upper shoulder bed, Cromer Knoll. Density and neutron exhibit similar responses. Such responses can be

misleading while steering the well especially if the well is faulted into one of the shoulder beds, in that it will be very hard to figure if the exit has been made through the roof or the bottom as both the formations show similar responses. The only log that shows good distinguishing ability here is the Gamma Ray which shows very low values for the Cromer Knoll, moderate values for the reservoir and very high values for the basement. We can also see that the oil water contact goes undetected as there is no distinct log response at the corresponding depth.

2.3. WELL PLACEMENT CHALLENGES IN THE FIELD

As discussed in section 2.2, we do observe some distinct log features but they cannot be expected to be consistent and will often be misleading or lack the ability to footprint the formations. Hence conventional geosteering methods may not be sufficient to accurately place the well in the reservoir. Following geosteering goals were identified for the field.

The first goal is to keep the well bore within the reservoir and avoid exiting into the upper or lower shoulder bed. This calls for an accurate detection of the reservoir boundaries.

The Second goal is to steer the wells maintaining a stand off from the oil water contact. The oil water contact is generally detected by the resistivity responses but as seen in the log responses discussed in the last section, resistivity responses do not aid in detecting the contact.

The third goal is to identify the lithology within the reservoir. As discussed in the lithology description of the wells, the oil shows are not consistent all through the reservoir. As the goal of geosteering is not just to place the well in the reservoir but in the best part, we need to map the variations within the reservoir accurately to identify the sweet spot.

The fourth goal is to identify the post exit position of the well in the event of an exit. As already discussed the downhole information in the field can be often misleading, besides uncertainties like faults cannot be accounted for beforehand. Hence it is very important to consider the possibility of exit and plan for a corrective measure when devising the steering strategy.

3. DEVELOPMENT OF DECISION MATRIX

3.1. BASIC LWD TOOLS

Logging while drilling is the measurement of the formation properties as the hole is drilled through the use of the measurement tools integrated in the BHA or it can be said that it is a technique of conveying well logging tools downhole as part of the bottom hole assembly. LWD works with the MWD to transmit the complete or partial measurement information to the surface via mud pulse telemetry. Thus, LWD is an extension of MWD where we measure the formation physical properties in addition to the directional data and drilling parameters. LWD suite also has a memory which stores the logging information as a formation is logged and the complete information can be retrieved after the run.

The working principles of logging while drilling tools are similar to the wireline tools which have an advantage of measuring the formation properties before any significant fluid invasion as the formations are logged as they are drilled or shortly after, depending on the distance of the sensor from the bit. Furthermore, many of the deviated wellbores especially the extended reach wells prove to be difficult or sometimes impossible to be logged by conventional wireline measurements. However, the wireline logs have a better quality control as they work under stable hole conditions whereas the LWD tools work in a dynamic environment where the log quality may be disturbed due to the irregular BHA motion while drilling as in stick slip or shock.

The formation measurements made downhole are recorded against time as LWD, unlike the wireline logs, has no means to record depth. The depth is measured at the surface i.e. the driller's depth against time using a clock which is synchronized with the one in the tool. The time index is then used to merge the downhole measurement-time data to give the measurement-depth data. The LWD tools are of two types, azimuthal and circumferential.

Circumferential tools record measurements 360° around the borehole. Hence, the measurements are an average of the properties distributed round the borehole and do not indicate an approaching geological event.

Azimuthal tools record measurements which focus on a sector of the bore hole, rather than the average around the bore hole, and thus help in determining the direction of an approaching geological event. These tools scan the bore hole during BHA rotation and the information acquired is binned into azimuthal sectors. The resolution depends on the type of measurement. Gamma ray can be resolved into four quadrants around the borehole which are presented as Up, Down, Right and left. For density each quadrant can be sub dived into 4 sectors which gives a total of 16 sectors around borehole. The most tightly focused measurement is the laterolog resistivity which can be resolved into 56 sectors around the borehole.

It is the directional ability of the azimuthal tools which makes them the primary source of information that helps guide the well path in an appropriate direction to avoid or encounter a geological event downhole.

The information presented to a geo-steering team might be overwhelming, so it is very important to compartmentalize the information into geonavigation and formation evaluation information. The geonavigation information must be prioritized when placing the well because geo-steering often requires a quick response and wading through the information which doesn’t really affect the steering decision will interfere with the decision making process. Before the horizontal section is kicked off, the geo-steering team must separate the data required for geo-steering from the one required for the complete reservoir evaluation. The reservoir evaluation can wait until the well has been placed in the desired interval. In the following section we will discuss the working principles and applications, with respect to well placement, of several LWD tools used for geosteering

3.2. PROPAGATION RESISTIVITY

Propagation resistivity has a similar working principle as the induction resistivity tool run on wireline. The induction resistivity tool uses a transmitter coil which on being excited by an alternating current launches electromagnetic waves that induce eddy currents into the formation which in turn induce a secondary magnetic field that induces a voltage in the receiver coil set. The secondary magnetic field measured gives a direct measure of the conductivity. This is the basic working principle of the tool and it requires

a precise coil positioning i.e. exact number of turns to cancel the primary magnetic field's flux so as to measure the secondary magnetic field only. The transmitting and receiving coil set of an induction tool are supported on a mandrel which is lowered downhole via wireline. The induction tools work in a stable or static environment and thus it is possible to maintain the precise coil positioning through the tool run. The working principle of the induction and the propagation resistivity tools is essentially the same, the difference being the operating frequencies and the tool design.

The LWD propagation resistivity, like their wireline counterparts, also use transmitter and receiver coils but incorporate the coils on a drill collar which is run downhole along with BHA to make measurements in a dynamic drilling environment where drill collars are generally subject to shocks and these shocks are in most cases strong enough to destroy any precise coil positioning. Thus the LWD propagation resistivity tool has to be the one in which the positional stability is not very demanding. This is generally achieved by using a transmitter and receiver pair arrangement as shown in Figure 3.1, the transmitter and receiver array are basically coil loops disposed in the recess formed circumferentially around the drill collar. Precise coil positioning does not matter because the phase shift and attenuation can be measured over a pair of coils. As can be seen in the figure, the two transmitter coils at the top and bottom transmit an electromagnetic wave into the formation and the phase shift and attenuation are measured across the two receivers. The propagation tools operate at high frequencies, 400 KHz - 2 MHz, unlike the induction tools which operate at the lower frequencies like 10 KHz – 100 KHz. The phase shift and attenuation measurable by these simple pair of coils increase rapidly with the frequency, so the measurements are pretty much reliable at high frequencies but at the same time higher frequencies mean higher dielectric effects on the measured signal. The 2 MHz frequency thus selected is a compromise between minimizing the dielectric effects and ensuring a reliable phase shift and attenuation measurements. If we go further than 2 MHz we will have to deal with dielectric interpretation issues. The phase shift and attenuation measured across a receiver pair can be used to derived resistivity of the formation. The propagation resistivity is generally expressed as phase shift or attenuation resistivity.

Phase shift (Φ) is the ability of a formation to resist electrical conduction as derived from the change in position of the peaks of the electromagnetic wave generated in a propagation resistivity measurement as shown in Figure 3.1. The phase shift depends mainly on the resistivity of the material with a small dependence on the dielectric permittivity. However the dependence on the dielectric permittivity increases at high resistivities. The phase shift is converted to resistivity assuming that the dielectric permittivity is related to the resistivity by a simple algorithm. For 2 MHz measurement the typical range is 0.2 to 200 ohm-m, above 200 ohm-m the dielectric effects become too variable and it is preferable to use dielectric resistivity. Phase shift is generally measured in degrees.

Attenuation or amplitude (A) is the ability of a formation to resist electrical conduction as derived from the reduction in amplitude of the electromagnetic wave generated in a propagation resistivity measurement as shown in Figure 3.1. The attenuation depends almost solely on the resistivity and is thus converted to it by using a simple algorithm. For a 2 MHz measurement, the typical range is 0.2 to 50 ohm-m, above 50 ohm-m the dependence of attenuation on resistivity is too small to be measured accurately. Attenuation is generally measured in dB.

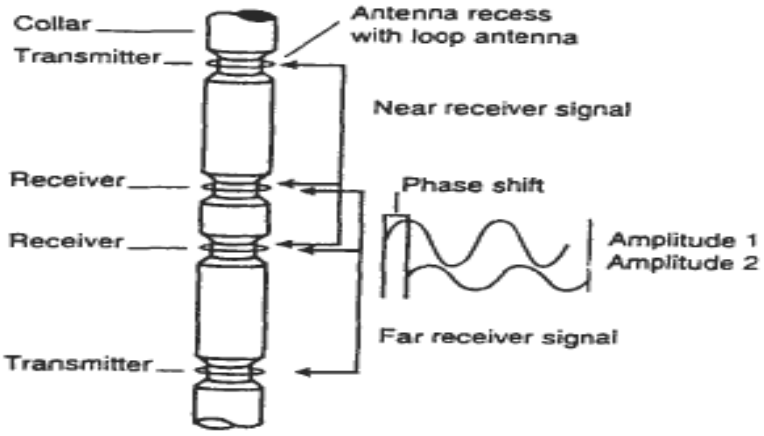

Figure 3.1. A typical LWD propagation resistivity transmitter and receiver arrangement to measure phase shift and attenuation (Lyons, 1996).

The propagation resistivity measurements can be thought of an AC circuit around a volume of rock which acts as a resistor. Ohm's law, which was used to define the resistance across a volume of rock for a DC circuit is extended to the AC circuits by the concept of electrical impedance. The mathematical expressions for the concept can be found in Appendix B.

Propagation resistivity is perhaps the most important tool for well placement owing to its large depth of investigation which can be as long as 18ft depending on the conductivity contrast. It is the only proactive LWD to date that has been tested in the field. However, the propagation resistivity tool used for well placement is azimuthal. Azimuthal sensitivity of the directional resistivity tools serves as the major advantage over the conventional propagation resistivity tools. For instance, if we are drilling in a reservoir sequence sandwiched between the shale beds and the wellbore exits the reservoir, we would know that the wellbore has exited reservoir interval because the resistivity measurements will show a low reading and the gamma ray will show a high reading but there is no way to figure out if the well has drilled out through the roof or the floor of the reservoir, the corrective action in this case depends on the knowledge of the local geology and making an educated guess which always involves some uncertainty. The conventional tools also lack the ability to identify the boundary from a good enough distance, owing to their short depth of investigation, to allow trajectory changes to maintain the well in the reservoir. The azimuthal propagation tools achieve their direction ability by using a combination of coaxial and tilted or transverse transmitter and receiver antennas. The details on how the tilted antenna arrangement makes the tools azimuthally sensitive and different available propagation resistivity tools from major contractors are discussed in Appendix C.

3.3. FEATURES OF DIRECTIONAL LWD RESISTIVITY

The features of directional propagation resistivity that can be used for well placement are as below.

Polarization horns were identified in the induction tools response at a bed boundary and were earlier considered as unfortunate anomalies in the log response but later their importance was realized and now they are considered as an accurate bed

boundary marker. This is very useful specifically for steering because to place a well accurately in a bed we need to identify its boundaries. The polarization horns occur at the boundaries with good resistivity contrast where the resistivity response becomes unexpectedly high and is seen as a distortion on the logs. The polarization horns are caused due to polarization at the boundaries which is caused by the discontinuity of the electric field crossing a boundary. When the induced currents cross a bed boundary, they must be the same for the entire current loop across the two beds because the electrons cannot vanish. But the two beds here are of different resistivity, so to obey ohm's law the electric field must be different in the two beds. This discontinuity in the electric field causes polarization or the charge build up at the boundary. Thus the received signal is very strong and is distorted into a polarization horn. The magnitude of the polarization horn is a function of the resistivity contrast between the beds and the dip angle and is mathematically represented as below (Luling, 1991).

$$(R_1 - R_2)^2 . sin^2(\theta_{dip}) / (R_1 . R_2 (R_1 + R_2)) \quad (1)$$

Where R_1 & R_2 – resistivity of the two beds across the boundaries in ohm.m θ_{dip} is the $_{Dip}$ angle in degrees

Up and Down resistivity -The resistivity measured by the sensors for all spacings and all the frequencies are binned into 32 regularly spaced sectors around the azimuth. The azimuth in this case is not with reference to the true north or the grid north but with reference to the high side of the hole. Hence, the azimuthal distribution here is as if we are looking through the center of the bore hole with the top being the high side of the hole, as shown in the Figure 3.2. The azimuthal resistivity measurements are available as the BHA rotates. The 'Up' resistivity or the high side resistivity measured when the tilted coils face up is the average resistivity from the top bins generally 1 and 32. The 'down' resistivity or the low side resistivity which is measured when the tilted coils face down is the average resistivity from the bottom bins generally 16 and 17 (Bejarano et al., 2010).

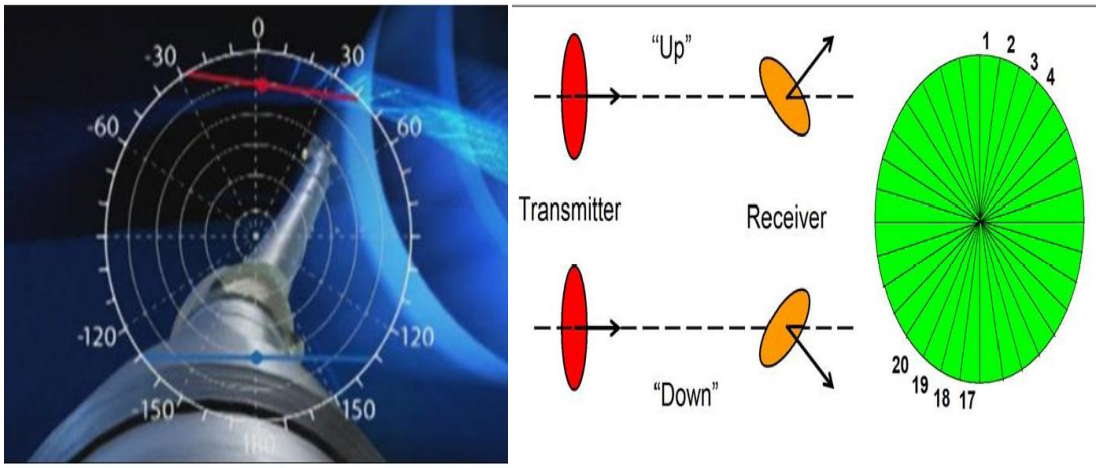

Figure 3.2. Azimuthal representation with respect to the bore hole (left), Up and down resistivity measurements by the tilted receiver antenna (right) (Diaz et al., 2009).

Figure 3.3 shows an example of how up and down resistivity helps in identifying the reservoir boundaries. Figure 3.3 shows the simulated azimuthal deep resistivity response for a wellbore drilling through the bottom boundary of the reservoir to a conductive zone.

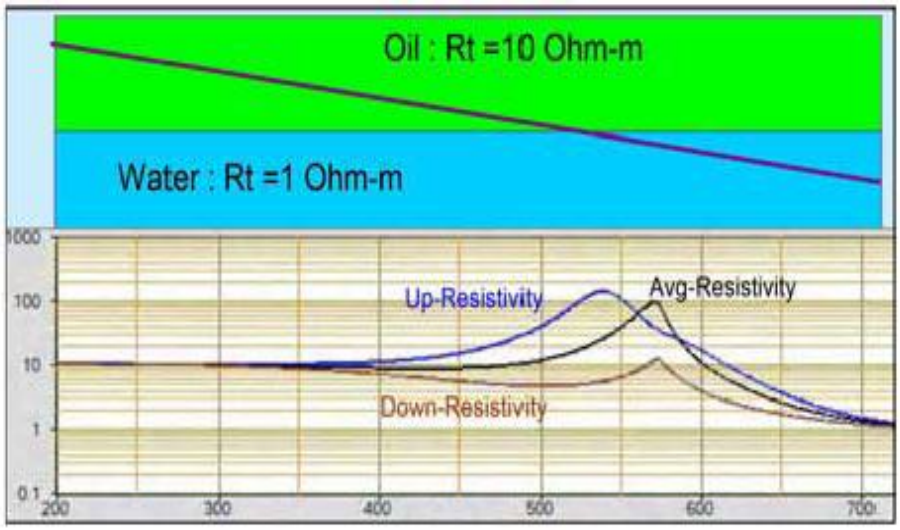

Figure 3.3. Wellbore crossing the reservoir boundary through the floor of the reservoir to a conductive water bearing zone (Bittar et al., 2010).

It can be seen in Figure 3.3, the up resistivity reads a higher value as it is focused on the reservoir and the down resistivity reads a lower value as it is focused on the conductive zone. The average resistivity curve which is the mean resistivity from all the sectors does indicate a polarization horn as the well intersects the boundary, because it responds to both the beds at that point, but is unable to indicate the direction of exit. The separation between the two curves can be seen well before the intersection with the boundary which demonstrates the early boundary identification by the deep azimuthal measurements. The up and down resistivity curves from longer spacings will identify the boundary earlier than the curves from shorter spacing between the transmitter and receiver. Figure 3.4 shows the simulated azimuthal deep resistivity responses when the wellbore drills through the roof of a conductive boundary.

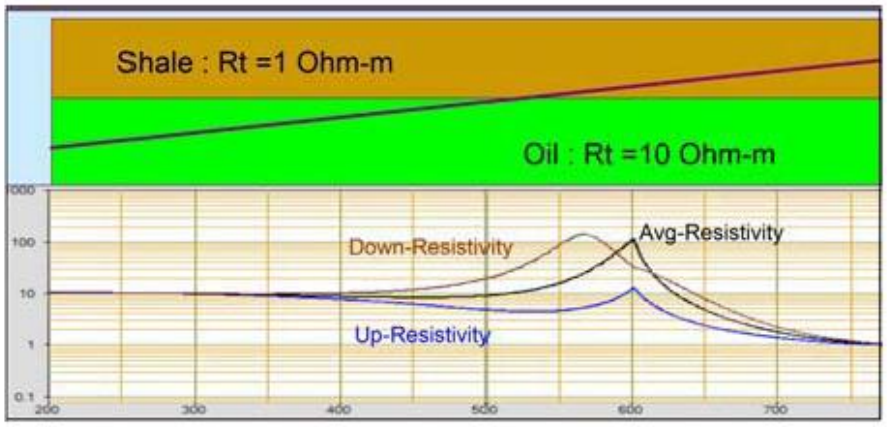

Figure 3.4. Wellbore crossing the reservoir boundary through the roof of the reservoir to the conductive shale (Bittar et al., 2010).

As can be seen in Figure 3.4, the separation in the up and down resistivity curves appears as the well nears the conductive formation towards the roof of the reservoir and in this case the readings of the two curves are reversed i.e. the down resistivity reads high and the up resistivity reads low.

Geosignal -The Geosignal is the difference between the measurements (phase shift and attenuation) measured from the opposite azimuthal orientations of the tool. It is expressed in degrees for the phase and dB for the attenuation.

Geosignal = Bin (i) – Bin (i+16) (2)

Where Bin (i) is the phase or attenuation reading from ith bin and Bin (i+16) is the phase or attenuation reading from the opposite bin if the resolution of the tool is 32 sectors

The signal detection threshold for the geosignal is set at the electrical noise floor of the resistivity tools which is 0.005 dB for the attenuation and 0.03 degrees for the phase measurements. The geosignal will only appear above the threshold values. When the resistivity tool is rotating in a homogenous formation the geosignal amplitude would be zero as the measurements from opposite azimuthal orientations are equal within the homogenous formation and they cancel out each other. This point within a reservoir where the geosignal is zero is known as the electrical midpoint of the reservoir. When the well bore is near the upper or lower boundary of the reservoir, the geosignal will have some amplitude which is increases exponentially with the distance to the boundary and also depends on the resistivity contrast between the reservoir and the shoulder bed. As a general rule, the geosignal points from the most resistive to the least resistive medium as shown in Figure 3.5

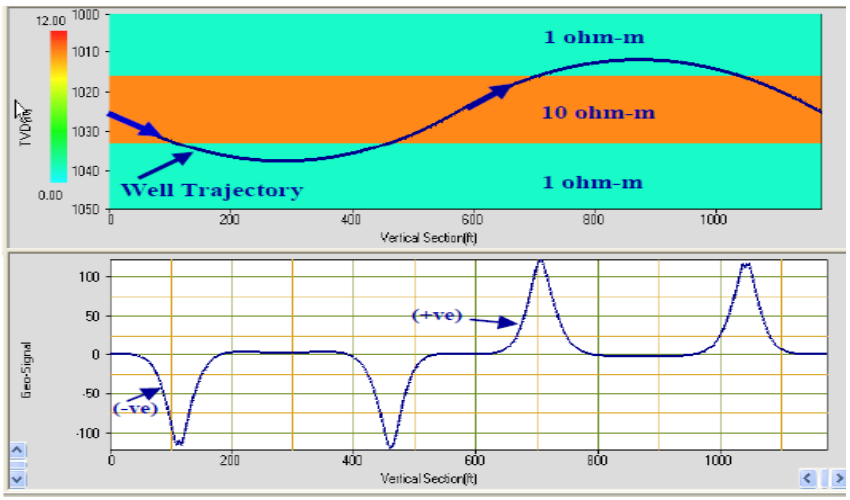

Figure 3.5. Wellbore trajectory through a reservoir – conductive bed and reservoir bed sequence and the corresponding geosignal response (Diaz et al., 2009).

As can be seen in Figure 3.5, the geosignal points from a higher resistivity boundary to a lower resistivity boundary. Through inversion, the geosignal can determine distance to the boundary in real time and with great accuracy.

Electrical midpoint and saddle point - The concepts of electrical midpoint and the saddle point have to be understood to efficiently interpret the response of the propagation resistivity tools. When navigating through a reservoir of a particular thickness, the midpoint of the reservoir is known as the physical midpoint. The electrical midpoint is however determined from the directional resistivity response or the geosignal and is defined as the point where the directional resistivity response or the geosignal becomes zero. It may or may not coincide with the physical midpoint of the reservoir. As discussed earlier, a directional resistivity response is the difference between the resistivity responses from the two opposite quadrants or sectors and assuming a good boundary contrast, the depth of investigation tool will be 18ft.If a reservoir is 36ft or more in thickness the physical midpoint of the reservoir will coincide with the electrical midpoint because in this case the tool does not respond to the shoulder beds, as the reservoir is thicker than the DOI of the tool, but only to the reservoir. Thus the resistivity response from the opposite quadrants will be the same, given the reservoir is fairly homogenous, and will cancel out each other. This is the simplest case where the electronic midpoint is established fairly easily within the reservoir.

Now let’s discuss a few cases where the thickness of the reservoir is less than the DOI of the tool i.e. it responds to the shoulder beds all the time through the course of the well. Figure 3.6 shows a wellbore traversing through a reservoir, 10 ohm, is surrounded by the shoulder beds of equal resistivity, 1 ohm.

Referring to Figure 3.6**,** as the wellbore traverses through the reservoir it responds to the shoulder beds at all times and as it approaches the physical midpoint, 115 ft, of the reservoir the directional signal becomes zero. This is because even though the tool is sensitive to the shoulder beds, the resistivity of the shoulder beds being the same, the tool records similar resistivity responses on either side or opposite quadrants at the physical midpoint which cancel each other. So, the electrical midpoint coincides with the physical midpoint of the reservoir in this case too.

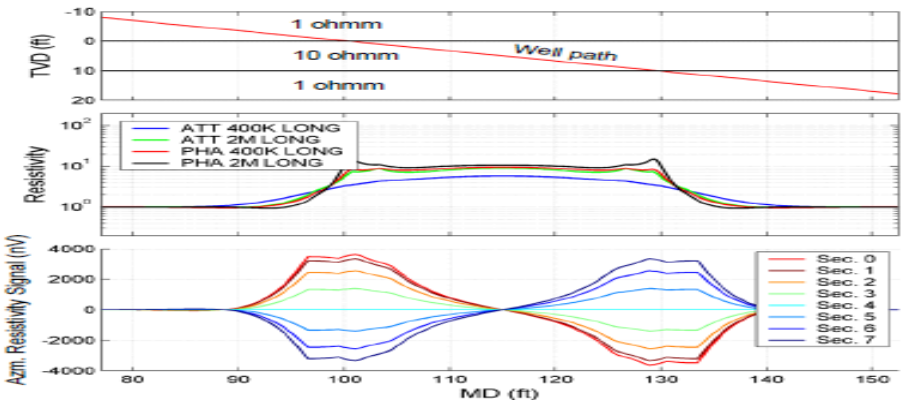

Figure 3.6. Well path through a reservoir surrounded by the shoulder beds of similar resistivity and the corresponding propagation resistivity responses (Bell et al., 2006).

If the resistivities of the shoulder beds in the above case are different from each other, the electrical midpoint will not coincide with the physical midpoint. Figure 3.7 shows such a scenario where the similar reservoir is surrounded by the shoulder beds of different resistivities, 1 ohm and 2 ohm.

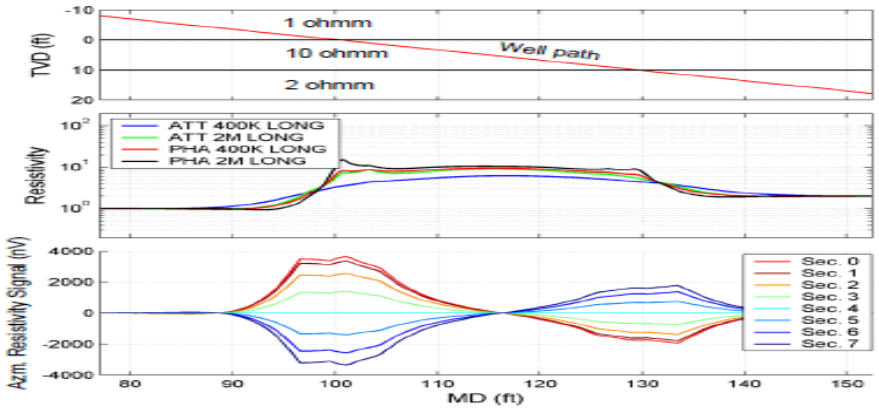

Figure 3.7. Well path through a reservoir surrounded by the shoulder beds of different resistivities and the corresponding propagation resistivity responses (Bell et al., 2006).

As can be seen in Figure 3.7 the electrical midpoint does not coincide with the physical midpoint at 115 ft but moves to 117 ft, closer the more resistive formation or the lower resistivity contrast. Electrical midpoint is important to well placement and once

established it assures us that we are safely placed in the reservoir and the well can be than be drilled parallel to the dip of the bed following the midpoint. The placement of the well in a particular reservoir is however governed by the definition of the sweet spot for that particular reservoir. The variation in the electrical midpoint when drilling parallel to the bedding indicates varying thickness of the reservoir along the course or a sudden rise in amplitude indicates a fault.

A saddle point is the point along the course where the magnitude of the directional resistivity response dips to the minimum surrounded by two local maxima. The magnitude at the saddle point may or may not be zero. Figure 3.8 shows a scenario which can cause a saddle point.

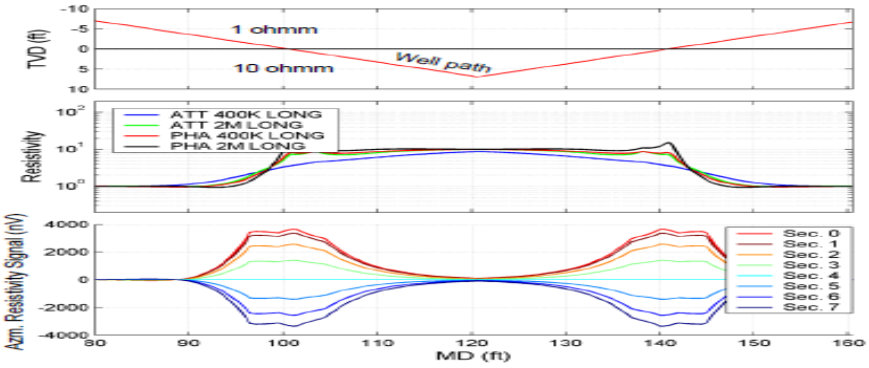

Figure 3.8. A 'V' shaped well path through a fairly flat reservoir and non-reservoir interface (Bell et al., 2006).

It can be seen in Figure 3.8 that the maximum response is recorded when the well intersects the boundary and the minimum amplitude i.e. the saddle point is recorded at the lowest trajectory point within the reservoir. A similar response can be observed when the well trajectory is relatively flat and traversing a curved resistive boundaries. Several scenarios which can cause a saddle point are shown in Figure 3.9. An understanding of the saddle point can thus help us identify the kind of scenario we are dealing with and can facilitate efficient well placement.

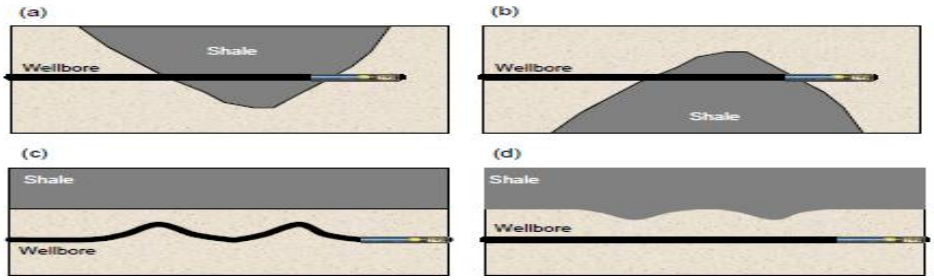

Figure 3.9. Several scenarios that can cause a saddle point (Bell et al., 2006).

Resistivity images - The propagation resistivity tools record the resistivity in a complete circumference i.e. 0°-360° around the borehole. The resistivity variation around the borehole is coded as a colored image where this variation is represented by different color tones. Dark tones indicate low resistivity whereas the light tones indicate high resistivity. The image is then presented to us in 2D, it is like cutting the circumferential image of the borehole from the high side and laying it out flat. The tracks 0° and 360° indicate the high side of the hole whereas the central track 180° represents the low side of the hole. Deep resistivity image logs used for the well placement are by convention presented as a horizontal log section as shown in Figure 3.10 with the MD increasing towards the right. Figure 3.10 shows an example of resistivity images when the well bore is traversing up dip (Top) and down dip (Bottom).

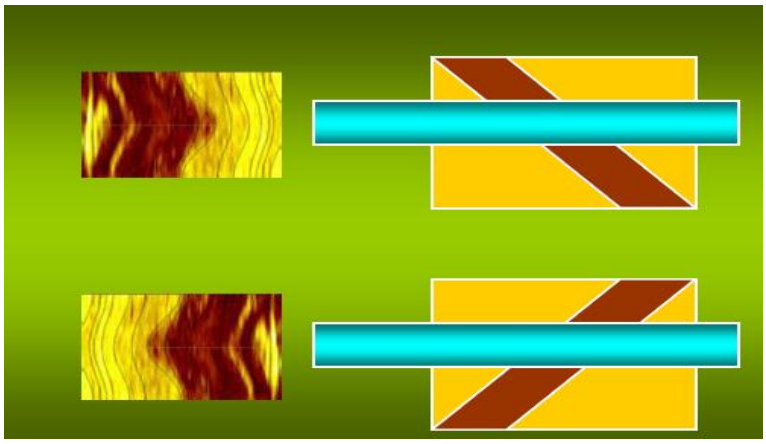

Figure 3.10. Smiling pattern (top) while drilling up dip and frowning pattern (bottom) while drilling down dip (Chemali et al., 2010).

The deep propagation resistivity images exhibit the typical ‘smiling’ and ‘frowning’ patterns for the up dip and down dip as the shallow images, as shown in Figure 3.10. Since the conventional shallow images such as GR, density etc. has a shallow depth of investigation they originate from a point just a few inches into the reservoir. For quantitative application, magnitude of the sinusoid is used to take a ratio to the borehole diameter to calculate the relative dip (Al-Musharfi et al., 2010; Bacon et al., 2009).

Dip calculation by sinusoid fitting is not applicable to the deep resistivity images because the depth of investigation is highly variable, depending on the resistivity contrast, and in all the instances is much more than the bore hole size. A unique feature of the deep resistivity images is the ‘bright spot’. The polarization horns which appear on the resistivity curves manifest themselves as bright spot on the resistivity images and hence indicate the presence of a boundary. Figure 3.11 shows the bright spots as indicated by the azimuthal resistivity array from different spacings. The bright spot is the most prominent for 48” spacing because of the larger DOI for the spacing as compared to other spacings. The bright spots appear when approaching a low resistivity shale or water contact from the high resistivity or at any boundary of good resistivity contrast. Hence when used together with the azimuthal resistivity and geosignal, they provide a good indication of the reservoir boundaries.

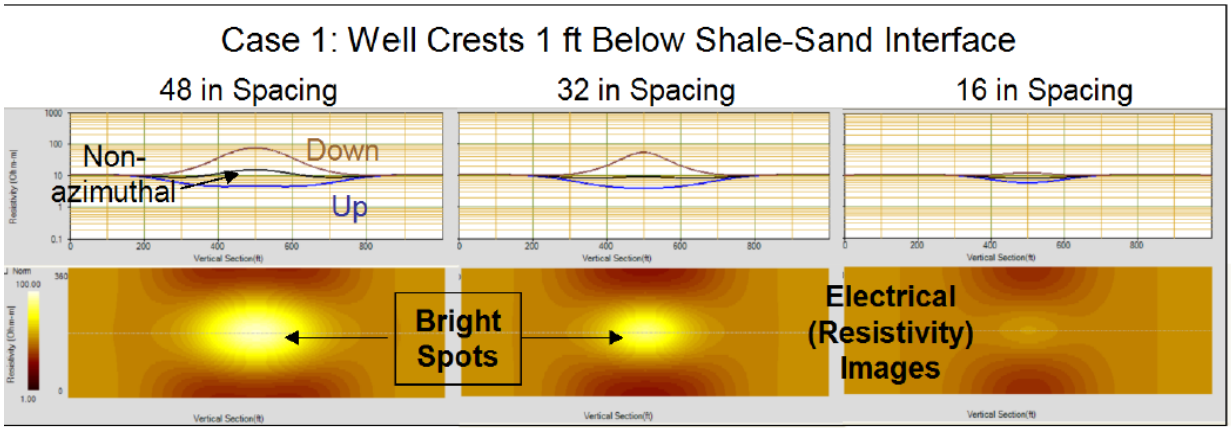

Figure 3.11. Bright spots from resistivity measurements from different spacings (Diaz et al., 2009).

There would always be a shift, between the bright spots indicated from the longer spacing to the ones from the shorter spacings, along the measured depth. The shift reflects the difference in depth of the electrical images and can readily be used to calculate the distance to the boundary along with the corresponding azimuth of the upper and lower boundaries. Hence, the relative dip can be derived by the angle between the two boundaries and the well bore path.

The images are categorized in order to simplify their interpretation. The major classification is known as the Theme and within each theme there are characteristic patterns called the Motifs which can be further divide into Submotif. These themes and motifs are given memorable and interesting names so they can be identified at sight and we know what kind of resistivity distribution or scenario we are dealing with. To understand how it works let's consider a theme "Landing the well". Figure 3.12 and Figure 3.13 show two motifs within this theme.

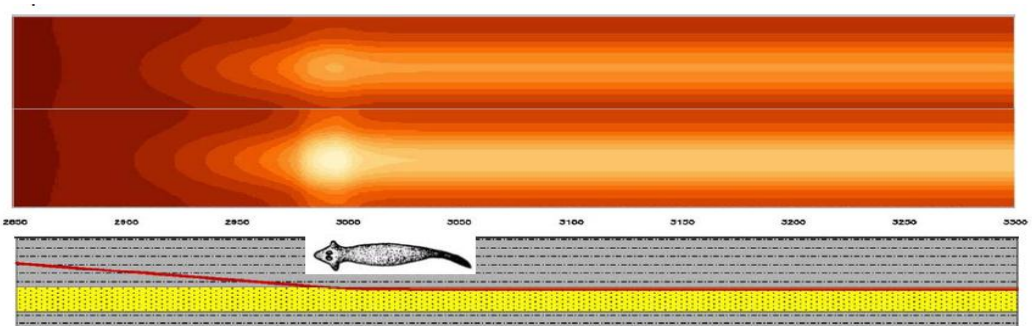

Figure 3.12. Motif 1 – Landing the well in the upper part of the reservoir and drilling parallel to the roof of the reservoir (Bacon et al., 2009).

Figure 3.12 shows a well being landed into the upper section of the reservoir and then drilling parallel to the roof with the corresponding resistivity images. As the well intersects the boundary, a bright spot is observed and as the well is drilled further parallel to the roof, lighter shade in the central track indicate a higher resistivity in the low side of the hole i.e the reservoir is below the wellbore. Darker shades in the upper and lower tracks indicate low resistivity above the wellbore. This motif is known as the flatworm

motif. The upper and the lower image are the two submotifs within it where the upper is for 10:1 resistivity contrast and lower for 100:1.

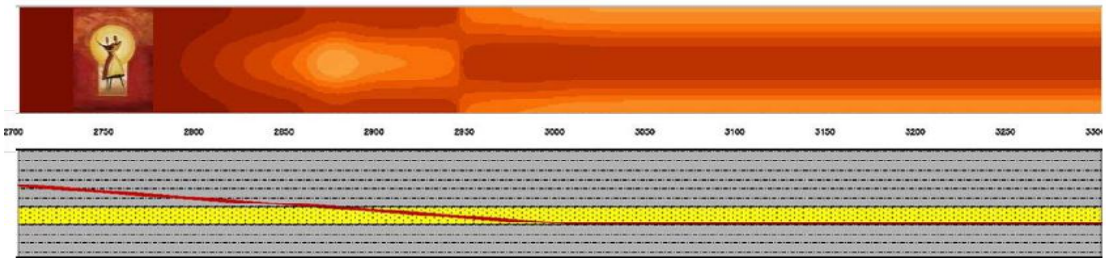

Figure 3.13. Motif 2 – Landing the well in the lower part of the reservoir and drilling parallel to the base of the reservoir (Bacon et al., 2009).

Figure 3.13 shows the second motif within the theme “Landing the well”. As the well intersects the upper boundary, a bright spot is observed. As the well traverses through the reservoir and electrical midpoint develops after which the color scheme is reversed and as the well is drilled parallel to the base of the reservoir, the lighter tones on the top and bottom track of the image indicate that the reservoir is above the wellbore. This motif is called the keyhole motif.

Similarly, many other themes and motifs describing a particular scenario have been identified and given names. If used during well placement they can help us make quick and efficient decisions in real time

3.4. APPLICATIONS AND THE LIMITATIONS OF THE PROPAGATION RESISTIVITY

- All the features discussed above when used in combinations provide a reliable source for identifying the reservoir boundaries well before intersection with the well bore and hence facilitate proactive geo-steering and but there must be sufficient resistivity contrast between the reservoir and the surrounding layers which is generally true for the reservoir shale sequence or for the reservoir water contact interface (Seifert et al., 2011).
- The main application of the propagation resistivity is in non-conductive muds such as fresh water muds or oil based mud as they cannot be used with conductive muds.

- Although the geosignal is an exponential function of the distance to boundary it is unable to detect the exact instance at which the well bore crosses the boundary in case there is an unexpected exit. Hence, the shallow measurement image like gamma image or density image must always be run in conjunction with the directional resistivity to calculate the relative dip immediately after an exit.
- In case of gradational resistive boundaries the inversion of the geosignals to determine distance to the boundary is not possible because the geosignal may not be reliable at boundaries which lack good contrast.
- Resistivity measurements are very useful in the carbonates where other measurements such as gamma ray are inconclusive.
- In cases where the reservoir is surrounded by very high resistivity layers such as zero porosity anhydrites the shallow laterolog measurements are preferred over the deep propagation measurements. The attenuation resistivity does not respond to very high resitivities and even the phase measurements are not reliable. The range and sensitivity of the geosignals are reduced significantly when approaching a high resistivity formation and also the polarization is reversed as it always points from high to low resistivity. Further, if the reservoir is very thin, the deep resistivity measurements would always be affected by the shoulder beds creating ambiguities in the resistivity curves and images.

3.5. LATEROLOG RESISTIVITY

Laterolog tools employ an emitting electrode to push a direct current through the borehole to the formation and the return current is sensed by a return electrode on the tool. The laterolog tools form a DC circuit where a current from a source passes through a resistor, which in our case is the formation, and the resistance is measured is given by the voltage drop between the source and the return electrode according to the Ohm's law, eq. xi. Thus the laterolog resistivity measurements require a complete circuit and can be used in the conductive borehole environments only (Griffiths, 2009).

$$r = V/I \tag{3}$$

Where r is the resistance measured by the tool in ohm, V is the Voltage drop between the source and return electrode in Volts, I is the current flowing from the source to the return electrode in ampere.

The resistance thus measured depends upon the volume of measurement whereas the resistivity is the property of the material. However, the two are related by a constant k factor which is generally the length between the measurement electrodes divided by the area that the current passes through. The k factor is constant for a given source – return electrode configuration. Eq. (4) mathematically represents the above relationship.

$$r = R.\frac{L}{A} = K.R \tag{4}$$

Where R is the formation resistivity in ohm.m, L is the characteristic measurement length in m, A is the area through which measurement current passes in m^2.

Figure 3.14 shows a typical laterolog tool, Geovision Schlumberger.

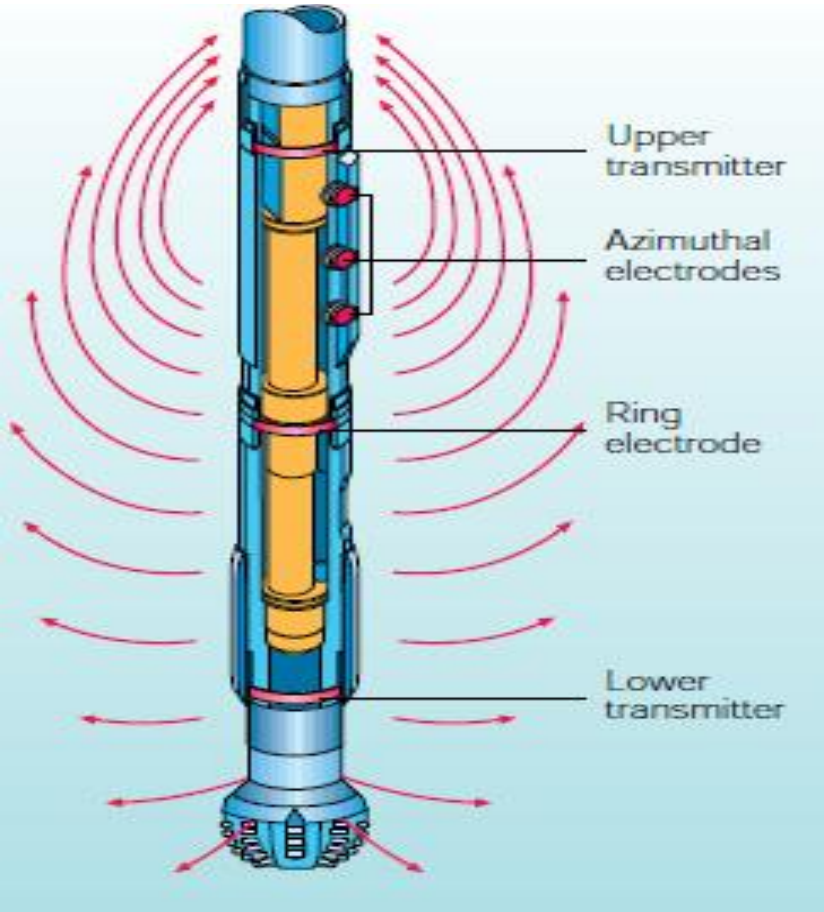

Figure 3.14. Geovision LWD, Schlumberger (Bonner et al., 2000)

Figure 3.14 shows that the tool employs toroidal transmitters and electrodes mounted on a steel collar. The Geovision tool provides four focused resistivity measurements via the three button electrodes and a ring electrode as can be seen in the figure. The three button electrodes provide multispaced azimuthal measurement, as the button electrodes at any point of time are oriented to scan a particular section of the borehole rather than the whole circumference, with the depths of investigation of about 1 inch, 3 inch and 5 inch respectively from top to bottom. The fourth focused resistivity measurement, the ring resistivity, is non-azimuthal in nature and averages the resistivity circumferentially around the borehole. However, it has a larger depth of investigation, up to 9 inches, as compared to the button electrodes. Two toroidal transmitters, shown as upper and lower in the figure, create current flows around the tool. Using two transmitters creates a balanced and borehole compensated resistivity measurement. The fifth resistivity measurement provided by the tool is the resistivity at the bit. The lower transmitter transmits an alternating current that induces a voltage in the collar below. The current flows down through the drill collar to the bit out into the formation immediately in contact with the bit. For this measurement the bit is used as a measurement electrode. Apart from the resistivity measurements the Geovision tool provides an azimuthal gamma ray measurement as well.

Laterolog resistivity has been successfully used in the field for well placement. The resistivity at the bit measurement measures the resistivity right at the bit, thus has the ability to see the significant resistivity changes in formation but again the formation has to be penetrated to observe the changes. However, RAB has one important application which is the identification of the marker beds. This application is known as geostopping and allows drilling to stop precisely at the casing or coring points (Bonner et al). Figure 3.15 shows one such example. It can be seen the RAB values are almost steady while drilling down until a point just where the top of the reservoir is encountered and the RAB increases. RAB is the first measurement to see reservoir top and just penetrated about 9 inch into the reservoir when the reservoir or the marker bed for coring was identified.

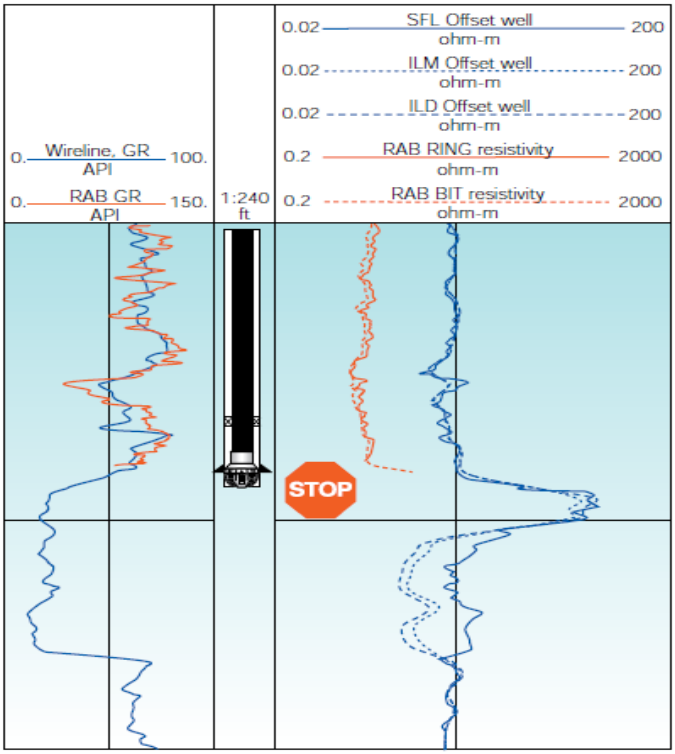

Figure 3.15. An example of Geovision RAB used for geostopping (Bonner et al, 2000)

As mentioned in the last section the three button measurements provide azimuthal resistivity at multiple depths of investigation, so we have the ability to look up or down the borehole while drilling but since the DOI is fairly shallow, the well placement based on laterolog measurements is largely reactive. The laterolog measurements also lack the polarization horn which is an important feature for the bed boundary detection and DTB, as discussed earlier. In spite of these limitations the laterolog resistivity is still an important tool for well placement owing to its higher resolution. The laterolog measurements like Geovision being more tightly focused can resolve the data into 56 azimuthal quadrants.

The propagation tools help us identify the boundaries with their large DOI but they do not tell us much about the reservoir we are presently in, especially in case of thin layers, as it may be responding to more than one layer. The laterolog tools on the other hand provide information about the current zone and their higher resolution images helps us identify the features like depositional facies, fractures and minor faults which may be

beyond the resolution of the propagation tools. Practically no reservoir is homogenous; there might be a few sedimentary variations within the reservoir itself. Figure 3.16 shows the depositional facies mapped by the real time laterolog images within a limestone reservoir traversed by the wellbore.

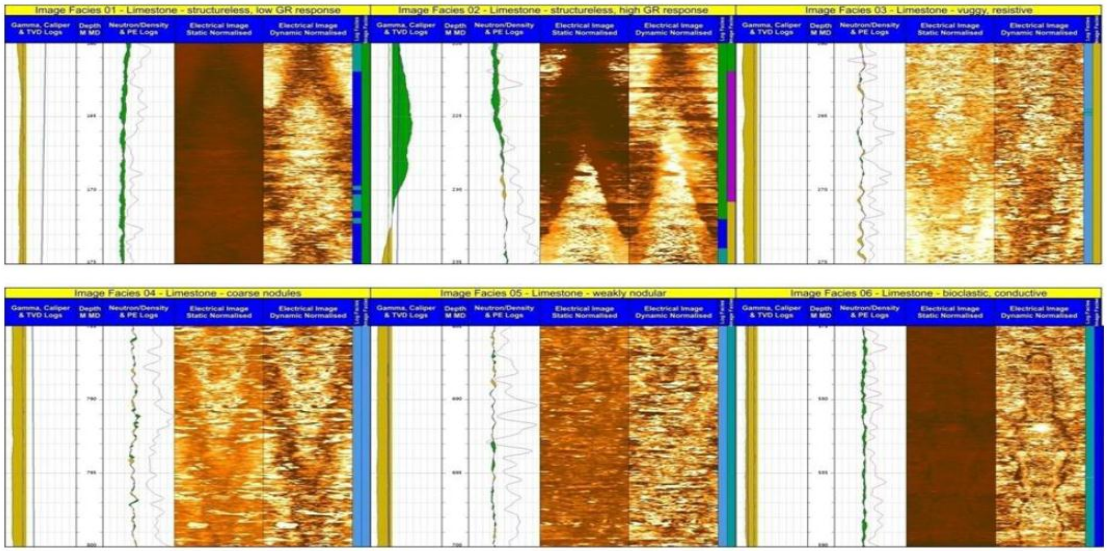

Figure 3.16. Real time laterolog resistivity images showing depositional facies within a reservoir (Bacon et al., 2010)

The purpose of geosteering is not just to stay in the reservoir but to place the well in the sweet spot of the reservoir i.e. the zone within the reservoir which has the maximum production potential. In the figure above, not only the bedding of the limestone has been delineated clearly but also the fabric and the sedimentology i.e. vuggy, coarser, nodular are successfully identified. No preference or target has been set here but if certain cutoffs are applied, we can identify the ideal depositional facies and can steer the bit following the targeted sedimentary facies using the high resolution images. This process is known as sedimentary steering or facies steering. As discussed earlier, the deep propagation tools work the best when there is a good resistivity contrast and when the reservoir bed is more resistive than the shoulder beds. So the propagation measurements may not very reliable in the reservoirs which lack a good resistivity contrast with the

shoulder beds or in carbonates surrounded by anhydrite or other denser material, which is more resistive than the reservoir, but to still steer effectively sedimentary steering needs to be employed.

Another important feature of the high resolution images is the identification of the natural fractures. In the reservoirs with low permeability and porosity, as in unconventional reserves, a well is considered successfully placed when it is in the zone of the formation most conductive to the hydraulic stimulation techniques i.e. it should intersect the natural fractures. One such example is shown in Figure 3.17.

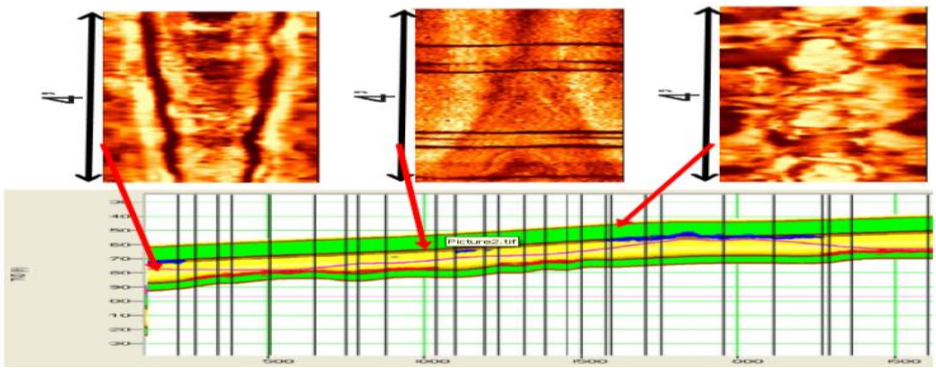

Figure 3.17. Real time laterolog resistivity images used to identify fractures within an unconventional shale reservoir (Market et al., 2010)

Figure 3.17 shows a well path traversing an unconventional reservoir. The well trajectory here is governed by certain cut off values for the gamma ray and resistivity within the reservoir. This criterion can be further refined using laterolog real time images to include natural fractures. The three images on the top of the figure represent three different positions in the reservoir – Lower (left), Middle (center), Top (right). The center image for the middle portion of the reservoir shows conductive fractures which are not evident on the images from the top or bottom of the reservoir. Thus, the real time images can show additional features and thus aid in geo-steering within the sweet spot of the reservoir which in this case is the middle lithofacies which is more prone to fractures.

Besides the real time applications of the laterolog tools discussed above, the complete set of high resolution laterolog data, which cannot be transmitted in real time

due to bandwidth limitations, can be downloaded from the memory of the tool later and is more useful for formation evaluation as it is subject to less distortion, polarization horns (Hu et al., 2006), and has a resolution which is even better than the real time features where the data compression techniques are used for real time transmission and a bit of resolution is lost as a compromise.

If the laterolog measurements are used in conjunction with the deeper propagation measurements, the long range bed boundary effect in propagation resistivity logs can be used to determine the relative position of the well bore within the reservoir and the shallow but high resolution laterolog measurements can target the sweet spot within the reservoir. Thus, it can be said that if used together the two measurements complement each other and yield a more precise well placement.

Apart from the features mentioned above the laterolog images follow the same pattern for the bed dips, the smiling and frowning pattern as discussed earlier, but prove to be more reliable source of calculating dips as they are more tightly focused compared to the propagation logs which are more prone to distortion. The laterolog measurements being shallow measurements can be used to pick dips by sinusoid fitting on the image. Another method to calculate dip for tools capable of up and down measurements is by measuring the offset between top and bottom measurements which is shown in Figure 3.18 as ΔD (Muddhi et al., 2005).

For our calculations we will use effective borehole diameter because the depth of investigation of the tool is not the same as the borehole diameter. The effective wellbore diameter is given by:

$$D_E = D_{BH} + 2\,X\,DOI \tag{5}$$

The angle of intersection of the borehole with formation is given by

$$\theta = \arctan\left(\frac{D_E}{\Delta D}\right) \tag{6}$$

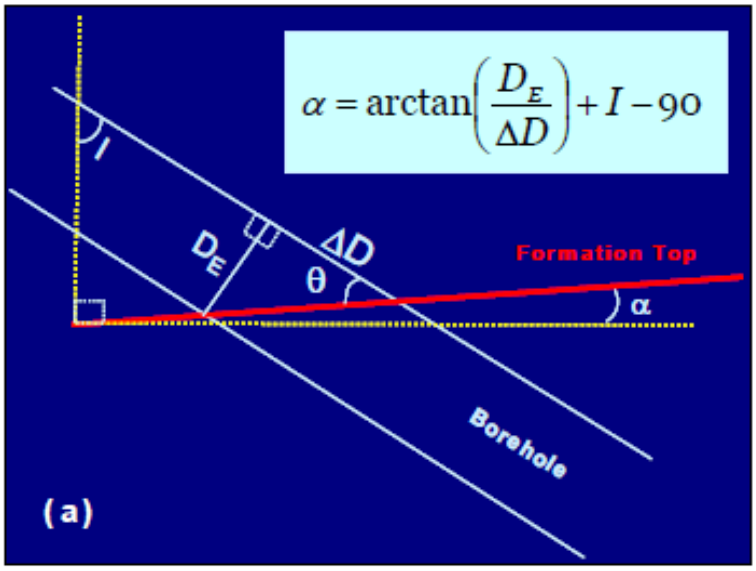

Figure 3.18. A well bore with an inclination I drilling through a bed dipping opposite to the borehole (Muddhi et al., 2006)

The apparent dip for the case shown in Figure 3.18 can be calculated by the following equation.

$$\alpha = \theta + I - 90 \tag{7}$$

If the bed is dipping in the same direction as the borehole as shown in Figure 3.19, we can use the equations xiii and xiv to give the apparent dip which in this case will be

$$\alpha = 90 - I - \theta \tag{13}$$

Where D_E is the effective wellbore diameter in inches, D_{BH} is the diameter of the borehole in inches, DOI is the depth of investigation of the tool in inches, θ is the angle of intersection of the borehole with formation in degrees, ΔD is the offset between the top and bottom measurements in inches, I is the inclination of the borehole in degrees, α is the apparent dip of the formation in degrees.

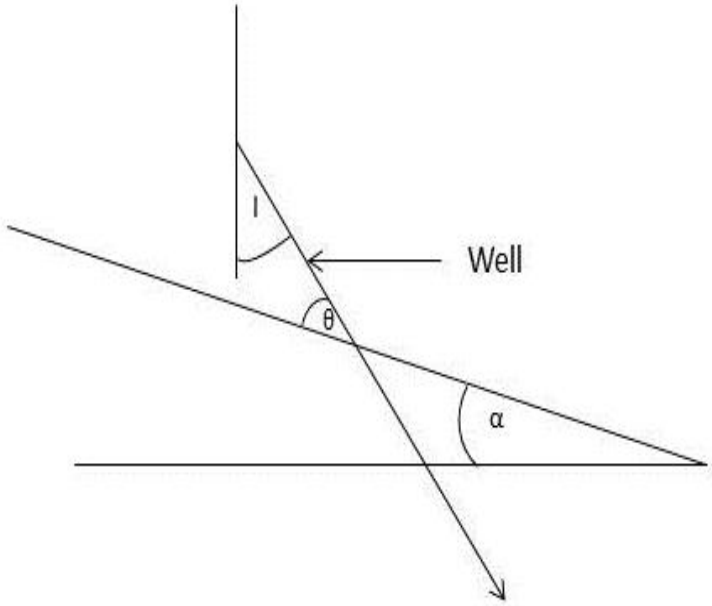

Figure 3.19. Wellbore drilling through a bed dipping in the same direction as the borehole

3.6. GAMMA RAY MEASUREMENTS

The GR measurements count the number of gamma rays emitted from the disintegration of three commonly occurring radioactive isotopes found in earth formations, Uranium (U), Potassium (K) and Thorium (Th). The gamma ray is generally used to measure the clay content of a formation because of higher concentration of these radioactive elements in the clay. The gamma ray measurements are relatively unaffected by the formation fluids such as water, oil and gas and can be used in conductive and as well as non-conductive drilling fluid boreholes, this property of the GR makes it a strong correlation tool and thus an important tool for well placement as correlation is a very important aspect of well placement as will be discussed later. Sometimes GR is used in the well placement LWD suite as a correlation measurement only. The gamma ray measurements are fairly shallow and the images are of low resolution but still can be used to pick the dips by using the same method as discussed in the last section.

The LWD gamma ray tools employ NaI scintillation detectors to measure the gamma ray count and are capable of azimuthal measurements. Figure 3.20 shows a typical azimuthal gamma at bit tool.

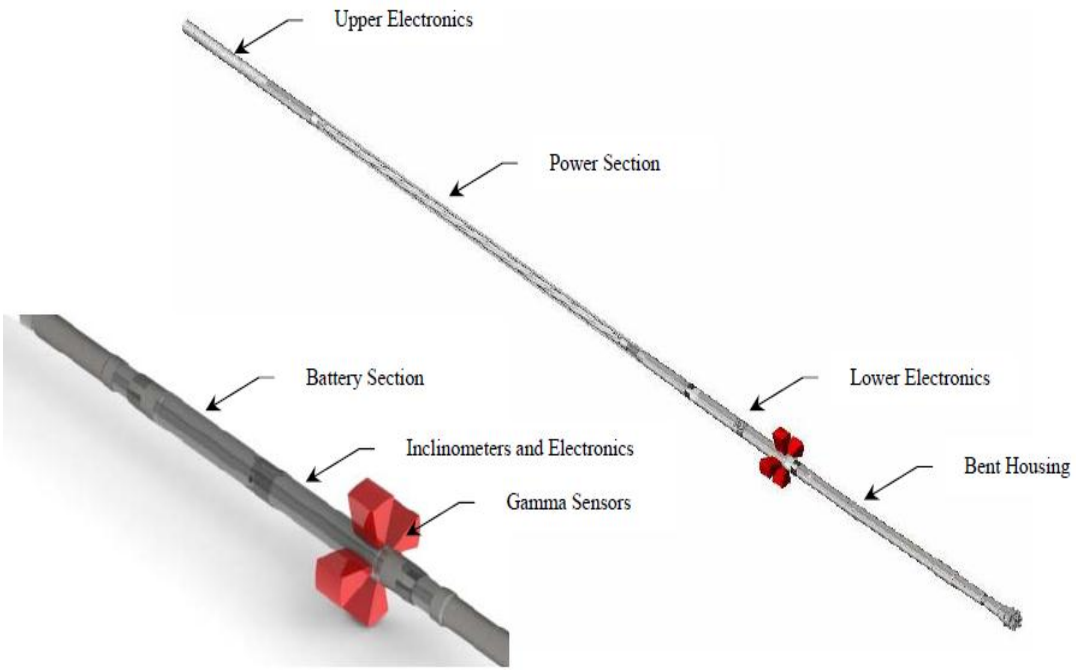

Figure 3.20**.** Configuration of gamma at bit tool (Pitcher et al., 2009)

The scintillation detectors are mounted 90° radially around the circumference of the tool. When rotating, the tool bins the azimuthal measurements into 16 quadrants and when sliding it provides 4 focused measurements around the borehole. The above shown configuration can be run only with the mud motors because the sensors for gamma at bit have to be 2m or 3m behind the bit, which is not possible when drilling with RSS as because the RSS has to be run immediately behind the bit. The gamma at bit is however an important tool when geosteering with mud motors because a portion of the well is drilled by sliding, when the string does not rotate, and as we have discussed earlier that the azimuthal measurements need rotation to bin the data into individual quadrants of a 360° circumference, other azimuthal tools are unable to provide information while sliding but the GAB tool still provides four directional measurements around the borehole owing to the sensors configuration. Figure 3.21 compares the density and GAB images acquired in real time while geosteering a well with mud motor. The white gaps in the density images represent the sections of the wellbore which were slided whereas The GAB images are consistent across the whole traversed path.

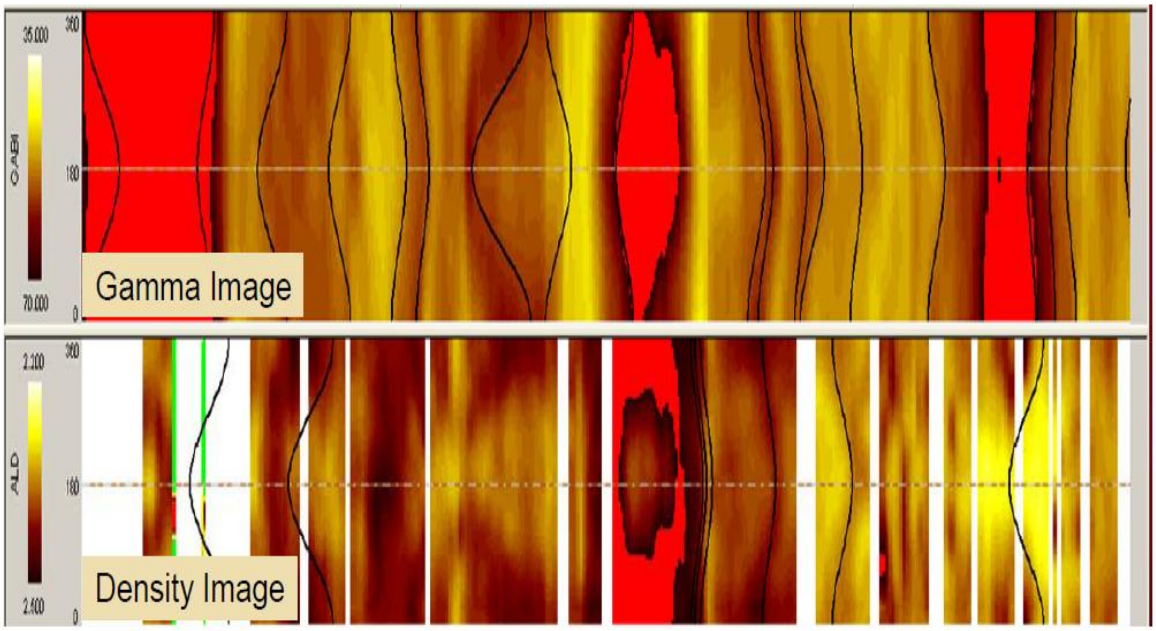

Figure 3.21. Comparison of the density and gamma images acquired across a well section (Pitcher et al., 2009)

Apart from being a strong correlation tool the gamma measurements have been successfully used for well placement to stay in the reservoir's sweet spot. The candidate reservoirs for this application are the ones with good gamma contrast or where the formations surrounding the reservoir have a characteristic value. The offset logs from a vertical well are used to set the upper and lower GR markers. The upper GR marker is used to identify the overlying layer and the lower is used to identify the underlying layer. The markers provide us a GR operating window and can also be used to landing the well into the reservoir. Figure 3.22 shows a well placed in such fashion. The top section is the real time GAB images where the scale is set between the upper and lower GR markers. The aim was to place the well between the upper and lower GR markers or within the scale of the top section. The red gaps in the image logs indicate that the data has gone off scale and an exit from the reservoir has been made, this can be confirmed by the bottom section of the figure which shows the traversed well path. Whenever an exit is seen on the logs, the up and down GR readings in the sixth section can be used to identify the direction of exit and the depth offset between the up and down measurements can be used to calculate apparent dip to steer the well back into the reservoir.

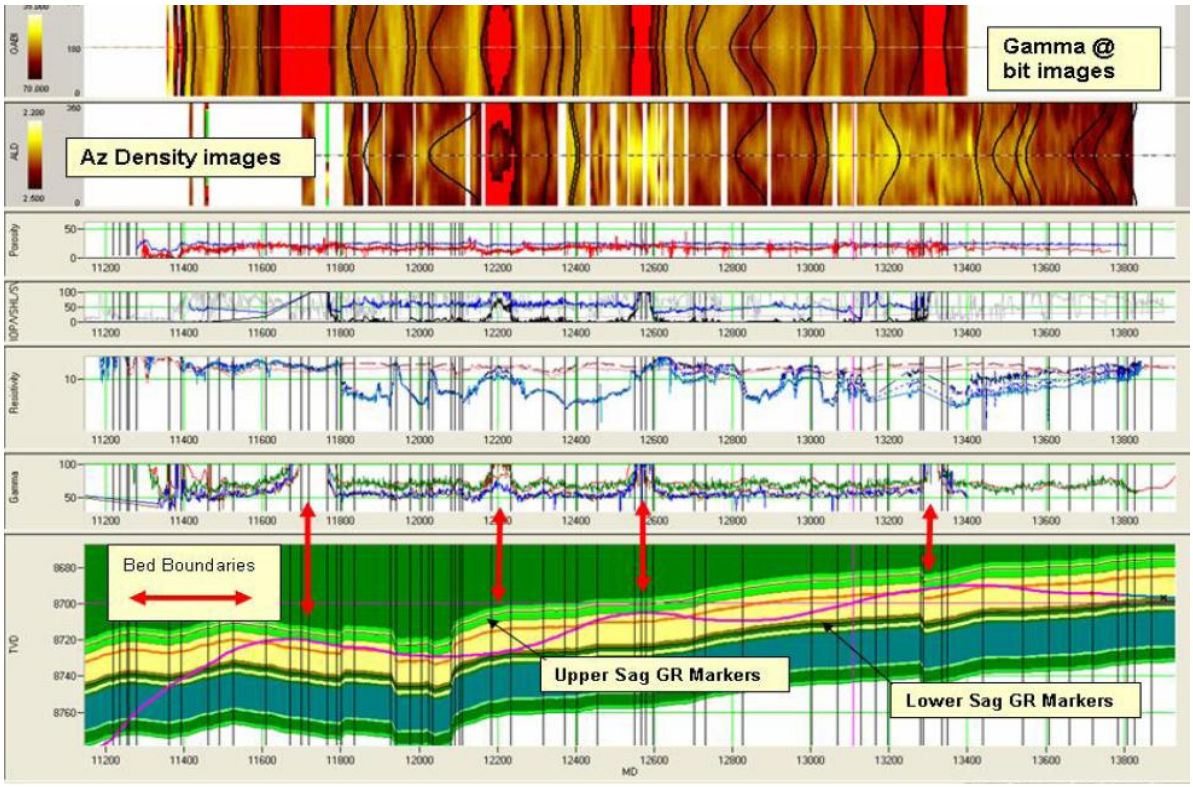

Figure 3.22**.** Example well log showing the traversed well path and the corresponding log data (Pitcher et al., 2009)

Another important application of the GR logs is the well placement in unconventional shale reservoirs where the sweet spot can be defined by following the kerogen in the reservoir (Market et al., 2010). The presence of kerogen, when it is 4% to 10%, complicates the porosity logs because it contains some gas filled porosity. However, the presence of kerogen can be accounted as it generally shows up as very high gamma ray readings on the gamma ray logs because of the uranium associated with it. Spectral gamma ray can be employed in real time to give the individual radioactive strength of uranium and well can be maintained in the sweet spot following kerogen.GR logs, however, have limited applications in the carbonates because of the inconclusive GR response in the carbonates (Muddhi et al., 2005).

3.7. DENSITY, PHOTOELECTRIC EFFECT AND NEUTRON

The density tools detect the bulk density of the formation by employing a radioactive source which emits gamma rays that interact with the electrons of the atom in

the formation. This interaction creates a scattering of the gamma ray energies where they lose some energy to the electrons. This process is called Compton scattering. The gamma rays with diminished energies are counted at the detector. The number of Compton scattering is directly related to the electron density which is converted to bulk density using a correlation between the number of electrons and atomic mass (Griffiths, 2009).

The density measurements are very shallow measurements with a DOI of approximately 50 to 60 cm, because the gamma rays are relatively easily stopped, and are capable of azimuthal measurements and imaging. The density images, 16 azimuthal sectors, do not have a high resolution as the resistivity images and are largely affected by the tool standoff and therefore may be misleading when the borehole rugosity is high. Figure 3.23 shows an example where the density measurements may have led to an inaccurate placement had it been the only information available.

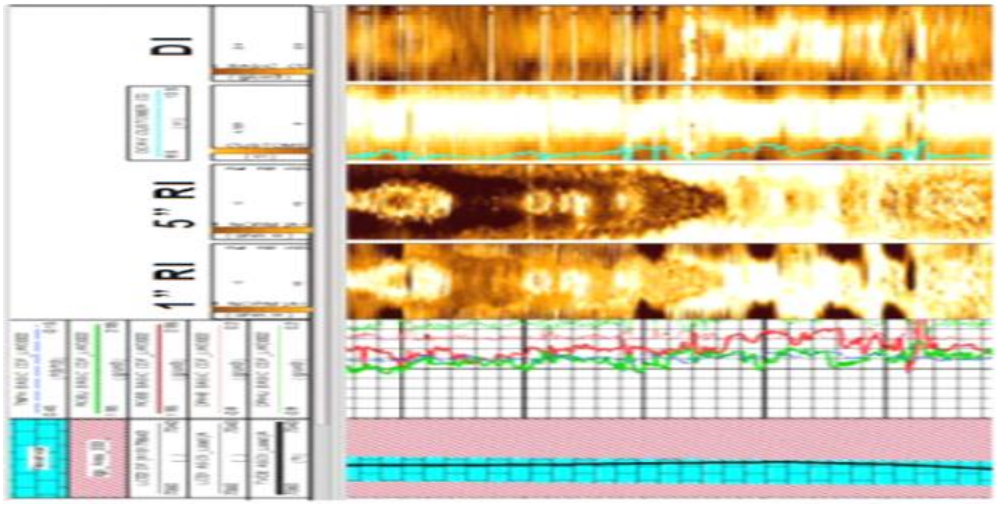

Figure 3.23. Comparison of the LWD density and resistivity data when exiting the reservoir from the top (Mudhhi et al., 2009)

The bottom section of the log shows the well (black line) traversing through a reservoir (blue portion) which is sandwiched between dense anhydrite layers. A point in this section shows the well path approaching the anhydrite from the top but the azimuthal density measurements in the section above indicate that the anhydrite is being approached

from the bottom as the bottom measurement reads higher density than the top density measurement but the 5" resistivity image at this point shows lighter density shades on the sides than the center of the image indicating that a high resistivity bed is being approached from the top. With more confidence in RI the well was steered down, thus maintaining it within the reservoir. The misleading information provided by the density can be attributed to the borehole rugosity. Thus, the azimuthal sensitivity is very important for the density measurements because the accuracy of the density data depends on azimuthally segregating the measurements affected by the large standoffs from the ones affected by the least standoffs. For a horizontal well bore, the low side density measurement generally has the least standoff and is taken to be accurate representation of the formation being logged (Jeniffer et al., 2009).

The density measurements also provide photoelectric measurement which can be used to determine lithology. The photoelectric factor is a measurement of the GR capture cross section of a formation. When low energy gamma rays interact with the electron in the formation, the gamma rays can be absorbed in a process known as photoelectric capture. The probability of a gamma ray being absorbed depends on the capture cross section of the formation which is measured in barns. 1 barn = 10^{-24} cm^{-2}. The photoelectric can be empirically estimated by (Glover, 2000):

$$P_e = (z/10)^{3.6} \tag{14}$$

The PEF can be converted to a volumetric PEF, U, by multiplying it with the electron density of the formation.

$$U = P_e \,.\, \rho_e \tag{15}$$

Where P_e is the photoelectric absorption index in barns/electron, Z is the atomic number, U is the volumetric photoelectric index in electrons/cc, ρ_e is the electron density of the formation in electrons/cc.

Table 3.1 shows the data distribution for common minerals and fluids.

Table 3.1. Photoelectric data distribution for common minerals and fluids (Glover, 2000).

Mineral	Formula	Molecular Weight	P_e	Z (equiv.)	ρ_b	ρ_e	ρ_a	U
Anhydrite	$CaSO_4$	136.15	5.055	15.69	2.960	2.957	2.977	14.93
Barite	$BaSO_4$	233.37	266.82	47.2	4.500	4.01		1070
Biotite			6.30				3.34	21.03
Calcite	$CaCO_3$	100.09	5.084	15.71	2.710	2.708	2.710	13.77
Dolomite	$CaCO_3.MgCO_3$	184.42	3.142	3.74	2.870	2.864	2.877	9.00
K Feldspar			2.86				2.62	7.51
Glauconite			5.32				3.95	21.00
Gypsum	$CaSO_4.2H_2O$	172.18	3.420	14.07	2.320	2.372	2.350	9.37
Halite	NaCl	58.45	4.169	15.30	2.165	2.074	2.031	9.68
Haematite	Fe_2O_3	159.70	21.48	23.45	5.240	4.987		107
Limonite			13.00				3.59	46.67
Magnetite	$MgCO_3$	231.55	22.24	23.65	5.180	4.922		113
Muscovite			2.40				3.29	7.90
Pyrite	FeS_2	119.98	16.97	21.96	5.000	4.834		82.1
Quartz	SiO_2	60.09	1.806	11.78	2.654	2.650	2.648	4.79
Siderite	$FeCO_3$	115.86	1.69	21.09	3.940		3.89	55.9
Sylvite	KCl	74.6	8.510	18.13	1.984	1.916	1.862	15.83
Zircon	$ZrSiO_4$	183.31	69.10	32.45	4.560	4.279		311
Shale	-		3.42	14.07	2.650	2.645	2.642	
Shaly Sand	-		2.70				2.41	6.52
Anthracite	-		0.161	6.02	1.700	1.749	1.683	
Bituminous Coal	-		0.180	6.21	1.400	1.468	1.383	
Pure Water	H_2O	18.02	0.358	7.52	1.000	1.110	1.000	0.398
Salt Water	120,000ppm NaCl		0.807	9.42	1.086	1.185	1.080	0.850
Oil	$(CH_2)_n$		0.119	5.53	0.850	0.948	0.826	$0.136\times\rho_{oil}$
Methane	CH_4	16.04	0.095	5.21	0.250		0.15	$0.119\times\rho_{gas}$

The photoelectric factor depends on the mean atomic number of the formation, eq. xvi, thus higher P_e indicates heavier minerals and lower P_e indicate light minerals. The above distribution can be used to delineate lithology. Since the gamma rays can be easily stopped and the gamma rays used to measure PEF are low energy waves, the PEF is the shallowest of all LWD measurements and is highly sensitive to borehole rugosity and mud conditions. The PEF measurements cannot be made in the boreholes with heavy mud because barite has a very high absorption index, 267 b/electrons as can be seen in Table 3.1, barite is such an efficient absorber of the gamma rays that it reduces the level of the gamma rays to too low to be measured accurately. However, if the conditions allow reliable PEF measurements, we can monitor the lithology changes in real time. The knowledge of lithology is required so that appropriate matrix density is used in

calculating formation porosity from the density measurements. Monitoring lithology in real time can help us stay in the reservoir and identify faults, a sudden change in lithology while maintaining an almost horizontal profile may indicate a fault (Efnik et al., 1999).

The neutron measurements are made by emitting neutrons from a radioactive source at high energies which lose energy as they interact with the elements in the formation. The tool's neutron detector will detect some of these neutrons, count rate, after they lose energy from the elastic collisions with nuclei in the formation. The high energy neutrons are moderated or slowed down mainly on collision with the hydrogen atom as it has the same mass as the neutron. The count rate at the neutron detector is inversely proportional to the amount of hydrogen or the hydrogen index of the formation which is given by

$$HI = \frac{H\ per\ cm^3 in\ the formation}{H\ per\ cm^3\ in\ water\ at\ 75\deg F} \tag{16}$$

When the HI is high, the count rate at the detector is low and the porosity is high. For low HI, the count rate is high and the porosity is low. Gas has a very low HI, oil and water though have almost similar HI, with the HI for oil being slightly less than HI for that of water (Griffiths, 2009). The density and neutron are generally used together in an overlay plot which is usually presented on a lithology compatible scale. For example, if we are using a limestone compatible scale then both the measurements should overlie in the water filled limestone of any porosity. Any separation of the curves indicates that either the fluid in the pore space is not fresh water or the lithology is not what is assumed for the scale. Figure 3.24 shows a typical neutron – density overlay plot on a limestone compatible scale. It can be seen that the two curves overlie for the freshwater filled limestone. When the freshwater is replaced by oil, the density response decreases because the density of oil is less than that of water and the neutron response also decreases as the HI of oil is slightly less than that of water. This separation is known as the hydrocarbon separation and is not very big for the presence of oil because of slight difference in the HI of the oil and water. In the next section where the limestone is filled with gas it can be seen that the separation is very big, gas separation. The much lower HI of gas as compared to the liquids reduces the neutron response significantly and may lead to

underestimation of the porosity. Other cases where the neutron response may be misleading are the presence of chlorine or shale, porosity is overestimated in both the cases. Section 6 in the figure shows the response to NaCl saturated water filled limestone, the neutron response here is increased because Chlorine is a good absorber of the neutrons and thus reduces the neutron count at the detectors. For this reason, the application of neutron logs is very limited when chlorine is present in the mud or as a mud filtrate. Section 7 shows the response to shale, shales contain clay which have a significant amount of water bound molecules on their surface. This increases the HI which in turn increases the neutron response.

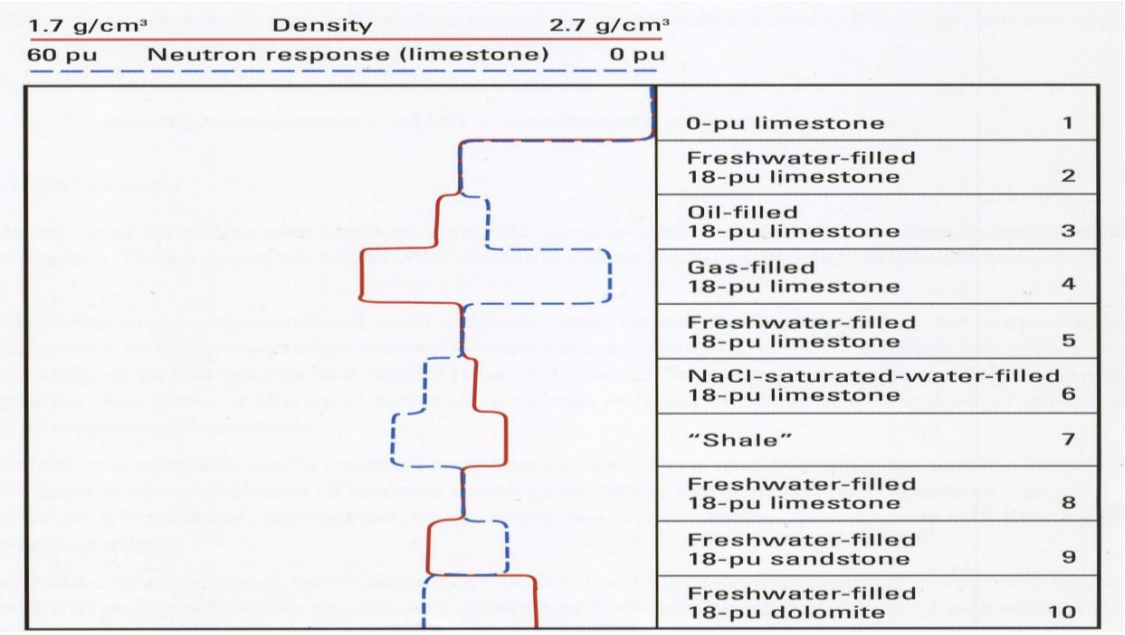

Figure 3.24. Neutron density overlay plot (Griffiths, 2009).

The above mentioned separations may complicate the formation evaluation but are generally advantageous as far as well placement is concerned. When steering in a gas reservoir the gas separation observed, a big separation when both density and neutron read low, gives us a qualitative idea of the presence of gas and thus may guide us through the sweet spot within the reservoir. As discussed above a separation with both density and neutron reading high may be attributed to shale, such a separation may while steering

will indicate an exit from the reservoir shale sequence or interbedded shales within the reservoir or zones of high clay content within the reservoir. As the density measurements are azimuthal, these separations can help guide the well path. The density and neutron LWD measurements find an important application in gas bearing carbonates as the gamma ray generally remains flat for such reservoirs, as mentioned in the last section, these measurements, complemented by deeper measurements to stay in the reservoir, can be utilized to steer within the sweet spot (Efnik et al., 1999; Akinsanmi et al., 2000). Figure 3.25 shows the ADN response for a well path traversing a gas bearing limestone.

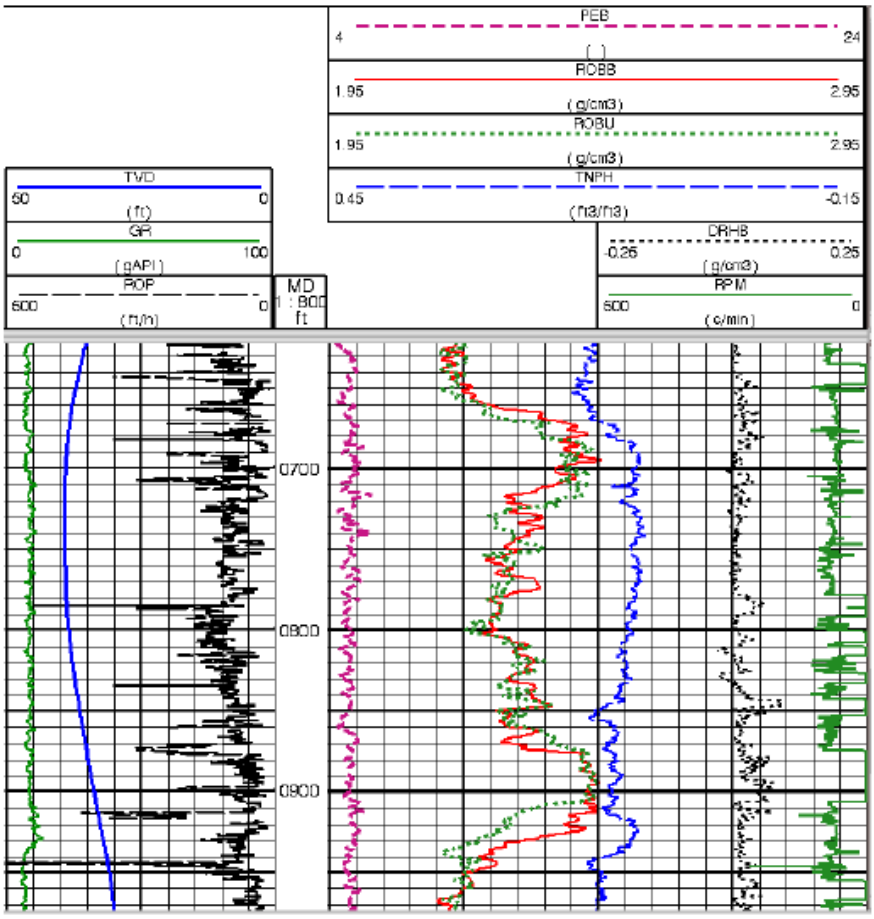

Figure 3.25. Azimuthal density neutron (ADN) response while steering through a gas filled limestone (Efnik et al., 1999).

The big separation in figure 3.25, with both density and neutron reading low, as can be seen from the top to about 675 ft indicate that the well is traversing through the sweet spot. At 675 ft the separation becomes narrow indicating the presence of a dense layer but the bottom density measurement saw the change first which means that the layer was being approached from the top, the well path was then steered up to return to the sweet spot. The big gas separation which appears again at about 720 ft indicates that the well returned to the sweet spot. In the bottom portion of the log, the separation again becomes narrow but this time the upper density measurement saw the change first, so the well was steered down to return it to the sweet spot.

3.8. FORMATION PRESSURE WHILE DRILLING

Formation pressure while drilling tools are used to measure the fluid pressure in the pores of the formation while drilling the wellbore. Figure 3.26 shows a typical formation pressure while drilling tool schematics, Geotap (Halliburton).

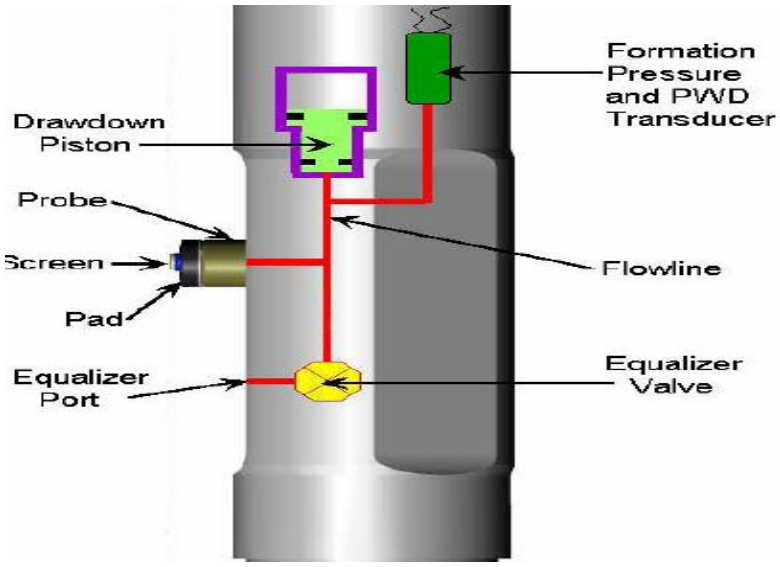

Figure 3.26. Geotap formation pressure while drilling tool, Halliburton (Neumann et al., 2007).

The FPWD has a similar tool design and working principle as their wireline counterparts. To make a pressure measurement the drilling has to be paused for a while

and the tool is positioned against the formation to be tested. A downlink command is sent to the tool and the probe shown in the above figure, already in extended position, extends out of the collar and presses against the borehole wall. At this point, a metal snorkel extends out from the center of the probe penetrating the mud cake and into the formation while the donut shaped rubber pad pressing against the borehole provides a hydraulic seal. The pressure on the formation is reduced in the process which allows the formation fluid to flow into the tool equipped with pressure gauges. The Geotap has two pressure gauges – strain gauge and quartz gauge, not shown in the figure. The test sequence can be seen in the Figure 3.27. Initially the pressure gauge reads the pressure in the borehole followed by a small increase in pressure which is observed when the tool sets as the snorkel compresses the mud cake. The pressure starts to drop at this point and a small pressure anomaly occurs just before the pressure drops below the formation pressure, this is the point at which the formation fluids flow into the flowline until the pretest piston stops. The pressure continues to build until it reaches the formation pressure. A second drawdown and buildup is then performed to improve the data quality. The testing is generally done with the pumps off and once the sequence is completed, pumps can be turned on to transmit the data to the surface.

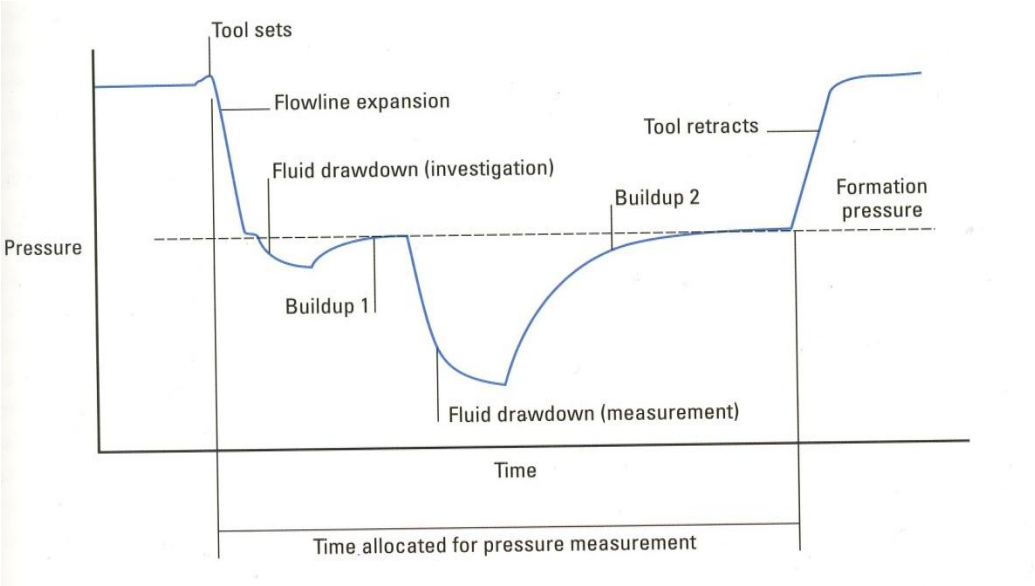

Figure 3.27. A typical test sequence for a FPWD tool (Griffiths, 2009).

One of the major applications of the FPWD tool is the identification of the fluid contacts. Figure 3.28 the pressure gradient for a well traversing a sand section. The gradients for fluid of a particular density always fall on the same line and as can be seen in the figure the gradient is pretty much uniform. The density of the fluid is calculated by:

$$P = 0.052 \,.\, \rho . TVD \tag{17}$$

Where P is the hydrostatic pressure in psi, ρ is the density of the fluid in lb/gal, TVD is the True vertical depth in ft.

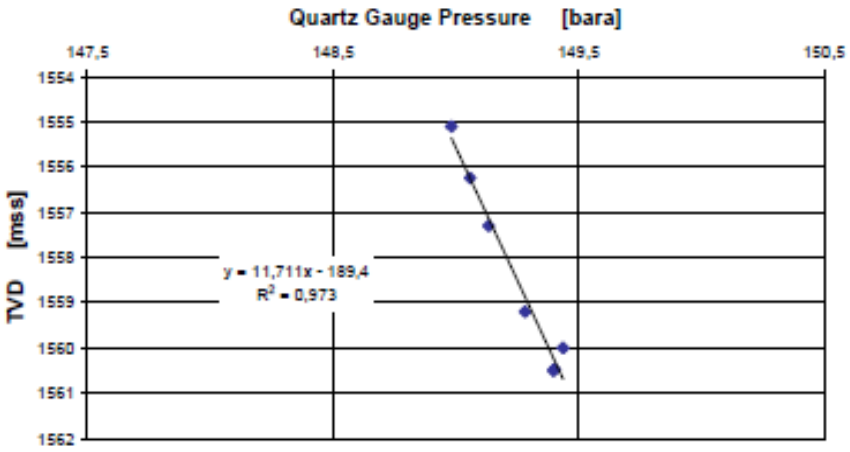

Figure 3.28. Pressure gradient achieved in real time while traversing through a sand section of a field (Meister et al., 2004).

The density of the fluid calculated based on the gradient above is 0.85 g/cc which fits the density of the oil in the reservoir being traversed confirming the well path being in the sweet spot of the reservoir. Figure 3.29 shows another real time gradient achieved in real time for a section of the well in the same field. The gradient with the red points shows the presence of gas as the density calculated here is 0.39 g/cc but at some point between 1575 m and 1600 m TVD, the gradient becomes very steep and the fluid density calculated for these points is about 1 g/cc indicating the presence of water. The interface

at which the gradient becomes steep is the gas water contact. Thus the fluid contacts when identified in real time could help guide the well path accordingly, in this case upwards, to place the well back in the reservoir.

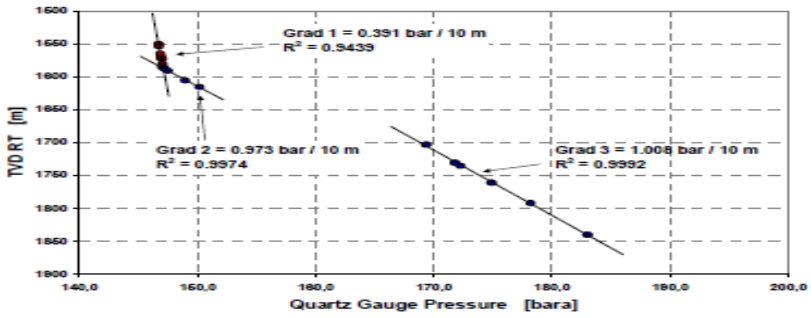

Figure 3.29. Pressure gradient achieved in real time while traversing through a gas bearing sand section of a field (Meister et al., 2004).

Another important application of the FPWD tools is the determination of the fluid mobility. The LWD tools that we discussed earlier define the sweet spot based on the hydrocarbon content and the effective porosity within the reservoir. However, for some reservoirs a few specific zones may have a good hydrocarbon content and effective porosity but may lack good permeability. To ensure an efficient well placement in this kind of reservoirs we define the sweet spot based on the fluid mobility and this is where the FPWD and NMR come into play to facilitate what is called mobility steering. The mobility of the fluid can be defined as a ratio of the formation permeability, the ability of the formation to transmit the fluid, divided by the fluid viscosity, the ease with which the fluid moves**.** The drawdown and buildup rates observed during the test tell us about the mobility or how freely the fluid moves. In the zones with good permeability and containing fluids of fairly low viscosity the drawdown and buildup times are pretty low because the fluid flows easily into the FPWD tool whereas the test sequence in the tight zones or the zones with high viscosity fluid is characterized by long drawdown and buildup times as shown in Figure 3.30**.** Other indicators of low mobility or tight zones are lost seal and supercharging. Lost seal is experienced in low permeability zones where the absence of mud cake does not allow a hydraulic seal to be formed between the pad and

the borehole wall (Griffiths, 2009; Neumann et al., 2007). When the mud cake is absent or quality of the mud cake is low against a low permeability formation, the mud cake cannot isolate the formation from the wellbore, thus the invasion continues and the pressure in the near wellbore area is higher than the native formation pressure, this phenomenon is called supercharging (Sarkar et al., 1998).

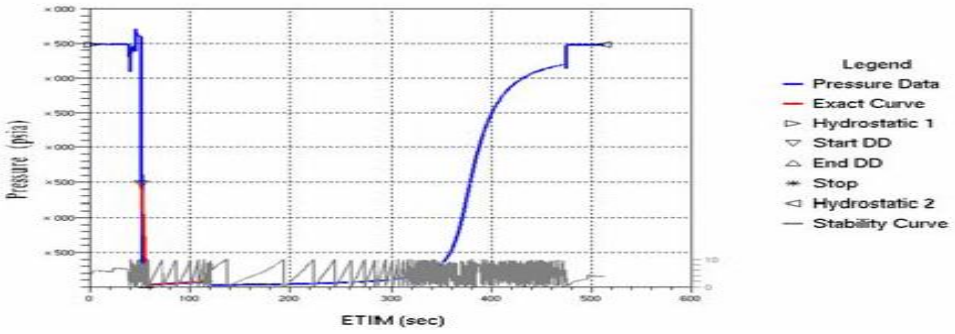

Figure 3.30. Test sequence as achieved in real time for a low mobility zone (Neumann et al., 2007).

For mobility steering, the FPWD tool is generally placed behind other important LWD tools such as resistivity, density and neutron which can solve for the effective porosity of the formation traversed. This ensures that we do not take “blind readings” in the low porosity or permeability zones. Generally, the formations with porosity less than 15% are not tested.

The reservoir under discussion in Figure 3.31 is a highly heterogeneous carbonate where the producible zones with fairly mobile oil are divided into zone A and zone B. A low porosity (LPZ) zone exists between the two and the zone B is underlined by a heavy oil or tar zone. The heavy oil or tar zone is located above the aquifer of the reservoir and prevents the aquifer from providing a natural drive for oil production. So, the aim here is to place an injection lateral in the zone B and as close to the producible oil/ heavy oil contact, called the oil/heavy oil contact (OHOC), to sweep the maximum producible oil from the bottom. Porosity is not an issue with this reservoir but mobility is the driving force here for a successful reservoir penetration, as the reservoir with LPZ as an

exception has a good porosity all through and even in the tar zone. After evaluating the reservoir complications final well plan called for an 8 ½" build section to be drilled through the Zone A and the LPZ and landed on top of zone B followed by 6 1/8" injection lateral in zone B. Figure 3.31 shows the real time pressure measurements made at the pressure points selected in the build section drilled through the Zone A and LPZ to the top of the zone B.

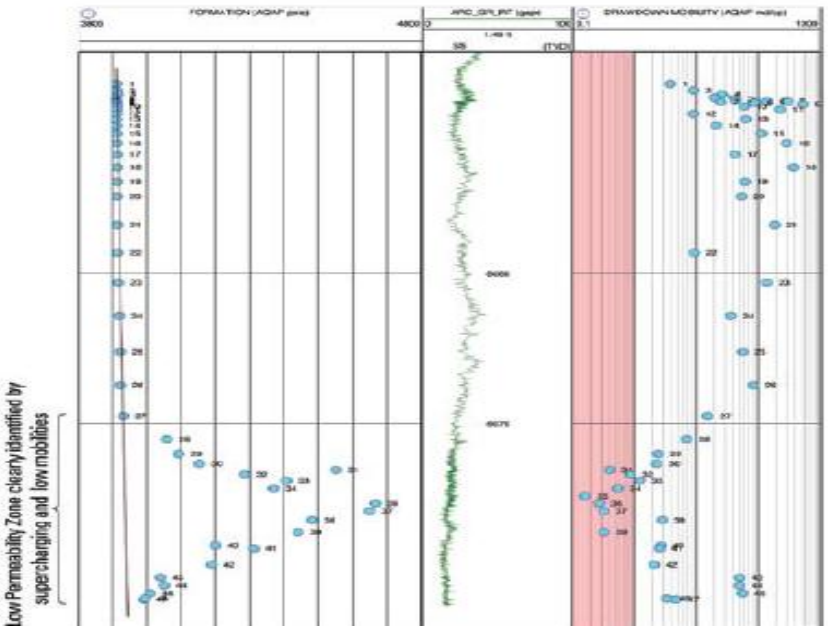

Figure 3.31. Real time pressure measurements made in the build section up to the top of Zone B. tests (Neumann et al., 2007).

Referring to Figure 3.31, the track on the left shows the pressure gradient, middle track shows the TVD and the track on the right shows the mobility calculated based on formation the pressure. It can be seen in the figure that the pressure gradient is pretty much steady as the well is drilling through the zone A and the fluid mobility is more than 10 md/cp for the most part. However, lower section of the log shows a steep deviation of the pressure gradient from the gradient line and decreasing mobility indicating that the well is now drilling through the LPZ. The supercharging continued to increase and the mobility decrease sharply as we drilled further through the LPZ, this response was

expected through the LPZ, till a point where the supercharging decreases again and the mobility increases indicating that the well is nearing the zone B. The build section was landed and now the 6 1/8" lateral was drilled in zone B. The steering events in the zone B are shown in Figure 3.32 along with the real time pressure measurements. Good mobilities were expected in the zone B, the challenge was to stay away from the tar zone but still as close to it as possible and also stay in the best mobilities of zone B. The third event in the figure is where a possible tar zone is detected on the observed steep deviation in pressure gradients and sharp decrease in mobility, the well was steered upwards at this point to get back to better mobilities. The steady gradient and fairly high mobilities after the point indicate optimum well placement (Neumann et al., 2007).

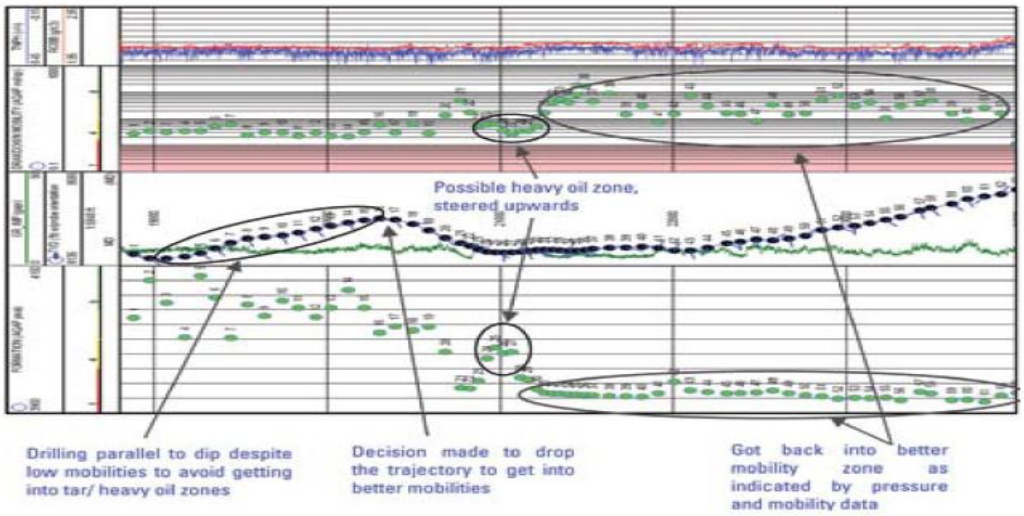

Figure 3.32. Real time pressure measurements made in the lateral section drilled through Zone B (Neumann et al., 2007).

The FPWD real time measurements allow us mud weight optimization by providing accurate pore pressure in real time and can also be used to drill horizontal wells with greater accuracy. Because of the uncertainties in surveying, discussed in Section 1.4, the actual course of a horizontal well may not be really horizontal. However, if FPWD measurements are made while drilling adjustments can be made to the trajectory to drill it across constant formation pressure and thus maintaining a horizontal profile. This

application is particularly useful when steering in thin reservoirs with tight TVD steering windows. Suppose if the sweet spot has been recognized in such a well and the dip of the reservoir bed is fairly flat, we can use the FPWD measurements to maintain the TVD for maximum reservoir contact.

The FPWD tools apart from their real time applications also have the ability to collect up to 15 fluid samples at the desired test points. These samples can be retrieved after pulling out of the hole and can be used for reservoir characterization.

3.9. SONIC WHILE DRILLING

The sonic tools emit a sound wave that travels from the source into the formation and back to the receiver. An array of equally spaced receivers is used to make the tool borehole compensated. The distance between the receivers is known, thus measuring the time difference between the arrivals at two different receivers gives the acoustic travel time per unit distance which is known as slowness, Δt, which is the inverse of the velocity and is measured in μs/ft.

The sonic while drilling find an important application for steering in the low permeability reservoirs such as unconventional shales. The production of the wells drilled in such reservoirs is governed by the success of stimulation operations on the well. Therefore the well placement in this kind of reservoirs calls for a well placement in the section of the reservoir which responds well to the stimulation techniques. If we consider the case of unconventional shales, we would like to place the well in the brittle section. Rock brittleness reflects the ability of the rock to fail under stress and maintain a fracture. The brittle shale, therefore is more likely to be fractured and turns out be a good producer. Ductile shale on the other hand is not a good producer because it tends to heal any natural or hydraulic fracture. So when steering in an unconventional shale, we would like to avoid the ductile shale and place the well in the brittle section. The brittleness index is a function of the Young's modulus and Poisson's ratio which can be estimated in real time using sonic while drilling and by the following equations**.** (Jeniffer et al, 2010)

$$\nu = (0.5\,.\left(\frac{V_p}{V_s}\right)^2 - 1)/(\left(\frac{V_p}{V_s}\right)^2 - 1) \tag{18}$$

$$E = \left(\rho \,.\, V_s{}^2\right).(1+\nu).2 \tag{19}$$

Where ν is the Poisson' ratio, V_p is the velocity of the compressional waves in ft/s, V_s is the velocity of the shear waves in ft/s, E is the Young's modulus in psi, ρ is the density of the rock in lb/gal.

Thus, the brittleness index estimated in real time can help place the well in brittle shale. This can be applied to other reservoirs as well if certain brittleness or rock mechanical properties can be associated with the zone we want to place the well in. Another important application of the sonic while drilling is to stay in the sweet spot. Figure 3.33 shows the coordinate axes of a sonic tool while drilling horizontally through thinly laminated layers. The compression P waves travel parallel to the axis of the tool in the formation, so the P waves will measure the horizontal or the x axis velocity. Whereas the shear S waves travel perpendicular to the axis of the tool, thus travelling in two directions – y axes and the z axes. It must be noticed here that the shear waves travelling in the y direction are within one layer i.e. the layer the tool is currently in and have a fairly simple route of propagation whereas the shear waves in the z direction respond to the surrounding layers.

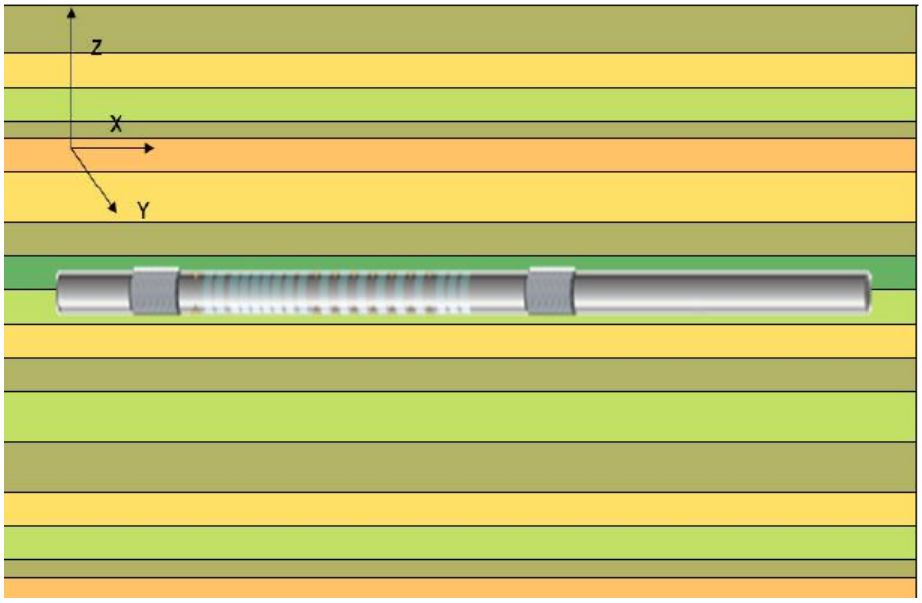

Figure 3.33. Coordinate axes system of a sonic while drilling tool when drilling horizontally in thinly laminated layers (Market et al., 2010).

The y shear waves will be faster because they are just travelling in the layer, the tool is currently in whereas the multiple layers slow down the z shear waves. Figure 3.34 shows a sonic log example from a horizontal section in an unconventional shale reservoir. The fast shear or the y shear (white) is constant all over the section indicating well placement within one layer whereas the z shear varies over the section. The point circled is the one where the slow shear approaches the fast shear indicating an increased brittleness in the surrounding layer.

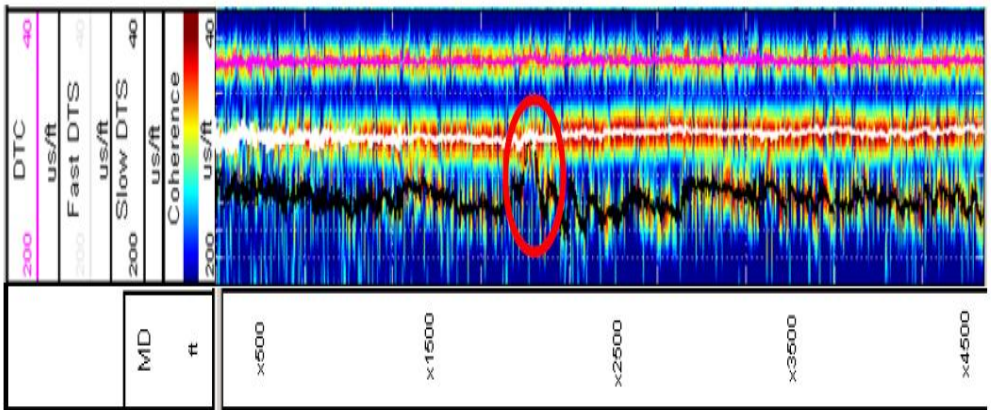

Figure 3.34. Real time sonic logs over a horizontal section in an unconventional shale reservoir (Market et al., 2010).

This is a very important application of sonic while drilling, as we discussed earlier that almost all the LWD tools provide an averaged response from multiple layers when traversing through thinly laminated layers. However, the sonic tool can delineate a thin layer with precision which allows us to steer within a thin layer by making adjustments to the trajectory to drill along the constant y shear slowness.

3.10. DECISION MATRIX

We can summarize the above discussions as a decision matrix which would help us decide on the LWD tool to be used for a particular problem. Figure 3.35 shows the devised decision matrix.

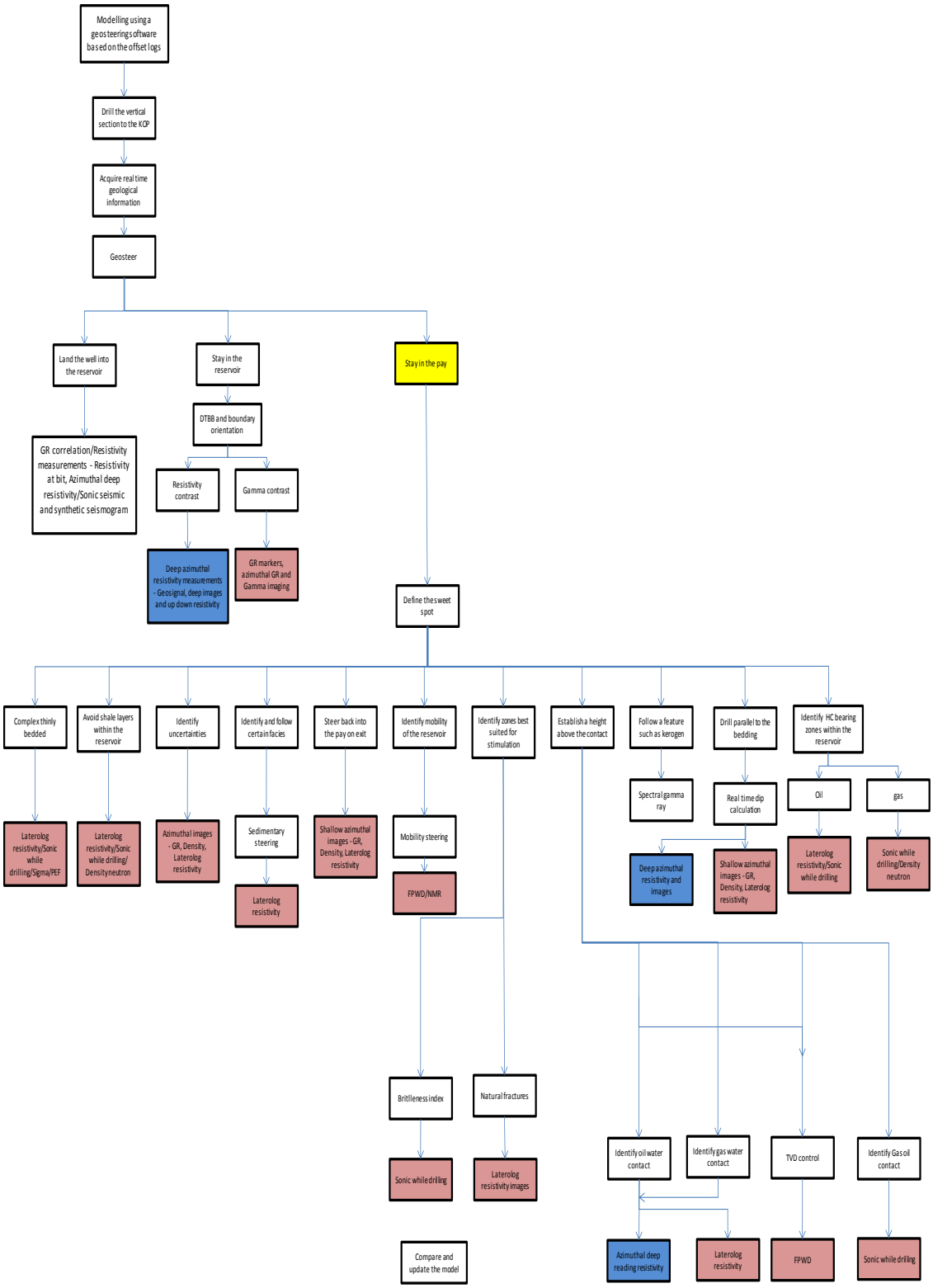

Figure 3.35. Decision matrix for the LWD tools

As can be seen in Figure 3.35 well placement can be broadly classified into three main aspects – Landing the well into the reservoir, Staying in the reservoir and staying in in the sweet spot. The following boxes below these three aspects show a particular scenario for each and the suggested tools as a proper flowchart. The blue colored boxes indicate a proactive method of geosteering, the boxes in pink indicate a reactive method and the yellow box indicates a combination of both reactive and proactive.

We have discussed the reactive and proactive methods of steering earlier but often placing a well optimally will be a combination of several challenges. For ex- a reservoir may have a good resistivity contrast with thinly bedded layers of shale within the reservoir and with certain uncertainties along the course, in this case an optimum LWD suite will be a combination of different LWD tools each addressing the respective challenge, as shown in the matrix, and the well placement calls for a "Proactive+Reactive" approach.

To ensure effective well placement we need to understand our reservoir and the well placement challenges to be addressed. There will always be uncertainties when placing the well which call for quick decisions and the well plan to be updated in real time. In order to do that we must understand the applications and limitations of each tool available and the decisions should be made on the basis of combined analysis of all relevent the real time information, as we have discussed and seen in some of the examples above that relying on just one information can be misleading at times.

3.11. APPLICATION TO THE FIELD

If we apply the decision matrix to the well placement challenges in the field of study, discussed in Section 2, the suggested LWD tools to meet the challenges are as below.

1. Gamma ray measurements can be used to differentiate between the Jurassic from the Triassic sediments below as we saw in Figure 2.3. Gamma ray has also shown an ability to mark the upper boundary of the Jurassic, Figures 2.1 through 2.3, even when the resistivity fails to do so. Also it is a strong correlation tool which can be used to identify the True Stratigraphic Position (TSP) of the well while drilling. However Gamma ray has a short depth of

investigation and cannot be used as a proactive tool. Hence it is recommended to use Gamma at bit to minimize the measurement lag while drilling and see the changes in GR responses as the bit cuts though the formation.

2. Deep azimuthal resistivity – The log responses in Figure 2.1 and 2.3 indicate a resistivity contrast between the Jurassic sandstones and the Cromer knoll. In such a scenario deep azimuthal resistivity can be used to proactively determine the distance and orientation of an approaching boundary. However, propagation resitivity tools need a conductive path and will not work with oil based muds.
3. Azimuthal density images - can be used to calculate the relative dip of the wellbore in real time and help us see if the well is traversing up or down with respect to the formation and density variation has also been observed between the sandstones of Jurassic and shoulder beds, Figure 2.1 and 2.3,.
4. None of the wireline logs shows sensitivity to the oil water contact. As per the decision matrix, the Formation pressure while drilling can be used to determine the oil water contact and also the low porosity zones where density and neutron do not work.
5. Azimuthal Laterolog resistivity – is a focused measurement and has the best resolution amongst all the LWD tools. We have also observed variations in resistivity responses within the Jurassic, Figure 2.2 and 2.3, and hence can be used to map the variations within the reservoir.

The suggested tools will be of assistance in geosteering but there still will be some associated uncertainties. As we saw in Figure 2.1 through 2.3, a certain distinct feature observed for a log measurement may be absent be absent in another well in the field. Hence we do not expect the log responses to be laterally extensive owing to the heterogeneity of the field. In the following sections we will evaluate the applicability of two other methodologies to geosteering, one is to evaluate the drilling data and other a statistical approach of hierarchal clustering and classification tree.

4. MECHANICAL PROPERTIES AND ROCK MECHANICS

4.1. INTRODUCTION

In this section we will analyze the variations in Mechanical Specific Energy and Uniaxial Compressive Strength to evaluate their contribution in distinguishing between the formations for well placement.

UCS is the unconfined compressive strength and is generally determined for a rock by the uniaxial compressive testing in the lab. For our analysis we will calculate it from sonic compressive travel time using the following equation.

$$UCS = \left(\frac{1}{k_1(\Delta t_c - k_2)}\right) + k_3 \tag{20}$$

Where UCS is unconfined compressive strength in MPa. and Δt_c is compressive travel time in μ sec/ft. k_1, k_2 and k_3 are constants based on lithology and their values for the respective lithology is given in Table 4.1 (Olea et al., 2008).

Table 4.1. The values of the constants for the respective lithologies.

Lithology	k1	k2	k3
Sandstone	0.0011	50.0000	3.4200
Shale	0.0013	50.0000	-2.6600
Combined	0.0012	50.0000	0.2200

MSE is the mechanical specific energy and is defined as the work required to destroy the given volume of rock. The MSE equation can be expressed in the terms of drilling parameters as (Teale, 1965)

$$MSE = \frac{WOB}{A_B} + \frac{120\,\pi \times RPM \times T}{A_B \times ROP} \tag{21}$$

Where MSE is the mechanical specific energy in psi, A_B is the area of the Bit in square inches, T is the applied torque in lb-ft, WOB is the weight on bit in lbf and ROP is the rate of penetration in ft/hr. All the input drilling parameters for the MSE calculation can be found in mud logs.

4.2. APPLICATION TO THE FIELD

MSE and UCS will be calculated for wells B and C from the field of study using the respective mud log and wireline files as inputs. The lithology of the wells and the well placement goals have already been discussed in Section 2. A graphical representation of the properties with respect to the lithologies is presented in Figure 4.1 and 4.2.

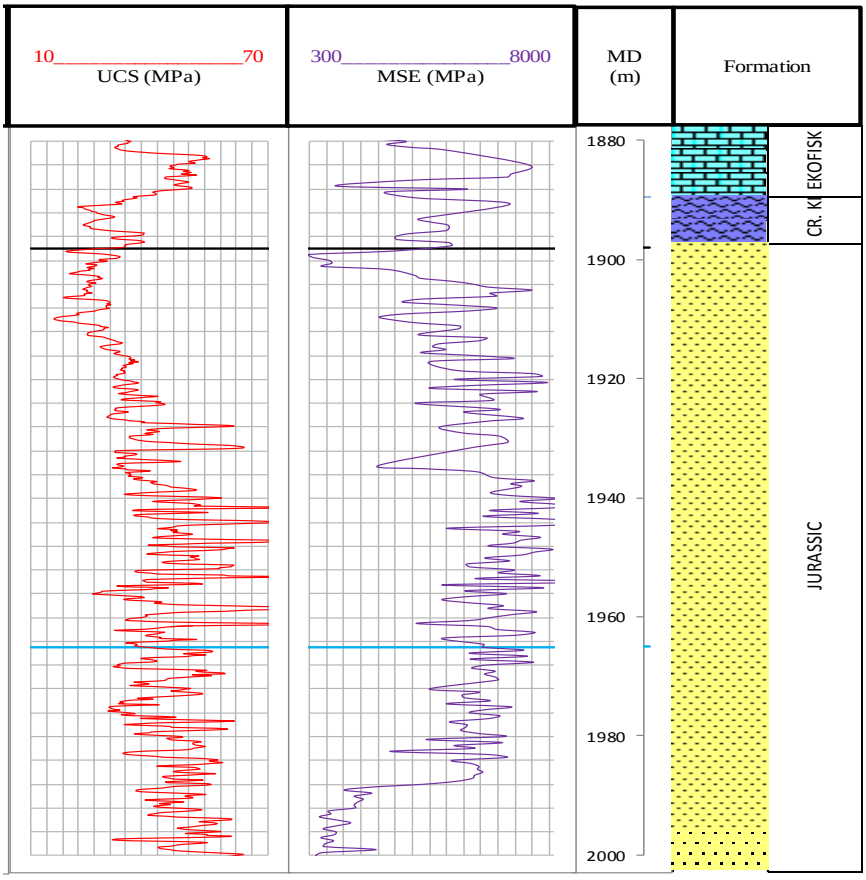

Figure 4.1. MSE and UCS values for the formations of interest for well B

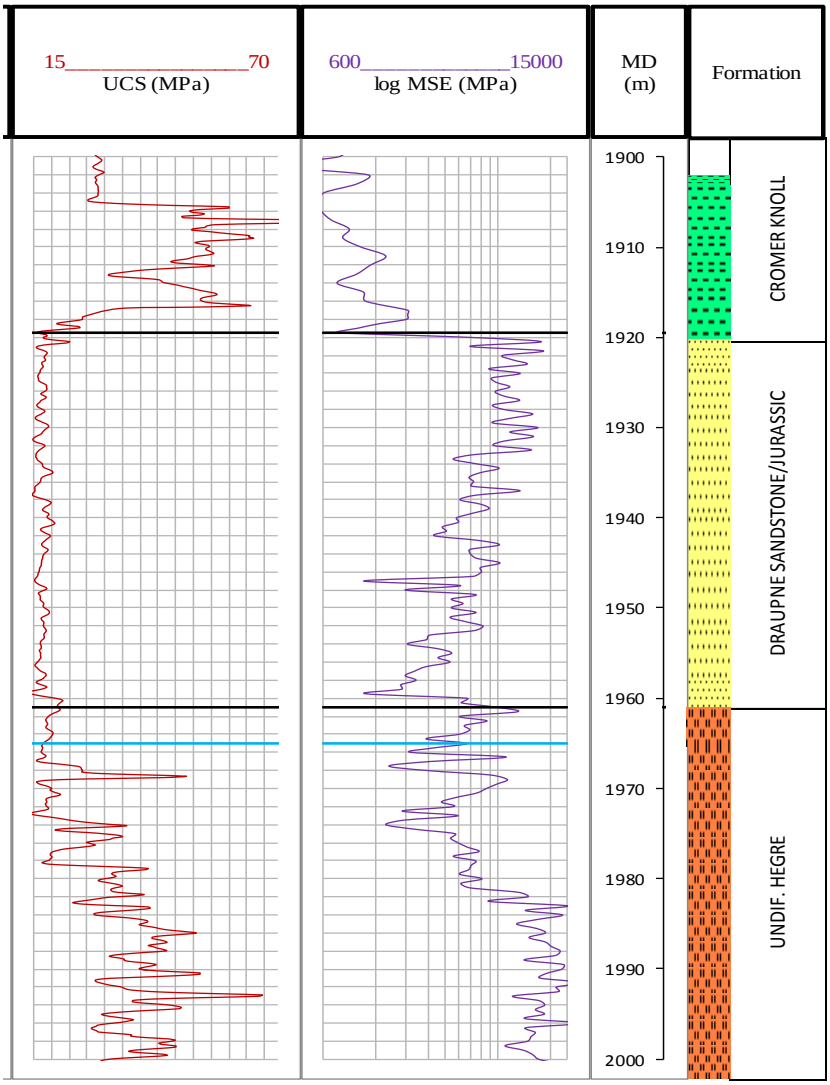

Figure 4.2. MSE and UCS values for the formations of interest for well C

For a particular property to be of assistance to well placement, the set of values for that particular property must be significantly different for each formation with minimum or no overlap. As we can see in Figures 4.1 and 4.2, both the properties show variation amongst the respective formations. To confirm if the variations are significant we will conduct a statistical analysis on the dataset of each property for the two wells. The statistical test that will be used for the analysis is the one way analysis of variance with the formations being the predictor variables and the values of a particular property

being the response variable. The tests will be conducted for 95% confidence intervals by setting alpha to 0.05.

4.3. RESULTS

The results of the analysis are listed for each well as per the property. Figure 4.3 shows the box plot of the UCS values for the well C.

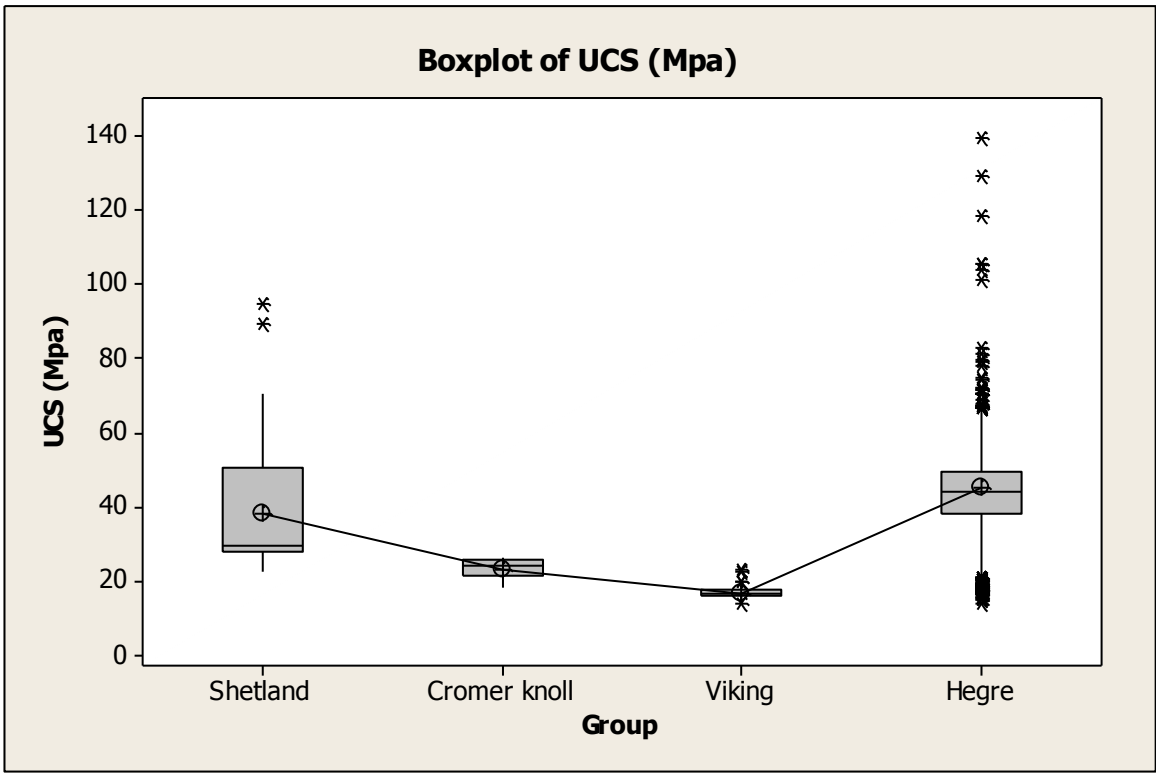

Figure 4.3. The box plots of the UCS values for the well C.

In Figure 4.3, the line that connect the means of the UCS boxes for each formation indicates that the mean UCS value are different for each formation which is also confirmed by the analysis of variance for which we got a p value of 0 which is less than the value of alpha,0.05. To check if the means are significantly different we will use the Tukey method for comparing the UCS means for all the formations. Table 4.2 shows the results shows the results of Tukey method analysis.

Table 4.2. Tukey comparison results for well C

Group	N	Mean	St. dev	Grouping
Shetland	194	37.91	13.52	B
Undif. Cromer Knoll	56	23.24	2.71	A B C
Viking	439	16.89	1.15	C
Hegre	1063	44.89	35.9	A

Means of the formations are grouped based on statistical difference between them in Table 4.2. The formations that do not share a letter have significantly different means. It can be seen in the table that all the formations except for Cromer Knoll have significantly different means and can be distinguished from each other. The mean and the standard deviations listed in the table are for 95 % confidence intervals minimizing the outliers. As can be seen the dataset for each formation has a unique spread except for the Cromer Knoll. Figure 4.4 shows the boxplot of the UCS values for well B.

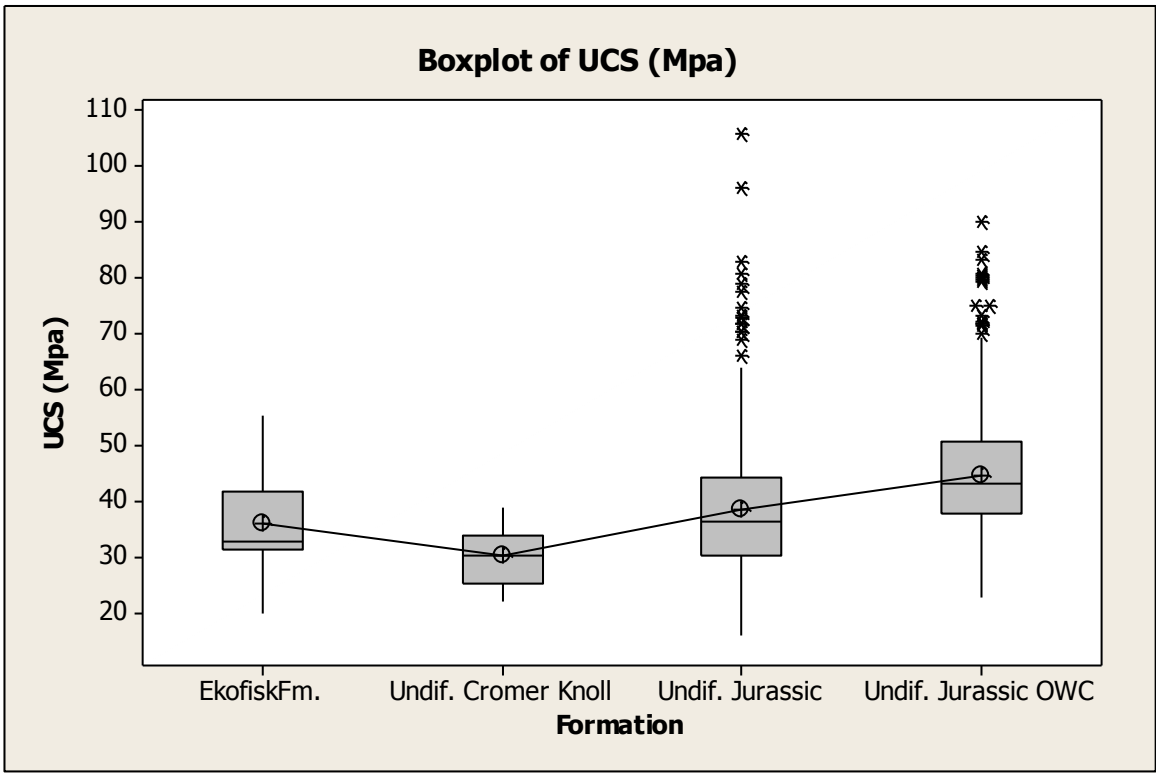

Figure 4.4. The box plots of the UCS values for the well B.

In Figure 4.4, 'Undif. Jurassic' is the part of the Jurassic formation above the oil water contact and hence is the target region with respect to well placement whereas Undif. Jurassic OWC represents the formation below the oil water contact. If we look at the figure it seems that the UCS means are significantly different for the formations. However, we can also see some overlap between the data spreads .To confirm the difference between the means, the results of the Tukey comparison are listed in Table 4.3.

Table 4.3. Results of Tukey method comparison for well B

Group	N	Mean	St. dev	Grouping
EkofiskFm.	194	35.88	8.28	C
Undif. Cromer Knoll	56	30.16	4.92	D
Undif. Jurassic	439	38.55	12.66	B
Undif. Jurassic OWC	1063	44.41	9.45	A

It can be seen in Table 4.3 that the means for the four formations are classified into four groups with a different letter for each formation which shows that the UCS means are significantly different. However, the overlap that was seen in the boxplot is confirmed here by the standard deviations for each group which indicates that none of the formations here have a unique spread for the data.

Figure 4.5 shows the boxplot of MSE values for well B. The values of MSE are in MPa and as can be seen in the figure, the MSE means for the formations are significantly different. There is some overlap between the spread of the dataset but is comparatively much less than that for the UCS dataset and if the outliers are ignored, there is a clear distinction between Undif. Jurassic formation above and below the oil water contact.

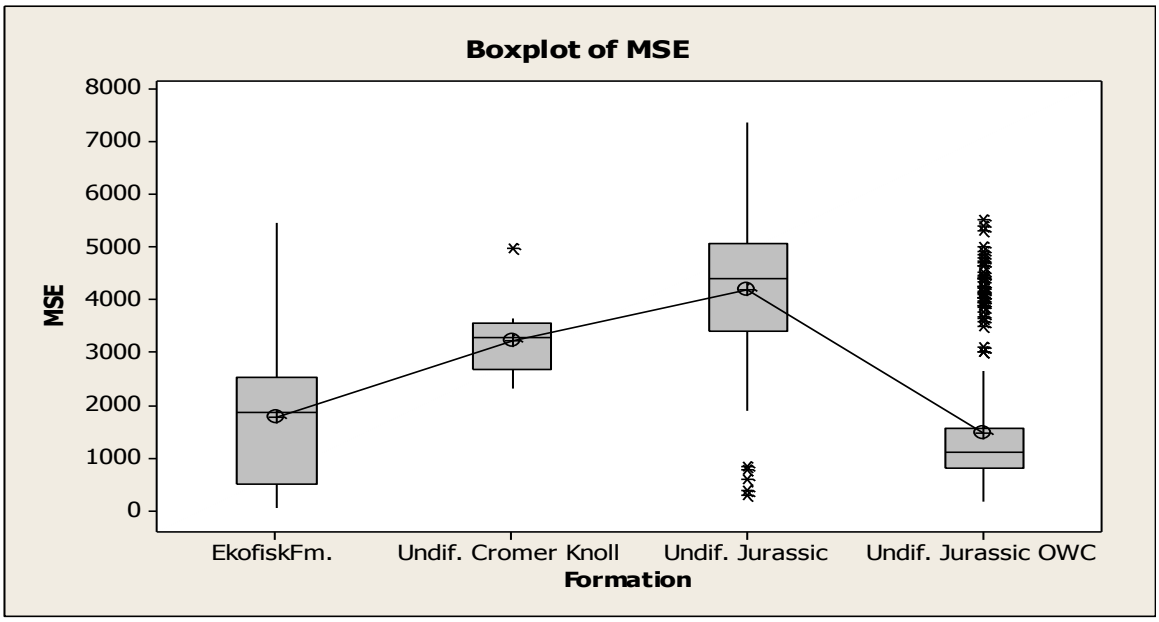

Figure 4.5. The box plots of the MSE values for the well B.

Table 4.4 shows the results of Tukey comparson.

Table 4.4. Tukey comparison results of MSE datset for well B

Group	N	Mean	St. dev	Grouping
EkofiskFm.	49	1765	1390	A
Undif. Cromer Knoll	12	3227	735	B
Undif. Jurassic	117	4188	1319	C
Undif. Jurassic OWC	369	1448	1109	A

It can be seen in Table 4.4 that the total number of observations are much lower for each formation as compared to those for UCS. MSE was calculated from the mud logs and UCS was calculated from the wireline sonic logs which have a much higher sampling rate than the mud logs. The table confirms that the difference in the means is significant for all the foramtions except for the Ekofisk and Undif. Jurassic OWC which share a common grouping letter. Also the standard deviation for the Jurassic formation above and

below the OWC shows a clear distinction between the two. Figure 4.6 shows the MSE boxplot for well C.

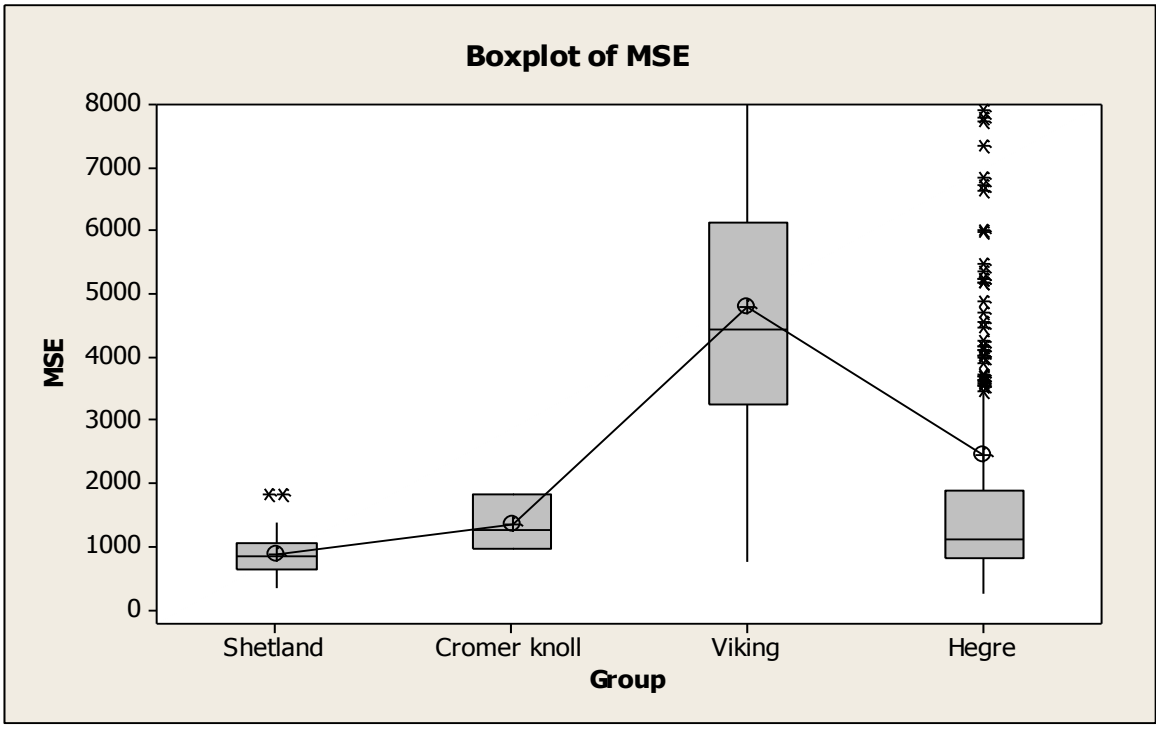

Figure 4.6. The box plots of the MSE values for the well C.

Figure 4.6 shows a clear difference between the MSE means for the formations. The spread of the data is also different for formations; however there is a major overlap between the Hegre and the Cromer Knoll group. Table 4.5 shows the Tukey comparison of MSE means for the formations.

Table 4.5. Results of Tukey method comparison for the MSE values for well C.

Group	N	Mean	St. dev	Grouping
Shetland	31	877	343	C
Cromer knoll	3	1339	440	A B C
Viking	81	4791	2325	A
Hegre	385	2447	3278	B

Table 4.5 confirms that the MSE means of all the formations are significantly different except for Cromer Knoll which cannot be distinguished from any of the formations. The uniqueness of the MSE data distribution for each formation is represented in Figure 4.5. Based on the standard deviations, we can infer that the dataset for formations do have different spread but there is a major overlap between the Cromer Knoll and the Hegre group. However, it must be noted that the thickness of the Cromer Knoll for well C is very limited i.e. 1.1m and we just had 3 data points as indicated by Table 4.5. Hence the MSE results for the formation as shown and discussed above may not be a good representation of the MSE spread for the formation. If we compare the MSE values for well C, Figure 4.6, with the MSE values for well B, Figure 4.6, we see that the MSE range is fairly close for the formations from two wells and it follows a similar trend i.e. increasing from the top shoulder beds to the reservoir and then dropping off at the basement. The UCS values do a good job in distinguishing between the formations for well C, Figure 4.3, but are of little help in well B, Figure 4.4.

4.4. APPLICATION TO WELL PLACEMENT

The mechanical properties analyzed above can be used for real time well placement if they are capable of distinguishing between the formations. As discussed in the last section the UCS values were able to distinguish well between the formations for well C but were of little help for well B. However, if we look at Figure 4.3 and 4.4 the UCS values follow the same trend starting from the Ekofisk down to the lower shoulder bed. Thus, the UCS might be able to distinguish well between the formations in some cases but this ability may not be transferable to the other wells, as we have seen for well B that even the UCS means for the formations were not significantly different. For the these properties to be used for well placement the whole data distribution for a formation has to be unique or else the information from the lower end or the higher end, which coincides with the data distribution of other formations, of the data distribution will always be misleading.

Based on the above analysis, it can be concluded that MSE performs better than the UCS. However, there were some uncertainties associated with MSE as well. For well B it was not possible to distinguish between the Ekofisk and the section of the Jurassic formation below the oil water contact based on MSE. The two formations are not

immediately next to each other but in fact make up the upper and lower shoulder beds, respectively for this particular scenario but even these two formations should have a unique signature from the well placement's perspective because there is always a probability of the well faulting into either of the formations and such an uncertainty cannot be accounted for beforehand. In that case the similar properties of the two formations will make it very difficult to determine if the well has made an exit or faulted. For well C, the uncertainty can be attributed to the limited thickness of Cromer Knoll. If we compare the two properties, it can be said that the MSE performs better than the UCS in distinguishing between the formations, as is evident from the boxplots.

The best way to utilize these properties for well placement is to understand the trend of both the properties for a particular well and use them together to distinguish between the formations when placing the well in real time. If we consider both the properties for well B, we can see that MSE values distinguish well between the formations except for the Ekofisk and the section of Jurassic below oil water contact but if we refer to the UCS data for the well we can see that these two formations have distinct UCS signatures and can be easily distinguished. The information required to determine MSE and UCS are the mud logs and the sonic logs, respectively, which are generally recorded when drilling a well. Thus it can be concluded that even with some associated uncertainties both the properties still help distinguish between the formations and can assist well placement in the field of study.

5. CLUSTERING AND CLASSIFICATION TREE

5.1. STEERING CHALLENGES IN HIGHLY HETEROGENEOUS RESERVOIRS

As discussed earlier, the purpose of geosteering is to place the well in the best part of the reservoir. This task becomes more challenging with the increasing heterogeneity of the reservoir as the distinct features of LWD measurements like polarization horns, bright spot etc. may not exist in such scenarios or even if they do they may not be laterally extensive through the course of the well. Practically almost all the reservoirs are heterogeneous and the lithological variations within the reservoir can get very complex. For example – Turbidites are composed of several layers of fine grained sand or silt interbedded within the hydrocarbon bearing reservoir. The resistivity response in such an anisotropic scenario cannot be trusted to differentiate between the productive and the non-productive section of the reservoir as the response is reduced giving an idea of poor reservoir quality even if the reservoir is full of hydrocarbons. For this reason turbidites are also known as the low resistivity pay.

Several such scenarios can exist and the heterogeneities can be attributed to the variation amongst a broad range of physical properties such as grain size, sorting, texture, mineralogy, cementation etc. Since the distinct well placement features, if any, are not laterally extensive it is practically impossible to select a particular tool and use it as the primary steering tool. One of the ways to deal to deal with such a scenario is to use a comprehensive LWD suite with all the advanced LWD tools as a particular tool may exhibit a certain distinct well placement feature at certain different points along the well path if not constantly through the course of the lateral. Such a LWD suite has to be accompanied by high bandwidth telemetry such as wired drill pipe to convey the huge set of information to the surface in real time. However such an approach is not practically feasible owing to the cost implications. Another problem with this approach is that it complicates the steering further rather than simplifying it. As we discussed in the first chapter that the real time information available will always be overwhelming and in order to make quick real time decisions about the well trajectory we need to prioritize or

compartmentalize the information i.e. separate the ones needed for well placement from those for formation evaluation. By using a huge set of LWD measurements we just add to the real time information and complicate the decision process as too much information will be misleading at most instances rather than assisting the well path. An understanding of the uncertainties and a method to characterize them is paramount to the success of well placement in such scenarios and that is where the concept of facies is applied.

5.2. FACIES

The heterogeneities in a rock body can be attributed to the variations in various physical properties such as grain size, sorting, cementing, texture, mineralogy etc. which can be categorized as facies which refers to a body of rock with specified characteristics. A rock body may consist of several facies depending on the heterogeneity (Altunbay et al., 1994). The sedimentary facies can be categorized into two types:

Lithofacies are the facies based on petrological characters such as grain size and mineralogy and when based on fossil content facies are known as biofacies.

Electrofacies are the distinct patterns derived from a data set which has several well logs as the subsets. Electrofacies and lithofacies are closely related and the difference between them, if any, depends on the level of details or the logging data used to define the electrofacies .The lithofacies are identified from the cores, several analyses are conducted on the core and the facies are identified based on the distinct physical properties such as mineralogy, appearance, cementation etc. and hence it can be said that the lithofacies are the detailed and complete characteristic units of a rock body. The electrofacies are identified from the well logs, which are also a function of the physical properties of the logged formation or rock, as the clusters or the set of log responses that characterize a rock type and allows it to be distinguished from others. Thus the identification of both the facies types has the same basis and it can be said that the electrofacies build an image of the lithofacies which means that a particular lihtofacies can contain more than one electrofacies. The more complete the logging program the better the image represents the actual lithofacies (Serra et al., 1982). In the next section, we will discuss a method to identify the electrofacies or the clusters from the well log data.

5.3. PRINCIPAL COMPONENT ANALYSIS AND HIERARCHAL CLUSTERING

5.3.1. Methodology. The principal component analysis is a way of identifying underlying patterns in a data and expressing the data in such a way as to highlight their similarities and differences. This technique is particularly useful when working with a dataset of high dimension as patterns could be hard to find in such a dataset. In our case each well log used is a dimension and hence we can expect to work with high dimension data as we will always be dealing with a set of well logs (Smith, 2002).

The first step in calculating the principal components is to normalize the data as the input well logs have different units. Each dimension is subtracted by the mean and divided by the standard deviation. The mean subtracted is the average across each dimension.

To understand the spread of the data we use variance which is a measure used to understand the spread of data and is given by the following equation.

$$var\ (X) = \frac{\sum_{i=1}^{n}(X_i - \overline{X})^2}{(n-1)} \tag{22}$$

Where X_i is a data point from the dataset, $\overline{X}$ is the mean of the dataset and n is the total number of observations in the dataset.

Variance explains the distribution of the dataset with one dimension, to extend the measure to a dataset with high dimension we use covariance which incorporates similar mathematics and explains how different dimensions of a dataset vary with respect to each other. The equation for the covariance is pretty much similar to the variance and can be expressed as below.

$$covar\ (X, Y) = \frac{\sum_{i=1}^{n}(X_i - \overline{X})(Y_i - \overline{Y})}{(n-1)} \tag{23}$$

Where X_i & Y_i are the data points for the respective dimensions X & Y from the dataset, $\overline{X}$ & $\overline{Y}$ for the dimensions X and Y of the dataset and n is the total number of observations in the dataset.

As we are working with more than one dimension, there is more than one covariance measurement that can be calculated. Hence a covariance matrix is generated for the whole dataset. An example of a covariance matrix for a three dimensional data is given below.

$$\begin{matrix} cov(x,x) & cov(x,y) & cov(x,z) \\ cov(y,x) & cov(y,y) & cov(y,z) \\ cov(z,x) & cov(z,y) & cov(z,z) \end{matrix}$$

The dimension of the covariance matrix depends on the dimensions in the dataset. Covariance matrix will always be a n x n square matrix where n is the dimensions in the dataset.

Next step is to calculate the eigenvectors and eigenvalues for the covariance matrix. Eigenvectors of a square matrix are the non-zero vectors that after being multiplied by the square matrix remain parallel to the original vector. Each eigenvector has a scalar multiple called the eigenvalue which is the factor by which eigenvector is scaled when multiplied by the matrix. The mathematical expression for the idea is as below.

$$Av = \lambda v \tag{24}$$

Where A is the square matrix, v is the eigenvector and the scalar λ is the eigenvalue.We can rewrite the equation (24) as

$$(A - \lambda I)v = 0 \tag{25}$$

Where I is the n x n identity matrix

In order for a non-zero vector to satisfy the equation $(A - \lambda I)$ should be non-invertible and hence

$$\det(A - \lambda I) = 0 \tag{26}$$

The eigenvalues can be determined by solving the equation (26). The determined eigenvalues can then be used in eq (25) to determine the corresponding eigenvectors for each.

The Principal components are then calculated for the whole dataset by a linear combination of the eigenvectors. The number of principal components generated is equal to the number of variables or the dimensions of the dataset. Since the principal components are generated from the eigenvectors which are mutually perpendicular, no two principal components are mutually dependent or correlated.

Once the important principal components have been identified, we use them as inputs for the hierarchal clustering to split a heterogeneous formation into the possible homogeneous clusters. The method that we will use for hierarchal clustering is the centroid method. The distance between the two clusters is the squared Euclidian distance between their means and is given by the following equation.

$$\boldsymbol{D_{KL}} = \|v_{\boldsymbol{K}} - \boldsymbol{v_L}\|^{\boldsymbol{2}} \tag{27}$$

Where D_{KL} is the distance between the clusters C_K and C_L, $\boldsymbol{v_K}$ is the mean vector for a cluster C_k and $\boldsymbol{v_L}$ is the mean vector for a cluster C_L.

This method of clustering is also known as agglomerative clustering. The hierarchal clustering is performed on the principal components using multivariate clustering in JMP and the results are represented by a figure called a dendrogram. The inputs, principal components, are plotted in a three dimensional space and each individual point in this space is treated as a cluster which are represented by the left side of the dendrogram. As we move towards the right side of the dendrogram the clusters with the shortest distance are merged all through the course till we have one large cluster of the dataset at the extreme right of the figure.

5.3.2. Example. To further explain the principal components analysis we will calculate the principal components for a simple two dimensional dataset shown in Table 5.1.

Table 5.1. The dataset used for analysis.

x	y	x'	y'
1.00	2.00	-1.72	-1.78
5.00	9.00	-0.80	-0.70
7.00	11.00	-0.33	-0.39
6.00	10.00	-0.56	-0.54
4.00	8.00	-1.03	-0.85
3.00	6.00	-1.26	-1.16
10.00	15.00	0.36	0.23
11.00	17.00	0.60	0.54
9.00	14.00	0.13	0.08
8.00	12.00	-0.10	-0.23
13.00	20.00	1.06	1.01
15.00	25.00	1.52	1.78
14.00	22.00	1.29	1.32
12.00	18.00	0.83	0.70

Table 5.1 shows a two dimensional dataset. x' and y' are the normalized values of the dimensions x and y. Looking at the data we know that the y increases with x. The Covariance matrix for the above dataset is a 2 x 2 square matrix and was calculated using equation (23).

$$A = \begin{pmatrix} 1 & 0.993 \\ 0.993 & 1 \end{pmatrix}$$

The eigenvalues were calculated using equation (26)

$$\lambda = \begin{pmatrix} 1.99 \\ 0.0071 \end{pmatrix}$$

The corresponding eigenvectors for each eigenvalue were calculated by solving for equation (25) and are presented as the columns of the matrix below.

$$v = \begin{pmatrix} 0.707 & -0.707 \\ 0.707 & 0.707 \end{pmatrix}$$

The two eigenvectors calculated above represent an arrow pointing from the origin (0,0) to the points (0.707,0.707) and (-0.707, 0.707) and can be represented graphically by using their characteristic equation of line which is y = x for the first vector and y = -x for the second vector. Figure 5.1 shows a plot of the standardized data points along with the two determined eigenvectors.

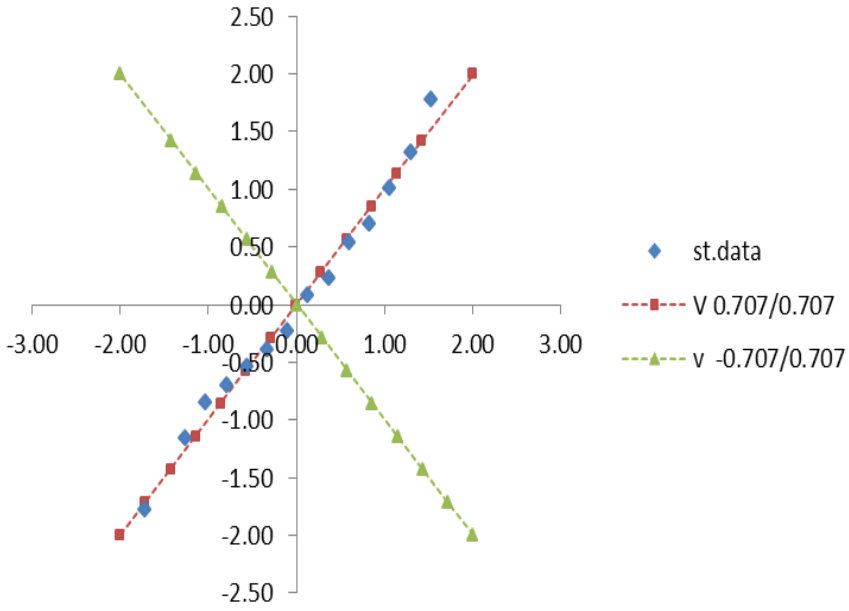

Figure 5.1. A plot of the determined eigenvectors and the standardized data.

The standardized data points are represented by the blue markers in the figure. The red line shows the eigenvector $\begin{pmatrix}0.707\\0.707\end{pmatrix}$ for the eigenvalue 1.99 whereas the blue line shows the eigenvector $\begin{pmatrix}-0.707\\0.707\end{pmatrix}$ for the eigenvalue 0.0071. It can be seen in the figure that both the eigenvectors are perpendicular to each other and one of them coincides with the data points as if drawing the line of best fit for the data. The other eigenvector gives us other, less important information that all the points follow the main line but are off by some amount. Hence we can ignore the second eigenvector and hence the second principal component without losing any significant information. Similar procedure is followed even for when conducting the PCA on datasets with very high

dimensions and this is how the PCA reduces the dimensionality of a dataset without any significant loss of information. In all cases, the principal component will have the capability to explain a major proportion of the data which decreases with the descending eigenvalues. This aspect of PCA is particularly useful for our purpose as we will be dealing with datasets comprised of several well logs. It is much easier to identify patterns in the dataset by analyzing a few principal components rather than each well log separately.

For the example above, the first principal component is generated by multiplying the eigenvector with the corresponding dimension at each point. For the first data point with dimensions – x=1 & y=2, Table 5.1, the first principal component is calculated as

PC1 = 0.707*1+0.707*2 = 2.121

All the principal components are generated in a similar way for the whole dataset using their respective eigenvectors. In this case however, only the first component is of significance and is sufficient to explain the whole data.

Our goal here is to divide heterogeneous formations into homogenous sub groups, so we have to deal with datasets with high dimensions i.e. comprising of several well logs. The higher dimensions can make the manual calculation of eigenvectors and eigenvalues very complicated. Thus, commercial statistical software will be used for our analysis. To demonstrate the results of the software we will conduct the analysis on a dataset from the well E in the field of study. The dataset comprises of 7 well log measurements for 5 formations - Ekofisk, undifferentiated Cromer Knoll, Cromer Knoll sandstone, Granite wash and fracture basement. The multivariate analysis will generate n number of principal components from PC1 to PCn, if n number of log curves were used. For our data set we have 7 well logs, hence the multivariate analysis generated 7 principal components. Each subsequent principal component is the linear combination of the variables that has the greatest possible variance and is uncorrelated with all previously defined components. Figure 5.2 shows the scree plot, generated from the analysis, which is a plot of eigenvalues with respect to the corresponding principal components and Table 5.2 shows the eigenvectors.

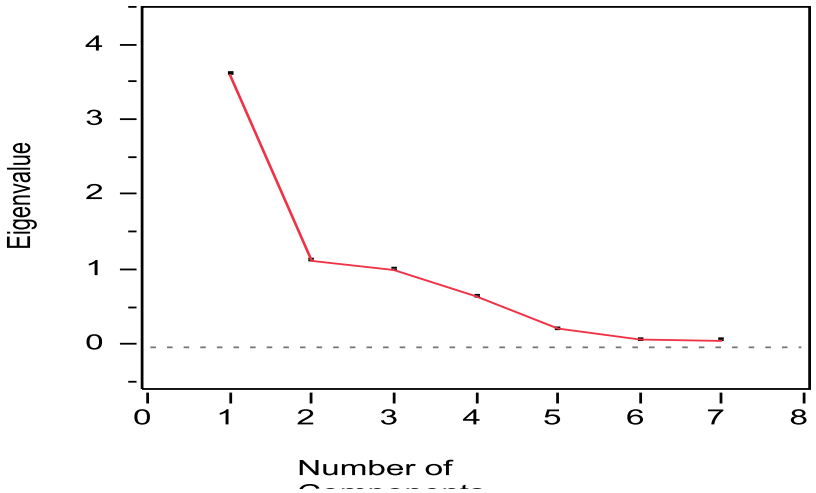

Figure 5.2. The scree plot for the principal components as determined for well E.

Table 5.2. The eigenvectors for each component with respect to the variables.

Eigenvectors

	Prin1	Prin2	Prin3	Prin4	Prin5	Prin6	Prin7
SRD	-0.09920	0.25480	0.89205	0.26253	0.23437	0.02252	0.07164
SRS	-0.19738	0.78934	-0.03950	-0.35159	-0.40901	0.21138	-0.02895
SNPHI	0.48703	-0.11155	0.06415	0.20999	-0.21608	0.80838	-0.04438
SGR	-0.27885	0.29275	-0.37809	0.82298	0.04240	0.04215	0.11274
SDTC	0.44491	0.37165	-0.13539	0.02483	0.47731	-0.11973	-0.63469
SDTS	0.47124	0.27020	-0.13099	-0.11194	0.30598	-0.08375	0.75802
SRHOB	-0.46500	-0.05238	-0.14190	-0.27004	0.63863	0.52745	0.04384

The eigenvalues are representative of the portion of information that can be represented by a principal component as the total sum of the eigenvalues is equal to the number of variables used in the analysis. A graphical representation of the eigenvalues with respect to the principal components allows the analyst to figure the importance of each component. The eigenvectors in Table 5.3 are the coefficients with respect to each variable which can be used to generate the principal components for each point in the dataset. As can be seen in Figure 5.2, the first component has the maximum slope which reduces with the following components. Table 5.3 shows the percent of information explained by each PC along with the corresponding eigenvalues.

Table 5.3. The percent of variation explained by each principal component along with the corresponding eigenvalues.

Eigenvalues

Number	Eigenvalue	Percent	20 40 60 80	Cum Percent	ChiSquare	DF	Prob>ChiSq
1	3.6505	52.150	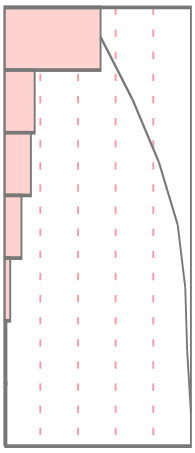	52.150	7359.96	27.000	<.0001 *
2	1.1602	16.574		68.724	3996.24	20.000	<.0001 *
3	1.0388	14.840		83.563	3258.80	14.000	<.0001 *
4	0.6886	9.837		93.400	2011.37	9.000	<.0001 *
5	0.2579	3.684		97.084	482.154	5.000	<.0001 *
6	0.1114	1.591		98.676	12.865	2.000	0.0016 *
7	0.0927	1.324		100.000	0.000	0.000	.

It can be seen in the above table that about 93.4 % of the variation in the given dataset can be explained by the first four PCs. PCs of higher order contain very little information which in some cases may be considered as noise and can be ignored. However if the higher order principal components include variations that are due to the events that appear on one log and that have not been accounted for in any of the other principal components, they cannot be considered as noise (Serra et al., 1982). Referring back to Table 5.2 we do not see any such variations in any of the higher order components and the first four components are sufficient to explain the variations. So, we will consider only the first four components for the cluster analysis and ignore the last three and this is how we reduce the dimensionality of a given dataset without losing any significant information.

The hierarchal clustering was then performed using the identified 4 PCs as inputs. The clustering was done by formation. Figure 5.3 shows the hierarchal clustering done for the Ekofisk formation using the calculated principal components as inputs and the centroid method for clustering.

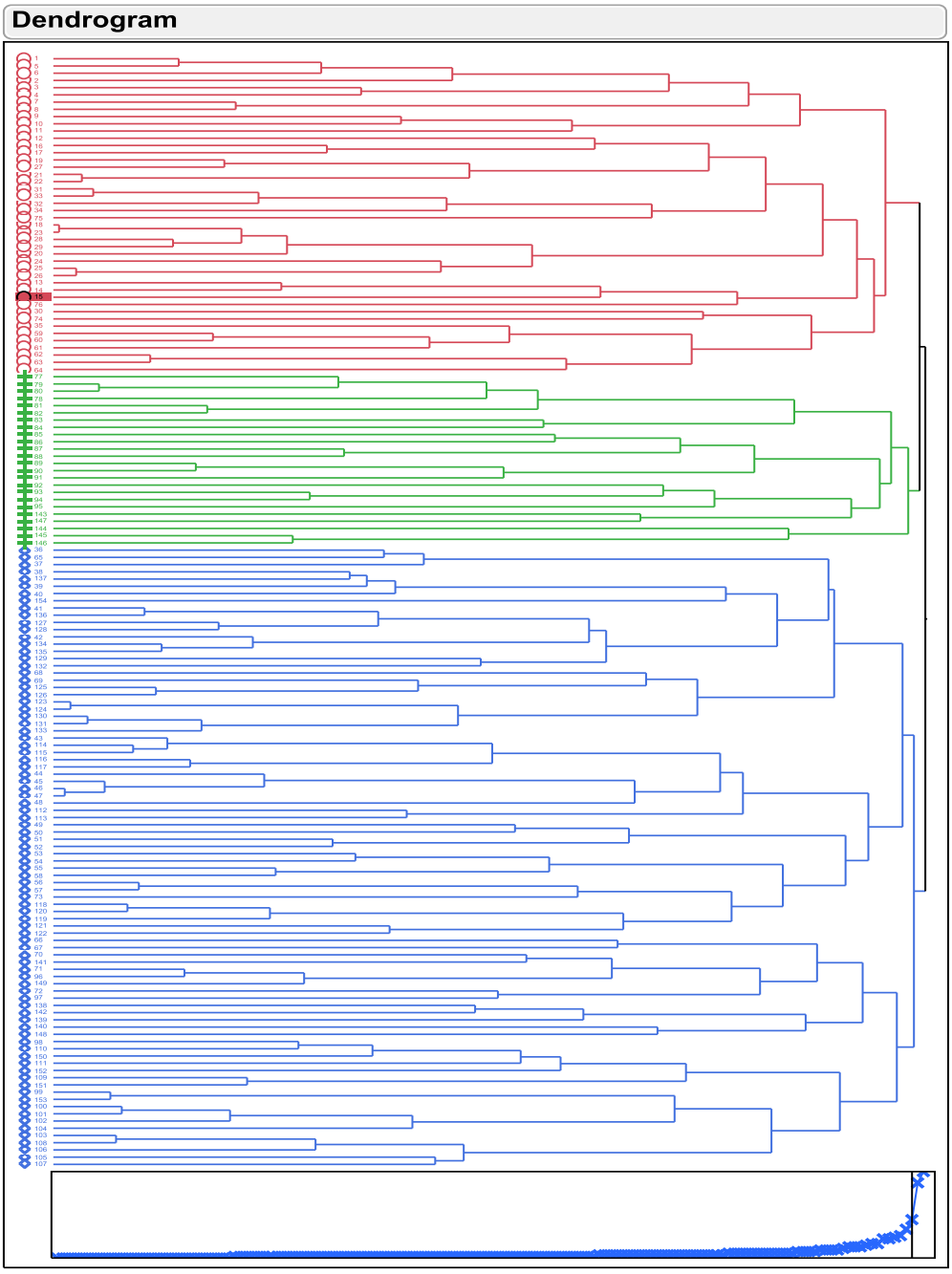

Figure 5.3. The hierarchal clustering for Ekofisk using the centroid method.

At the left side of the figure every single point which represents a particular set of principal components in the three dimensional space is treated as an individual cluster and at the extreme right of the dendrogram we have one big clusters that comprises of all the information. The scree plot below the dendrogram has a point for each cluster join

and the ordinate shows the distance that was bridged to merge the clusters at each step. It can be seen in the scree plot that the distance increases steadily as we move towards the right until at a point where a break is observed i.e. the distance suddenly jumps up. Our goal is to pick the optimum number of clusters in between the extreme left and the right sides. However, there is no defined criterion to pick the optimum number of clusters. The cluster distance information shown in the scree plot below must be combined with some knowledge about the dataset that we are dealing with to pick the right number of clusters. For this particular scenario, we know that Ekofisk formation is fairly homogeneous and hence we do not expect huge variation or clusters within it. Hence picking just the three clusters, which are the maximum distances apart, from the end of the scree can explain the variations within the formation. If we do not have enough knowledge about the heterogeneity of the formation we must pick the number of clusters at the break point to account for all the variations within the formation. Since, the criterion for the optimum number of clusters is not predefined we must make sure that we pick the number of clusters in such a way that all the significant variations or different patterns have been accounted for.

The cluster analysis performed above helps us to divide a heterogeneous formation into the several homogenous clusters since it is really difficult to deal with a highly heterogeneous formation as a whole. Once these homogeneous clusters are identified we need to set a criterion based on the well logs for each of the cluster and for this purpose we will use a decision tree which is discussed in the following section.

5.4. CLASSIFICATION TREE

5.4.1. Methodology. The clusters identified by the PCA and heirarchal clustering are placed against the corresponding log measurements, the original data set. A classification tree is then built to set a criterion for the recognition of each cluster based on well log data. Before we devise the tree for the identified clusters in the Ekofisk formation, let’s briefly discuss the components of the tree. Figure 5.4 shows a typical classification tree built for a particular dataset.

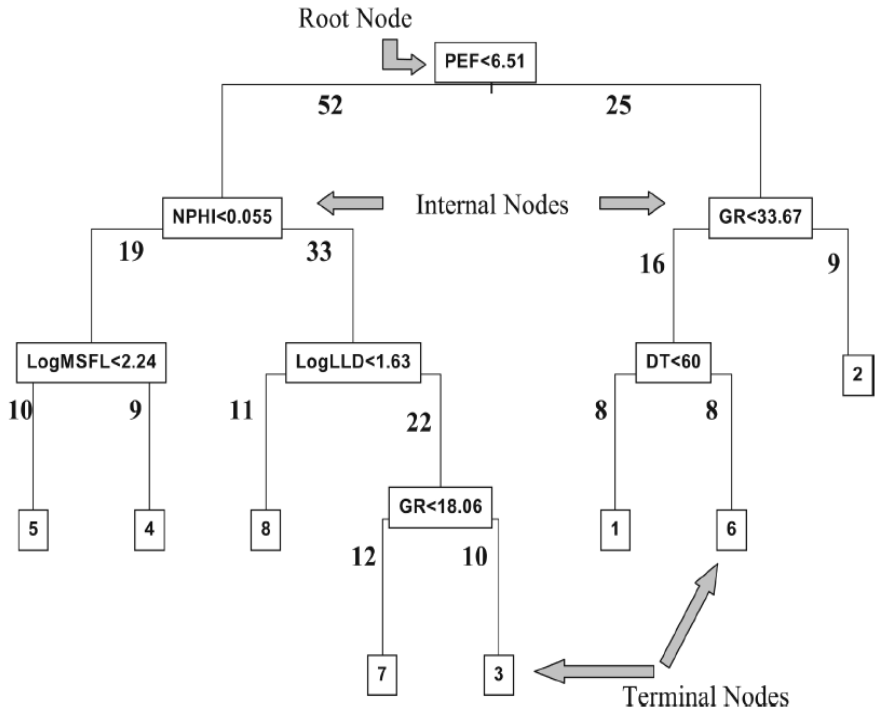

Figure 5.4. Graphical representation of a typical classification tree (Perez et al., 2005).

Figure 5.4 above shows the graphical representation of a classification tree which uses seven well logs, mentioned in the rectangular boxes, as inputs. For this tree we start with 77 samples of the respective well logs mentioned in the. The first criterion PEF<6.51 i.e. the topmost node which splits the samples between shaly sand and sands, PEF for shaly sands is about 6.52, forms the first node of the tree. The samples to left (52) are the ones which satisfy the criterion and the ones to the right (25) do not. The samples are further refined or split by applying additional criteria on the samples which form the internal nodes of the classification tree. The internal nodes and all the following nodes follow the same logic throughout to filter the available information until the process is terminated resulting into several terminal nodes. So a classification tree starts off with all the observations within a sample and uses different filters or splits to eventually terminate at the target clusters setting an identification criterion for each in the process (Perez et al., 2005).

The classification tree is based on the probability model approach and the tree is built around a central concept called deviance which is the quality of fit statistic for a model. The splits or the classifiers are chosen based on the reduction in deviance which is given by the following equation.

$$D_i = -2 \sum_k n_{ik} \ln(p_{ik}) \quad (28)$$

Where p_{ik} is the probability distribution at node i over the identified classes or clusters k, n_{ik} is the number of cases assigned to k at i. The probabilities can be estimated from the proportions at each node;

$$p_{ik} = n_{ik}/n_i \quad (29)$$

Where n_i is the total number of observations at node i.

Based on the equations above we can call deviance an ability to predict a certain class at a particular node. We start off with the root node of the classification tree with the maximum deviance as we have all the classes and all the observations at that particular node. Then we move down splitting the nodes at each point until the criterion for the terminal nodes is met. An ideal classification tree will be the one where the terminal nodes are reduced to a deviance of 0. The value of deviance will be 0 only if the number of y values for a particular class is equal to the y values of the sample at that node which means the node has been filtered to a particular class. Otherwise the nodes are declared terminal if the number of cases at a node drops below a set minimum or the maximum possible reduction in deviance for splitting a node drops below the set minimum.

The reduction in deviance at the parent node s from splitting into the child nodes t and u is given by.

$$D_s - D_t - D_u = 2 \sum_k \lfloor n_{tk} \, log(n_{tk} n_s / n_{sk} n_t) + \, n_{tk} \, log(n_{uk} n_s / n_{sk} n_u) \rfloor \quad (30)$$

Where D_s, D_t, D_u are the deviance at nodes s, t & u respectively; n_{sk}, $n_{tk,}$ n_{uk} are the y values for each class k at nodes s, t & u respectively; n_s, $n_{t,}$ n_u are the total y values at nodes s, t & u respectively.

5.4.2. Example. To better understand the process we will apply the concept of deviance to build a classification tree for the Ekofisk formation to reach the target clusters identified in the last section. Root node of the tree is the node before the 1st node of the classification tree and is not actually a part of the classification tree. The root node consists of all the values over all the given classes. The number of clusters identified for the Ekofisk formation in the last section was 3, Figure 5.3; we will call them a, b & c starting from the top of the dendrogram. The total number of observations (y values) for all the variables, well logs, at the root node is 154. The number of cases (y values) assigned to each class or clusters are:

n_a – 44, n_b – 24, n_c – 86

The probability of each can be calculated as:

$P_a = 44/154 = 0.2857$
$P_b = 24/154 = 0.1558$
$P_c = 86/154 = 0.558$

Hence the deviance can be calculated as:

$D = -2((44* \ln 0.2857) + (24* \ln 0.1558) + (86* \ln 0.558) = 299.7$

To build the classification tree, we apply different split criterion or the classifier which reduces the deviance at each node until the target classes are reached. To decide, the first split we will calculate the change in deviance for the entire range of the well log measurement considering each of the measurement as a possible split. The excel spreadsheet used for the calculation is shown in Figure 5.5.

					>=								<								
	Cluster	DTS		n	na	nb	nc	pa	pb	pc	dev	n	na	nb	nc	pa	pb	pc	dev	total dev	Δdev
3	c	114.649	3.5	154	44	24	86	0.28571429	0.15584416	0.55844156	299.678395	0	0	0	0	1	1	1	0	299.678	0.02161
4	c	115.824	3.8	153	44	24	85	0.2875817	0.15686275	0.55555556	298.508019	1	0	0	1	1	1	1	0	298.508	1.19198
5	c	116.36		152	44	24	84	0.28947368	0.15789474	0.55263158	297.327184	2	0	0	2	1	1	1	0	297.327	2.37282
6	c	116.372	3.333	151	44	24	83	0.29139073	0.1589404	0.54966887	296.135698	3	0	0	3	1	1	1	0	296.136	3.5643
7	c	117.318		150	44	24	82	0.29333333	0.16	0.54666667	294.93336	4	0	0	4	1	1	1	0	294.933	4.76664
8	c	117.467		149	44	24	81	0.29530201	0.16107383	0.54362416	293.719964	5	0	0	5	1	1	1	0	293.72	5.98004
9	c	117.986	1.54	148	44	24	80	0.2972973	0.16216216	0.54054054	292.4953	6	0	0	6	1	1	1	0	292.495	7.2047
10	c	118.415	3.954	147	44	24	79	0.29931973	0.16326531	0.53741497	291.259148	7	0	0	7	1	1	1	0	291.259	8.44085
11	c	118.441	1.356	146	44	24	78	0.30136986	0.16438356	0.53424658	290.011285	8	0	0	8	1	1	1	0	290.011	9.68872
12	c	118.502		145	44	24	77	0.30344828	0.16551724	0.53103448	288.751479	9	0	0	9	1	1	1	0	288.751	10.9485
13	c	119.062	2.787	144	44	24	76	0.30555556	0.16666667	0.52777778	287.479491	10	0	0	10	1	1	1	0	287.479	12.2205
14	c	119.213	6.146	143	44	24	75	0.30769231	0.16783217	0.52447552	286.195076	11	0	0	11	1	1	1	0	286.195	13.5049
15	c	119.259		142	44	24	74	0.30985915	0.16901408	0.52112676	284.897979	12	0	0	12	1	1	1	0	284.898	14.802
16	c	119.492	1.358	141	44	24	73	0.31205674	0.17021277	0.5177305	283.587939	13	0	0	13	1	1	1	0	283.588	16.1121
17	c	119.843	4.392	140	44	24	72	0.31428571	0.17142857	0.51428571	282.264686	14	0	0	14	1	1	1	0	282.265	17.4353
18	c	119.897	4.006	139	44	24	71	0.31654676	0.17266187	0.51079137	280.927939	15	0	0	15	1	1	1	0	280.928	18.7721
19	c	120.076	1.661	138	44	24	70	0.31884058	0.17391304	0.50724638	279.577412	16	0	0	16	1	1	1	0	279.577	20.1226
20	c	120.263	2.469	137	44	24	69	0.32116788	0.17518248	0.50364964	278.212804	17	0	0	17	1	1	1	0	278.213	21.4872
21	c	120.326		136	44	24	68	0.32352941	0.17647059	0.5	276.833809	18	0	0	18	1	1	1	0	276.834	22.8662
22	c	120.36		135	44	24	67	0.32592593	0.17777778	0.4962963	275.440108	19	0	0	19	1	1	1	0	275.44	24.2599
23	c	120.53	2.286	134	44	24	66	0.32835821	0.17910448	0.49253731	274.031369	20	0	0	20	1	1	1	0	274.031	25.6686
24	c	120.957		133	44	24	65	0.33082707	0.18045113	0.4887218	272.607251	21	0	0	21	1	1	1	0	272.607	27.0927
25	c	122.01	1.645	132	44	24	64	0.33333333	0.18181818	0.48484848	271.167401	22	0	0	22	1	1	1	0	271.167	28.5326
26	c	122.437	4.351	131	44	24	63	0.33587786	0.18320611	0.48091603	269.711452	23	0	0	23	1	1	1	0	269.711	29.9885
27	c	123.526		130	44	24	62	0.33846154	0.18461538	0.47692308	268.239022	24	0	0	24	1	1	1	0	268.239	31.461
28	c	123.752	5.104	129	44	24	61	0.34108527	0.18604651	0.47286822	266.749717	25	0	0	25	1	1	1	0	266.75	32.9503
29	c	125.238	3.948	128	44	24	60	0.34375	0.1875	0.46875	265.243128	26	0	0	26	1	1	1	0	265.243	34.4569
30	c	125.263	1.412	127	44	24	59	0.34645669	0.18897638	0.46456693	263.71883	27	0	0	27	1	1	1	0	263.719	35.9812
31	c	125.352		126	44	24	58	0.34920635	0.19047619	0.46031746	262.17638	28	0	0	28	1	1	1	0	262.176	37.5236
32	c	125.438	3.768	125	44	24	57	0.352	0.192	0.456	260.615318	29	0	0	29	1	1	1	0	260.615	39.0847
33	c	125.461	3.003	124	44	24	56	0.35483871	0.19354839	0.4516129	259.035167	30	0	0	30	1	1	1	0	259.035	40.6648
34	c	125.488	2.726	123	44	24	55	0.35772358	0.19512195	0.44715447	257.435429	31	0	0	31	1	1	1	0	257.435	42.2646
35	c	125.514		122	44	24	54	0.36065574	0.19672131	0.44262295	255.815586	32	0	0	32	1	1	1	0	255.816	43.8844
36	c	125.571		121	44	24	53	0.36363636	0.19834711	0.43801653	254.175098	33	0	0	33	1	1	1	0	254.175	45.5249
37	c	125.657		120	44	24	52	0.36666667	0.2	0.43333333	252.5134	34	0	0	34	1	1	1	0	252.513	47.1866
38	c	125.68	3.917	119	44	24	51	0.3697479	0.20168067	0.42857143	250.829905	35	0	0	35	1	1	1	0	250.83	48.8701
39	c	125.821	2.721	118	44	24	50	0.37288136	0.20338983	0.42372881	249.123999	36	0	0	36	1	1	1	0	249.124	50.576
40	c	125.9		117	44	24	49	0.37606838	0.20512821	0.41880342	247.39504	37	0	0	37	1	1	1	0	247.395	52.305
41	c	125.987		116	44	24	48	0.37931034	0.20689655	0.4137931	245.642356	38	0	0	38	1	1	1	0	245.642	54.0576
42	c	125.995	1.545	115	44	24	47	0.3826087	0.20869565	0.40869565	243.865243	39	0	0	39	1	1	1	0	243.865	55.8348
43	c	126.001	1.836	114	44	24	46	0.38596491	0.21052632	0.40350877	242.062966	40	0	0	40	1	1	1	0	242.063	57.637
44	c	126.241	1.459	113	44	24	45	0.38938053	0.21238938	0.39823009	240.234751	41	0	0	41	1	1	1	0	240.235	59.4652
45	c	126.514		112	44	24	44	0.39285714	0.21428571	0.39285714	238.379788	42	0	0	42	1	1	1	0	238.38	61.3202
46	c	126.628		111	44	24	43	0.3963964	0.21621622	0.38738739	236.497223	43	0	0	43	1	1	1	0	236.497	63.2028
47	c	126.658	2.115	110	44	24	42	0.4	0.21818182	0.38181818	234.586161	44	0	0	44	1	1	1	0	234.586	65.1138
48	c	126.784	8.307	109	44	24	41	0.40366972	0.22018349	0.37614679	232.645657	45	0	0	45	1	1	1	0	232.646	67.0543
49	c	126.817		108	44	24	40	0.40740741	0.22222222	0.37037037	230.674717	46	0	0	46	1	1	1	0	230.675	69.0253

Sheet1 | DTS | RD | RS | GR | DTC | RHOB | NPHI | Comparision

Figure 5.5. Spreadsheet for calculating change in deviance for DTS over the first node.

It can be seen in the figure above that all the DTS measurements have been placed against the corresponding DTS measurements. Since each measurement is considered as a possible split, the deviance for each of the resulting scenarios i.e. greater than equal to the measurement and less than the measurement is calculated. The sum of both is the total deviance for a particular measurement and when subtracted from the total deviance of the earlier node, which in this case is the root node with a deviance of 299.7, gives the change in deviance for a particular measurement and is calculated over the entire range of data. It is presented in the last column of the spreadsheet above as Δdev. The change in deviance calculated for DTS over its entire range is shown in the Figure 5.6 below.

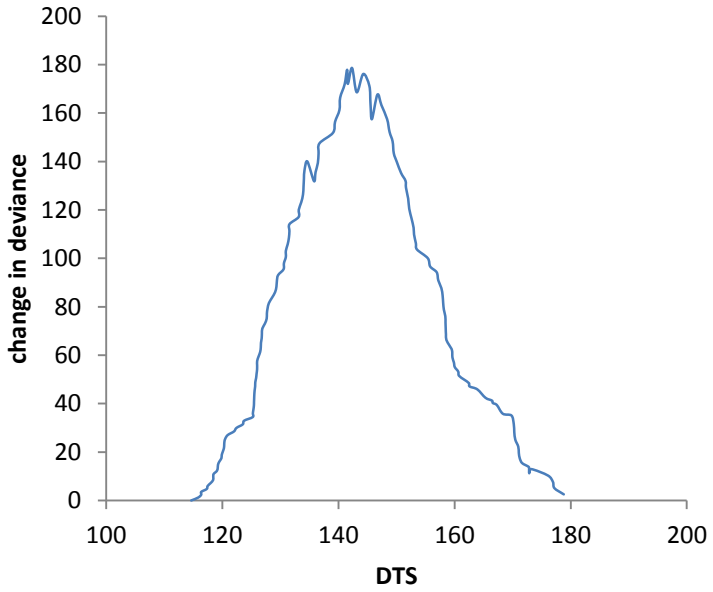

Figure 5.6. Change in deviance over the entire range of DTS.

The same method is applied to calculate the change in deviance for all the input well logs. Figure 5.7 shows a comparison between the change in deviance calculated for all the input well logs.

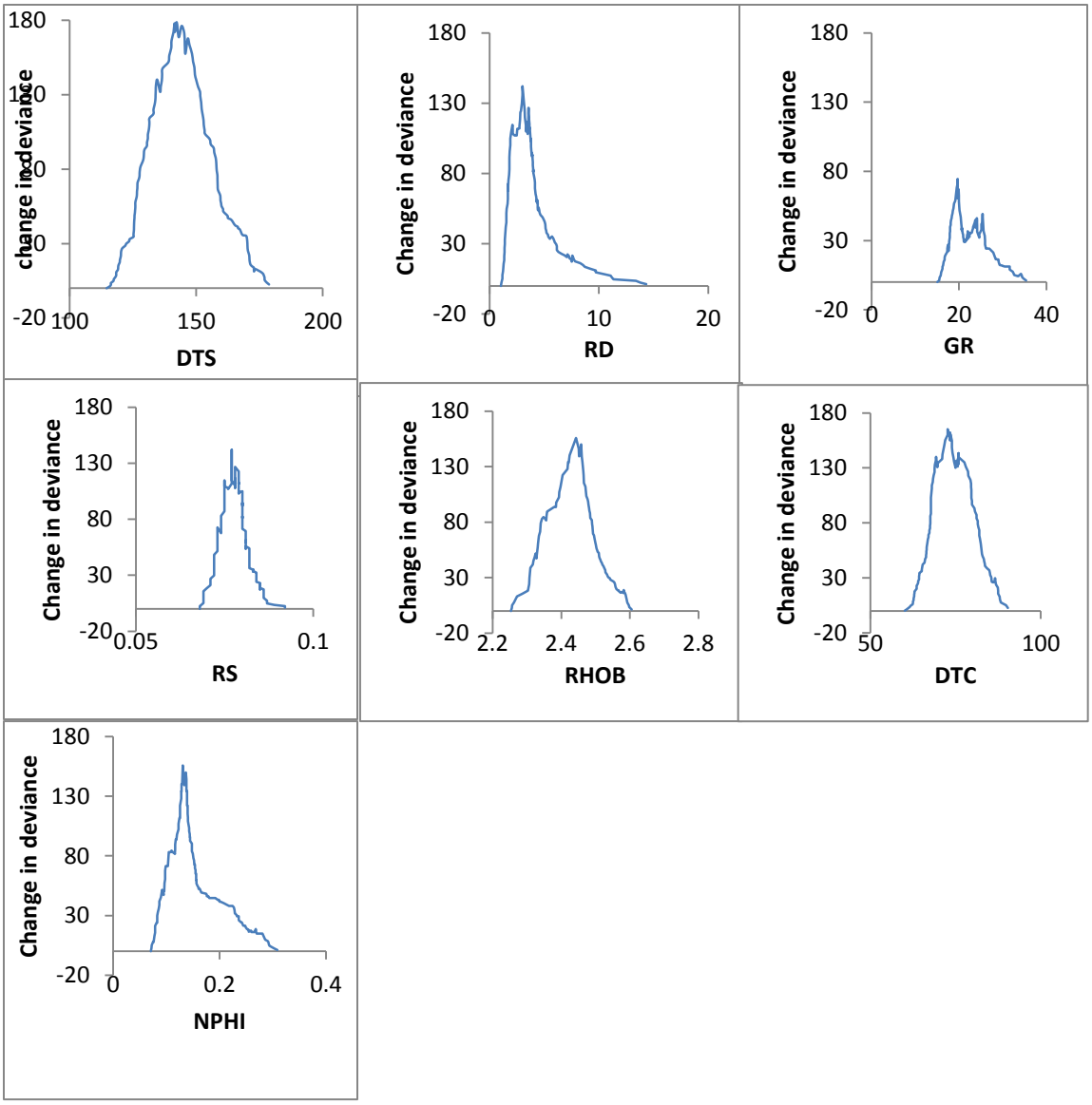

Figure 5.7. Change in deviance over the entire range of all the input well logs.

It can be seen in Figure 5.7 that the DTS log shows the maximum change in deviance at a value of 142.34 µs/ft. So this can be selected as the first split, >=142.34 and will be known as the parent node and the two resulting splits i.e. >142.34 and <142.34 will be known as the child nodes. The actual value for the split must be chosen such that

it is close to the identified split but not a part of the data set, in this case we chose 142, to avoid an unnecessary child node i.e.

142.34

$D_t(< 142) = 19$, $D_s(> 142) = 102.1$

The final classification tree for the Ekofisk formation developed following the procedure discussed above is shown in Figure 5.8.

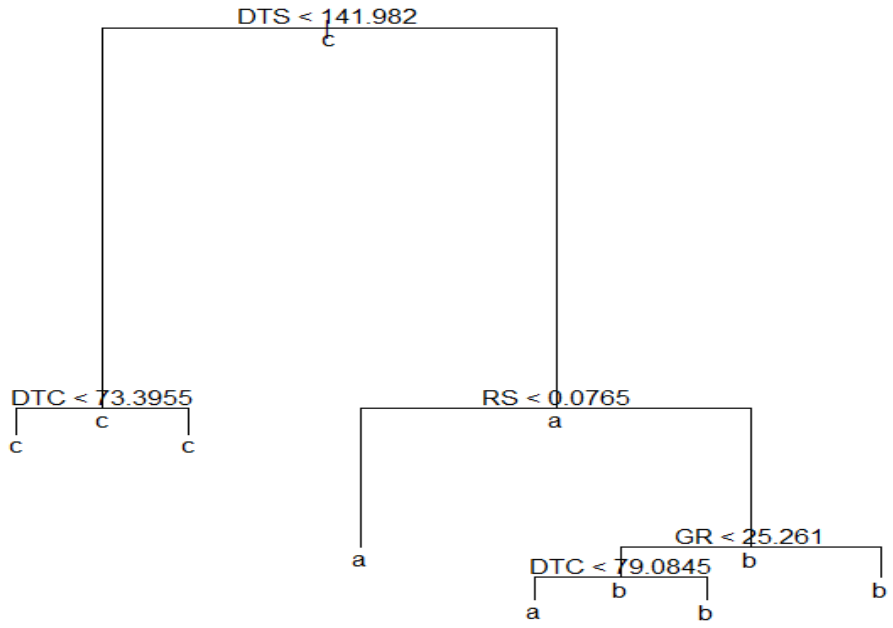

Figure 5.8. The classification tree developed for the Ekofisk based on the well log information from well E.

The decision tree developed for Ekofisk above to understand the procedure is a very simple decision tree because the formation is fairly homogenous and the identified clusters are fairly big and uniform. However, the decision trees can get very complex depending on the heterogeneity of the formation and the increasing number of target

clusters, thus making the decision criterion fairly complex. So certain methods have to be recognized to prune or snip the tree at an optimum point where the decision criterion for each cluster are fairly simple and without much misclassification. Figure 5.9 shows the change in deviance with the increasing number of nodes classification tree.

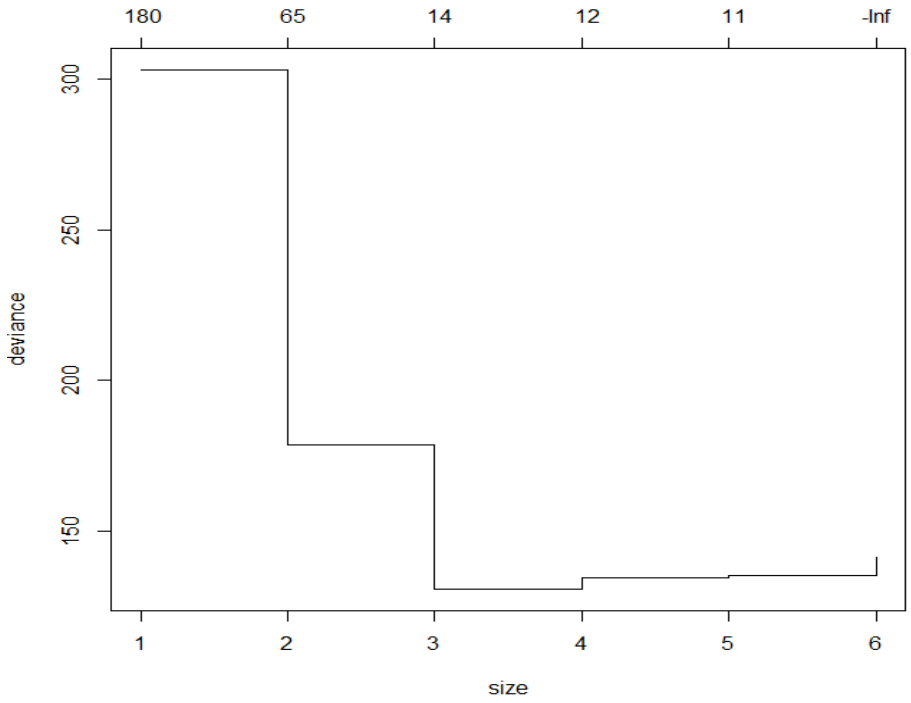

Figure 5.9. The change in deviance with the increasing number of nodes.

It can be seen in Figure 5.9 that there is a steep reduction in deviance as the size of the tree increases up to 3 nodes, increasing the number of nodes further increases the deviance rather than reducing it. As mentioned earlier that we start off a decision tree with the maximum deviance and reduce it with every node or split till the terminal node, the optimum number of nodes for this particular tree is 3 as there is no further reduction in deviance after that. So, we can snip the tree when its size is three nodes and call them terminal nodes. This result is exactly the one expected for the formation as the number of clusters identified for the formation in the cluster analysis was also 3.

5.5. APPLICATION TO FIELD

To verify the feasibility of the methods discussed above, we applied them to the actual field data from the field of study. Well log information from two of the wells in the field, well A and well D, will be used for the analysis. The well log information used was recorded for each well via wireline and comprises of Gamma ray, PEF, Sonic shear and compressive travel time, Bulk density, Neutron porosity, Resistivity measurements – Shallow, medium and deep. The formations of interest with respect to well placement for each of the well are presented in the following tables. Table 5.4 shows a lithological description of the reservoir and shoulder beds for well A.

Table 5.4. The lithological description of the reservoir and the shoulder beds for well A.

Depth interval (m)	Formation	Lithological description
1913 - 1925	Hod	Limestone
1925 - 1964	Jurassic	Sandstone and Conglomerate
1964 -2200	Triassic	Conglomerate, sandstone and Claystone

Table 5.4 shows the lithological description of the section of interest for well A. Good oil shows were observed in the Jurassic sediments with the most consistent shows being at the top of the formation and decreasing gradually to patchy towards the bottom of the formation and finally disappearing as the Triassic sediments were penetrated. Hence, an ideal well placement in this scenario would be a horizontal lateral maintained in the top portion of the Jurassic formation while avoiding an exit into the Hod formation above and the Triassic sediments below the reservoir.

Table 5.5 shows the lithological description for the section of interest for well D. The top shoulder bed for this scenario is Cromer Knoll whereas the section below comprises of Jurassic and Triassic sediments. Our well placement goal for this well is to distinguish the sandstone from the conglomerate and several clasts of granite present while also avoiding an exit into the Cromer Knoll.

Table 5.5. The lithological description of the reservoir and the shoulder beds for well D.

Depth interval (m)	Formation	Lithological description
1913 - 1925	Cromer Knoll	Limestone with ocassional chert layers
1925 - 2150	Jurassic/Triassic	Sandstone, conglomerate and several clasts of granite

The sections from the two wells will be divided into homogeneous clusters by using the principal component analysis and hierarchal clustering. The concept of deviance, discussed earlier, will then be used to set the decision criteria for the identified clusters. To reduce the noise in the well log information, each measurement was averaged over a meter of depth. As already mentioned, there is no defined criterion to identify an optimum number of clusters, each analysis was repeated several times with different number of clusters and matched with the lithology described in the core reports for each well to identify the optimum number of clusters and the classification tree. The results are presented in the next section.

5.6. RESULTS

The analysis for well A that exhibited the most appropriate match was the one with nine clusters. The identified clusters are presented in Table 5.6 along with the corresponding depth intervals and formations. It can be seen in Table 5.6 that the clusters ‘a’ and ‘b’ which constitute the Hod formation do not show up again down in the Jurassic or the Triassic formation as the hod formation is a totally different lithology than Jurassic or Triassic sediments, Table 5.4. However, the Jurassic and the Triassic sediments do share some common clusters. When matched with the core descriptions cluster ‘e’ represents the sandstone and comprises of a good 6m thick interval, 1928.2-1934.2, which can be a potential zone for geosteering. As already discussed one lithofacies can consist of two or more electrofacies or clusters, clusters ‘g’ and ‘i’ represent two electrofacies within the pebbly sandstone, clusters ‘f’ and ‘h’ represent two electrofacies within granite and cluster ‘j’ represents the conglomerate. The clusters show a good

match with core lithologies with some uncertainties at certain depths, for example the interval 1952.5 – 1954.8 which is actually sandstone as per the core lithology is identified as pebbly sandstone here. In order to be of assistance to well placement each cluster should have a distinct decision criterion. Figure 5.10 show the classification tree devised for well A.

Table 5.6. Identified clusters with the corresponding depth intervals, well A

Depth interval (m)		Formation	Cluster
1913	1913.26	Hod	a
1916.022	1925.166	Hod	a
1925.166	1916.022	Hod	b
1916.022	1928.214	Jurassic	d
1928.214	1934.31	Jurassic	e
1938.882	1940.406	Jurassic	e
1934.31	1935.072	Jurassic	f
1935.834	1937.358	Jurassic	f
1940.406	1941.168	Jurassic	f
1941.93	1942.692	Jurassic	f
1943.454	1944.216	Jurassic	f
1948.788	1949.55	Jurassic	f
1952.598	1954.884	Jurassic	f
1956.408	1957.17	Jurassic	f
1964.79	1965.552	Triassic	f
1970.124	1970.886	Triassic	f
1985.364	1986.888	Triassic	f
1935.072	1935.834	Jurassic	g
1937.358	1938.882	Jurassic	g
1941.168	1941.93	Jurassic	g
1948.026	1948.788	Jurassic	g
1949.55	1952.598	Jurassic	g
1954.884	1956.408	Jurassic	g
1957.17	1964.79	Jurassic	g
1965.552	1967.076	Triassic	g
1968.6	1969.362	Triassic	g
1970.886	1971.648	Triassic	g
1978.506	1980.03	Triassic	g
1984.602	1985.364	Triassic	g
1986.888	1987.65	Triassic	g
1944.978	1945.74	Jurassic	h
1973.934	1974.696	Triassic	h
1989.174	1996.794	Triassic	h
1997.556	1999.08	Triassic	h
1999.842	2000.604	Triassic	h
1945.74	1948.026	Jurassic	i
1946.502	1947.264	Jurassic	i
1967.076	1968.6	Triassic	i
1971.648	1973.934	Triassic	i
1976.22	1978.506	Triassic	i
1980.03	1984.602	Triassic	i
1987.65	1989.174	Triassic	i
1996.794	1997.556	Triassic	i
1999.08	1999.842	Triassic	i
1942.692	1943.454	Jurassic	j
1944.216	1944.978	Jurassic	j
1969.362	1970.124	Triassic	j
1974.696	1976.22	Triassic	j

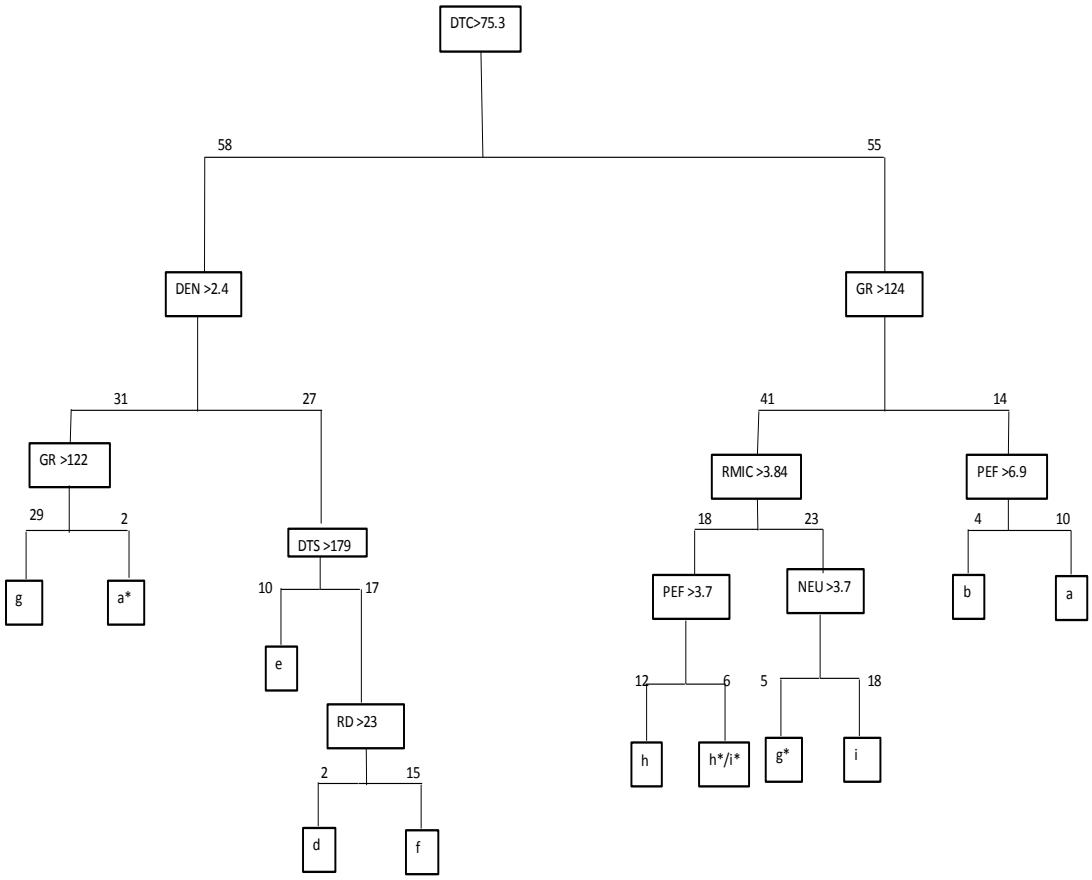

Figure 5.10. Classification tree for well A

Each rectangular box in Figure 5.10 represents a node and the classifier used for the split at that particular node is mentioned in the box. The number above the lines represents the observations, the one to the left denotes the observations that agree with the classifier and the one to the right denotes the observations that disagree. The small boxes where a particular decision criterion terminates are the terminal nodes and represent a cluster. As can be seen in the figure, all of the clusters have a distinct decision criterion. At some of the terminal nodes cluster name is followed by "*" and they represent the misclassification error for the analysis which is 13 for this particular analysis. However, the potential steering cluster i.e. 'e' has no associated classification error. Figure 5.11 shows the classification tree for the same section of well A devised for 12 clusters. It can be seen in Figure 5.11 that the misclassification error in this case is 87

which is much higher than the analysis conducted with 9 clusters, Figure 5.10. The clusters identified for the earlier analysis efficiently explained the variations within the section but the extra number of clusters here just complicate the process by adding to the number of nodes in the tree and are not actually required.

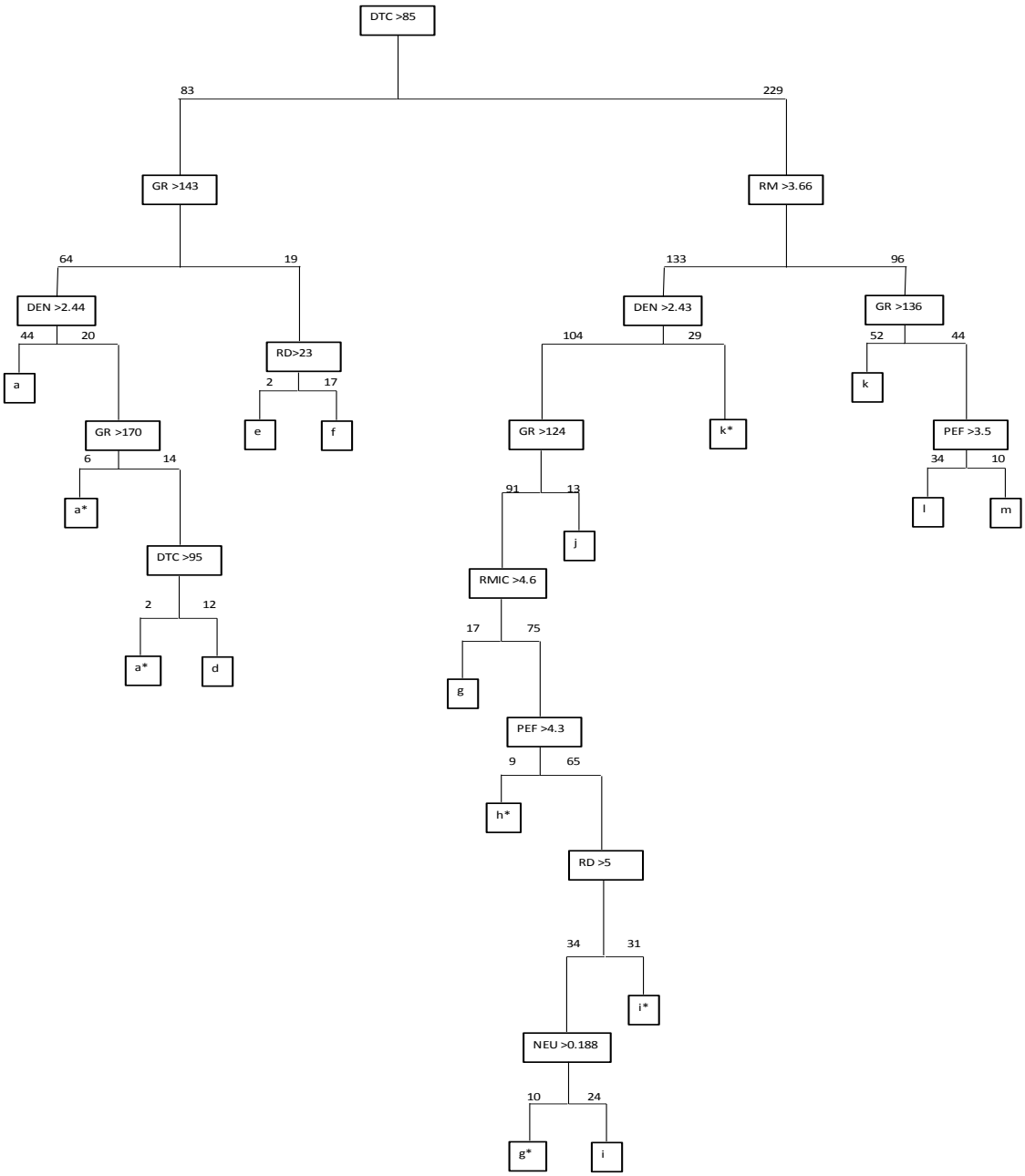

Figure 5.11. Classification tree for well A devised for 12 clusters

Results of Principal component analysis and hierarchal clustering for well B are presented in Table 5.7 with the corresponding depth intervals and Figure 5.12 shows the classification tree.

Table 5.7. Identified clusters with the corresponding depth intervals, well D

Depth interval (m)		Formation	Cluster
1931.518	1933.042	Jurassic	a
1934.566	1935.328	Jurassic	a
1957.426	1958.188	Jurassic	a
1971.904	1972.666	Jurassic	a
1978	1979.524	Jurassic	a
1981.048	1981.81	Jurassic	a
1983.334	1984.096	Jurassic	a
1917	1917.802	Cromer knoll	c
1917.802	1918.564	Cromer knoll	c
1925.422	1926.184	Jurassic	d
1930.756	1931.518	Jurassic	d
1933.804	1934.566	Jurassic	d
1935.328	1936.09	Jurassic	d
1971.142	1971.904	Jurassic	d
1977.238	1978	Jurassic	d
1990.192	1992.478	Jurassic	d
1918.564	1920.088	Jurassic	e
1920.85	1923.898	Jurassic	e
1984.858	1987.144	Jurassic	f
1993.24	1994.002	Jurassic	f
1997.812	1999.336	Jurassic	f
1928.47	1929.232	Jurassic	g
1929.232	1929.994	Jurassic	g
1938.376	1944.472	Jurassic	g
1945.996	1946.758	Jurassic	g
1947.52	1948.282	Jurassic	g
1948.282	1949.044	Jurassic	g
1950.568	1951.33	Jurassic	g
1953.616	1954.378	Jurassic	g
1955.14	1955.902	Jurassic	g
1960.474	1961.236	Jurassic	g
1961.998	1962.76	Jurassic	g
1980.286	1981.048	Jurassic	g
1992.478	1993.24	Jurassic	g
1999.336	2000.098	Jurassic	g
1937.614	1938.376	Jurassic	h
1944.472	1945.234	Jurassic	h
1946.758	1947.52	Jurassic	h
1949.044	1950.568	Jurassic	h
1952.854	1953.616	Jurassic	h
1961.236	1961.998	Jurassic	h
1963.522	1964.284	Jurassic	h
1966.57	1969.618	Jurassic	h
1969.618	1971.142	Jurassic	h
1972.666	1977.238	Jurassic	h
1981.81	1983.334	Jurassic	h
1984.096	1984.858	Jurassic	h
1987.144	1990.192	Jurassic	h
1994.002	1997.812	Jurassic	h
1924.66	1925.422	Jurassic	j
1926.184	1928.47	Jurassic	j
1929.994	1930.756	Jurassic	j
1933.042	1933.804	Jurassic	j
1936.09	1936.852	Jurassic	j
1936.852	1937.614	Jurassic	j
1945.234	1945.996	Jurassic	j
1951.33	1952.854	Jurassic	j
1954.378	1955.14	Jurassic	j
1955.902	1957.426	Jurassic	j
1958.188	1960.474	Jurassic	j
1962.76	1963.522	Jurassic	j
1964.284	1966.57	Jurassic	j
1979.524	1980.286	Jurassic	j

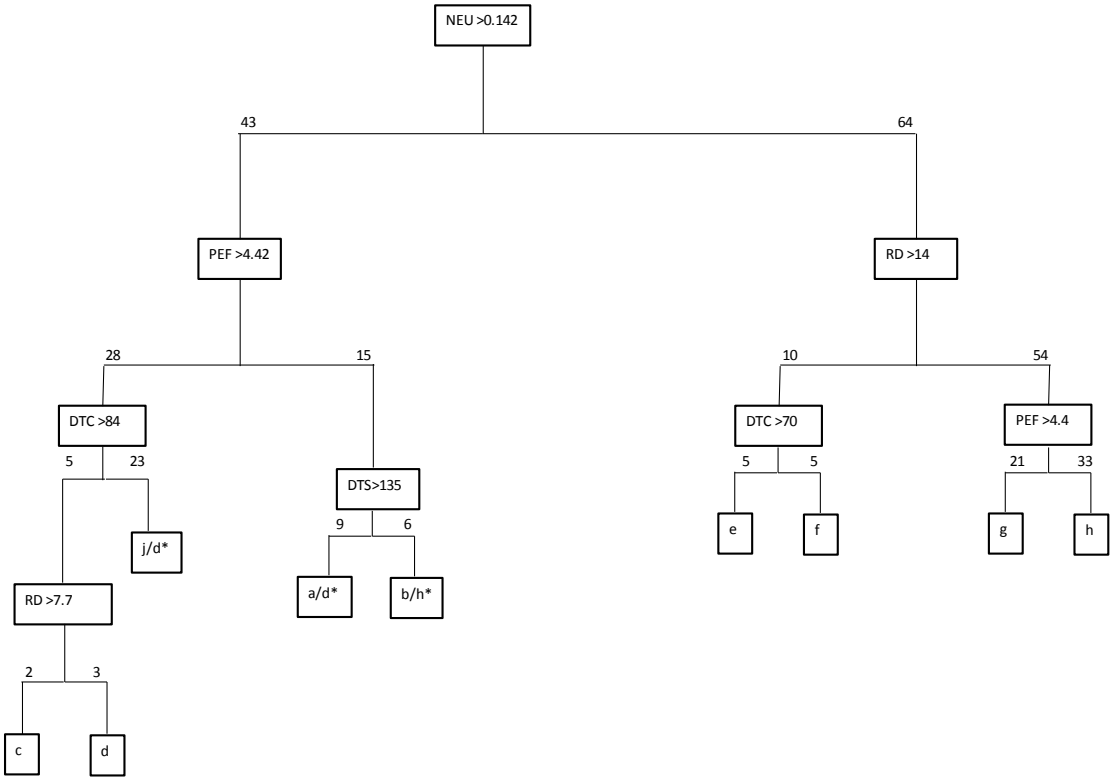

Figure 5.12. Classification tree for well D

It can be seen in Table 5.7 that Cromer knoll is comprised of just one cluster ‘c’ which does not repeat itself anywhere below Cromer knoll. The Jurassic/Triassic sediments below are comprised of 8 clusters. Cluster ‘e’ is present at the top of the Jurassic/Triassic sediments and does not repeat itself below. Correlation with the core lithology shows that it is a sandstone layer whereas the other clusters represent various clasts of granite and conglomerates with some uncertainties at certain depths. The uniqueness of the decision criterion for each cluster is confirmed by the classification tree for the section, Figure 5.12.

The misclassification error for the classification tree in Figure 5.12 was 5, which is very low and represents a good classification. All the clusters have a distinct decision criteria and efficiently explain the variations within the section.

The results presented here can be accurately used to distinguish between the potential and non-potential steering clusters as the identified clusters have distinct

decision criteria and efficiently explain the variations within the section, as verified with the core lithology. Picking the right number of clusters is very important for the accuracy of the analysis. The picked clusters should be able to account for all the variations within the section.

5.7. VALIDATION OF THE METHOD

In the last section we applied the method of classification tree to the highly heterogeneous Luno field and as is evident from the results the method can be used to define certain homogeneous regions within a heterogeneous body, using the small variations in the well log information, with a distinct classification criterion for each. To determine if the method can be used accurately for well placement we need to verify its transferability to other wells. To do that we will construct the classification trees for two similar sections of formation but from different wells using the same set of well logs as inputs. The two sections were picked based on the Gamma ray correlation. Figure 5.13 shows a section of Gamma ray responses for the fractured basement for the wells B and D.

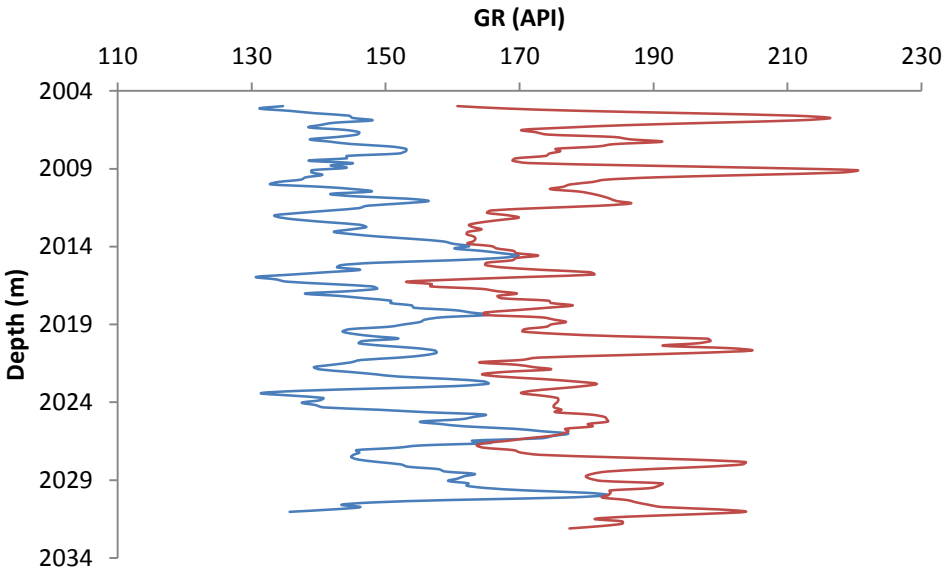

Figure 5.13. GR responses for a section of the fractured basement for the wells B and D.

Figure 5.13 shows the Gamma ray responses for the two sections of the fractured basement from different wells. The fractured basement is made up of fractured granite and is the basement or the lower shoulder bed for most of the Luno reservoirs. It can be seen in the figure that the gamma ray responses for both the selections follow almost the same trend with the numbers being a little higher for the well D. The thickness of the section for well D is 26m and the thickness for that of well B is 25 m.

The input logs used for the classification tree construction are Sonic compressive travel time, Gamma Ray, Neutron porosity, Bulk density, deep and medium resistivity. Same approach was used for the tree construction and the classifiers were selected based on the maximum change in deviance. Figures 5.14 and 5.15 show the devised classification trees for the sections of wells D and B respectively.

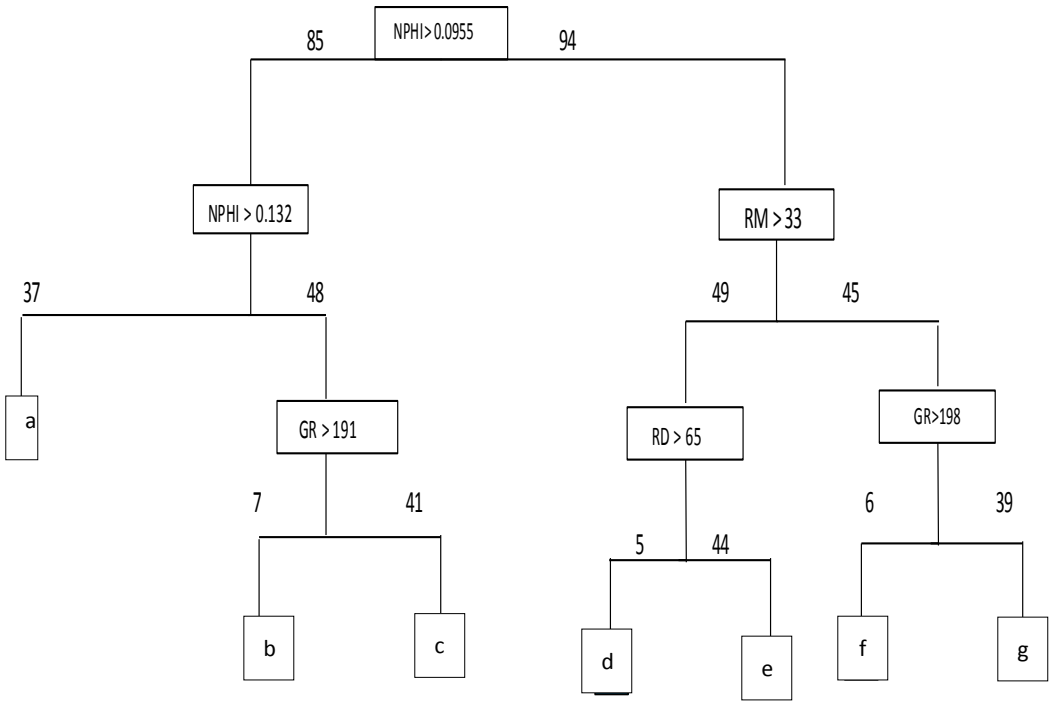

Figure 5.14. Classification tree for the selected section of fractured basement for well D.

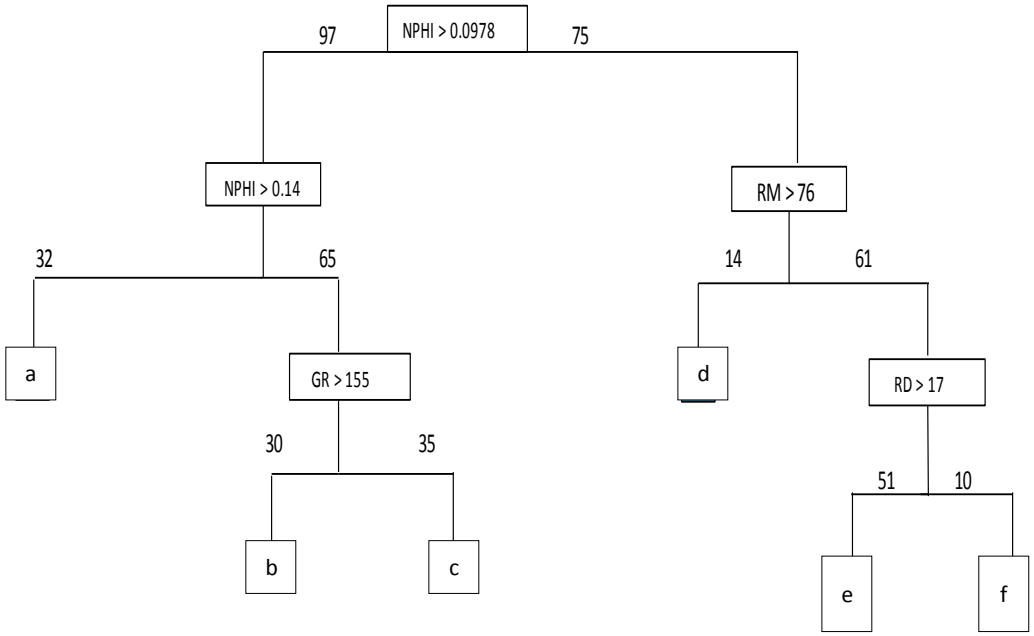

Figure 5.15. Classification tree for the selected section of fractured basement for well B.

It can be seen in figures 5.14 and 5.15 that the first classifier is same for both the sections i.e. NPHI and the values for the classifiers are fairly close as well – 0.0955 and 0.0978 for wells D and B respectively. As we move down the classification trees, the internal nodes follow a similar trend for both the sections with the classifiers being the same but the values being different. For example, the second or the last internal node for the left section of each tree is Gamma ray but well D has a higher classifier value i.e. 191 as compared to B, 155, which was expected as we have already seen in the gamma ray correlation, Figure 5.13, that both the sections do correlate but the responses for well D have values higher than B and hence we expect a similar trend for the log responses but different numbers for the two wells. The number of observations within the clusters are also different as a certain identified electrofacies or cluster is likely to have different thicknesses in different wells. Also the number of identified facies or the clusters are different for both the wells i.e. 7 for well E and 6 for well B.

5.8. APPLICATION TO WELL PLACEMENT

The clustering method discussed above descibes the possible variations in a reservoir and resolves a reservoir or a rock body into several homogenous compartments and the classification tree sets the classification criterion for each cluster. The classification criterion set by the tree are particularly useful when we are unable to identify certain distinct well placement features such as bright spots, polarization horns etc. For these features to exist we need the big contrast between the reservoir and the shoulder beds or the reservoir and the non-reservoir section but when using the classification tree we utilize the minor variations within the formation to quantify a classification criterion for the small homogenous bodies within the formation. The criterion is a robust one as we do not rely on a single log measurement or feature but instead we use a set of log measurements to define a certain cluster.

However, there is a limitation associated with the cluster analysis and that is the identification of the optimum number of clusters. The identified clusters for a particular formation must be able to accurately define different homogenous bodies within the formation such that they account for all the variations within the section but the statistical methods used lack a defined criterion. As we have seen in the last section picking an inaccurate number of clusters can have an adverse effect on the accuracy of the analysis. The approach will be most useful and accurate when the identified clusters are matched with the lithology from the core descriptions. If the clusters or the facies are identified accurately we just need to put them against the corresponding depths and the log measurements to devise a classification tree using the same approach that was discussed in the last sections. If the classification tree so constructed still cannot classify the clusters accurately, it means that the set of input well logs being used are not good enough to map the present facies.

The well logs used for all the classification trees discussed above were wireline logs which are more suitable as far as the construction of the tree is concerned. Wireline logs do not work in the same harsh drilling conditions as their LWD counterparts, hence are less prone to distortion and while quantifying the classification criterion for the clusters or the electrofacies we want the input information to be accurate. To extend the use of this method to real time well placement we need an algorithm into which the

desired LWD information, as per the classification tree, is fed and matched against the predefined classification criterion for the clusters to identify the cluster that the well is traversing. As per the results for well A discussed in Section 3.6, we do identify some clusters with good thickness in the desired part of the reservoir that can be potential targets for the well placement. Although each cluster has a distinct classification criterion, steering with the method would still be reactive because we have to drill into the formation to attain a few sample points that can be matched against the predefined criteria.

One of the other important applications of the method is that it helps demonstrate the sensitivity of each measurement with respect to the formation as a whole and each cluster as well. Referring to Figure 5.12, the classifiers in the classification tree for the well D are comprised of just five well logs out of the nine that were used as inputs. As already discussed, identifying and compartmentalizing the right information is a very important aspect of geosteering as the real time well path adjustment needs quick decisions on the fly. So we need to identify just the right amount of information that is good enough to map the formations of interest.

An LWD suite consists of various measurements with the sensors being placed at some distance behind the bit. Thus, it is very important to identify and have the most sensitive LWD tool right behind the bit so it responds to the current formation being drilled and avoid any unnecessary exits. The sensitivity of each measurement as demonstrated by the classification tree can help us prioritize the tools and thus decide their position in the LWD suite with the measurement of topmost priority, root node of the classification tree, being right behind bit followed by the other measurements, internal nodes, moving farther away from the bit in a descending order of assigned priority.

6. CONCLUSIONS

Three different methods to geosteer were studied and analyzed for the applicability on the field of study, located in the Norwegian North Sea. The conclusions based on the analysis are as below.

The decision matrix was developed based on the case study of various LWD tools and applied to the field of study to decide the LWD suite that can address the well placement challenges in the field. The decided LWD suite comprises of Gamma ray measurements as a correlate

on tool and to identify the conglomerates, Deep azimuthal resistivity as the bed boundary marker, Azimuthal density images for real time dip calculation, Azimuthal sonic measurements to distinguish between the reservoir and the conglomerates and Laterolog resistivity to accurately map the heterogeneities within the reservoir and identify the sweet spot. The identified tools have not been tested on the field yet but the certain log responses from the field indicate that the tool can be of assistance to well placement. However if we expect a field to have laterally extensive responses the decision matrix can be applied to the field with minimum uncertainty.

As identified from the decision matrix, Propagation resistivity is the only proactive geosteering tool but case study of Azimuthal Sonic tool indicate that the tool can have a good Depth of Investigation which depends on the porosity contrast and can be used as a proactive steering tool wherever the favorable conditions exist. However, the tool has not been tested in the field yet.

MSE and UCS demonstrated their ability to footprint formations but with some associated uncertainties like transferability of the properties between wells. Both the properties have demonstrated an ability to distinguish between the formations of interest but MSE clearly performs better than UCS in distinguishing between formations. These conclusions are however based on a limited dataset i.e. the well logs for two wells, if a bigger dataset will give us a better picture of the foot printing ability of each. Also the MSE values for the two wells were different, hence it must be used as a trending tool rather than a quantitative tool.

Classification trees accurately define quantitative decision criterion for the clusters identified using the hierarchal clustering method. The principal component analysis was used to reduce the dimensionality and redundancy in the well log data. As the results indicate, clusters can be distinguished from each other and each one has unique and robust decision criteria which does not depend on just one log but is defined by a set of those. However, there is no defined optimal criterion to pick an accurate number of clusters for the hierarchal clustering method. If the number of clusters picked is significantly different from the actual clusters or facies, the classification tree would still set classification criteria for each but the results might be complicated or oversimplified making the steering strategy less accurate in either case. If the picked number of clusters are less than the actual facies, it oversimplifies the classification tree and the criteria for the classified clusters may not be robust whereas if the picked number of clusters is more, the classification tree is more complex resulting in a higher classification error and a very thin clusters which offer a very tight steering window. Another important application of the classification tree is that it represents the log measurements actually required to define the identified clusters and also describes the sensitivity or the ability of each towards the clusters. Hence, the method can be used in conjunction with the decision matrix to decide on the LWD suite and also help us determine the placement of the decided LWD suite behind the bit with the most sensitive measurement being right behind the bit.

APPENDIX A

MINIMUM CURVATURE METHOD

Minimum curvature method uses the hole angle measured i.e the inclination and hole direction measured at consecutive survey points to generate a smooth circular, curve that represents the well path. Between each survey pair we calculate Δx, Δy and Δz at the survey points and sum them to define the position of the well bore in the 3D space at a particular point. The surveys at the two points or stations represent the vectors or the vectors, A_1B and A_2B in Figure 1.5, which are tangent to the well bore. A ratio factor, RF, is used to smoothen the tangent vector onto the well bore curve. Figure 1.5 shows a representation of the ratio factor, which is expressed mathematically as

$$RF = \frac{2}{\beta} * \tan(\frac{\beta}{2}) \text{ (rad)} = \frac{2*180}{\beta*\pi} * \tan(\frac{\beta}{2}) \text{ (°)} \quad (1)$$

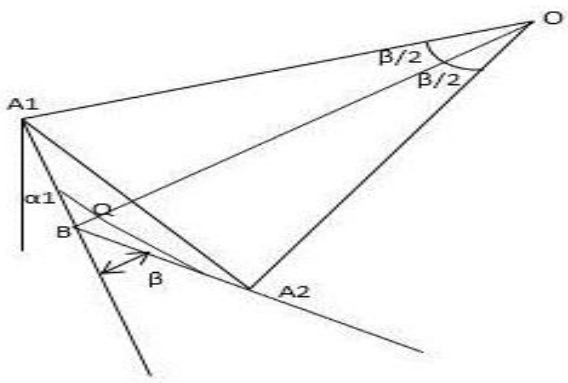

Figure A.1. Representation of minimum curvature ratio factor

Once the RF has been calculated the departures in the respective directions can be calculated by the following equations:

$$\Delta x = \frac{\Delta MD}{2}(\sin\alpha_1 . \sin Az_1 + sin\,\alpha_2 . \sin Az_2)RF \quad (2)$$

$$\Delta y = \frac{\Delta MD}{2}(\sin \alpha_1 . \cos Az_1 + sin\, \alpha_2 . \cos Az_2)RF \quad (3)$$

$$\Delta z = \frac{\Delta MD}{2}(\cos \alpha_1 . + \cos \alpha_2)RF \quad (4)$$

Where β is the Dog leg severity and is given by the following equation

$$\beta = \arctan(\cos(\alpha_2 - \alpha_1) - (sin\alpha_1 . sin\alpha_2(1 - \cos(Az_2 - Az_1))) \quad (5)$$

Where α_1 , α_2 are angle of inclination at points A_1 and A_2 respectively,Az_1, Az_2 are the azimuths at points A_1 and A_2, MD is the Measured depth, Δx is the departure in the West–East direction, Δy is departure in the North–South direction and Δz is the TVD departure.

APPENDIX B

MATHEMATICAL DESCRIPTION OF ELECTRICAL IMPEDANCE

Electrical impedance is the measure of the opposition to the alternating currents describing not only the relative amplitude of the voltage and current but also the relative phases or in simple terms we can say that the impedance is the resistance as applied to the alternating currents. It has two components; one is the frequency independent component which is given by

$$G = \sigma A/l \quad (1)$$

Where G is the Formation conductance, σ is the Formation conductivity (mmho), A is the Area through which the measurement current passes (m^2) and L is the Characteristic measurement length (m)

This equation is the governing equation for the laterolog measurements, as will be discussed later, expressed in terms of conductivity rather than resistivity. Now since the propagation resistivity tools work at a higher frequency, the frequency dependent term X i.e. the formation capacitance must be taken into. Formation capacitance is expressed mathematically as below.

$$X=i\omega\epsilon_s A/L \quad (2)$$

Where i is the imaginary unit and equal to sqrt(-1), ω is the Angular frequency and equal to 2πf and ε_s is the Formation dielectric constant

Thus, the complex conductance Z, inverse of impedance, can be given in the Cartesian coordinates by the following expression:

$$Z=G+iX \quad (3)$$

Where G, conductance, is the real part and X, formation capacitance is the imaginary part and the expression, Z, is the vector sum of the two quantities.
The amplitude,$|Z|$, and phase, ‹Z, of the conductance are:

$$|Z| = \sqrt{G^2 + X^2} \quad (4)$$

$\angle Z = arctan(X/G)$ (5)

The ohm's law, if mentioned in terms of conductance is given by:

$V = I/G$ (6)

Now for an AC circuit, if we replace the conductance G with the complex conductance, the total current that flows through the formation can be given by

$I_T = V.Z$ (7)

Plugging eq. (4), (5) and (6)

$I_T = (\sigma + i\omega\varepsilon) A/L.\ V$ (8)

It can be seen in the above expression that the tool's response depends on the conductivity and the dielectric constant of the formation and thus some correlation algorithm or chart must be used. Figure B.1 shows a correlation between resistivity and relative dielectric constant ε_r, which is dielectric constant of the material ε_s divided by the dielectric constant of the vacuum, devised by Schlumberger using hundreds of sandstone and carbonate core samples fully and partially saturated with water (Griffiths, 2009).

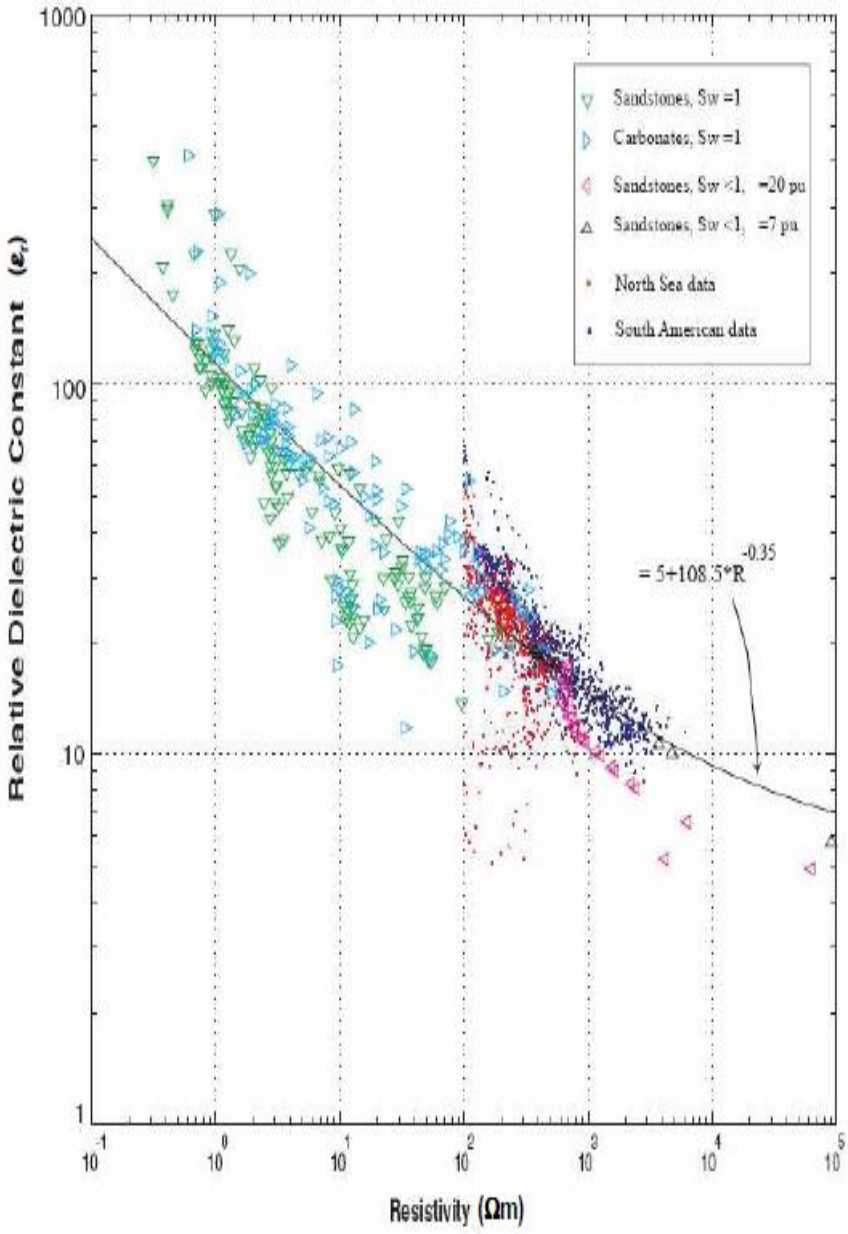

Figure B.1. Correlation chart for resistivity and relative dielectric constant (Schlumberger). (Griffiths, 2009)

APPENDIX C

AZIMUTHAL PROPAGATION RESISTIVITY TOOLS

Propagation tools are perhaps the most important tools and are the primary source of proactive geo-steering because of their large depth of investigation. Large DOI of the tool combined with the directional or azimuthal ability of the tool aids in steering the well path in real time. The propagation resistivity tool that we discussed above just gives us the basic working principle of propagation resistivity using co axial antennas which lack azimuthal or directional ability.

The top section of the Figure C.1 shows a 3D radiation pattern of an antenna along its coordinate axes, the antenna has its vertical axis in the z direction. The coaxial transmitter and receiver coils of the propagation resistivity tools can be thought of loop antennas with the loop being in the x-y plane and the vertical axis of the loop in the z direction. So the transmitting and receiving antennas would have a radiation and receiving pattern similar to that shown in the figure. Figure C.2 shows a 2D plot of the strength of the radiation, for the same antenna, with respect to the polar angle, angle off the z axis and azimuth, angle measured counterclockwise off the x axis. It can be seen that be maximum signal strength is at a polar angle of 90° i.e. in the x-y plane whereas the strength is constant at maximum with respect to the azimuth. This is a typical case when a coaxial transmitter and receiver are coupled; the receiving coil has the maximum sensitivity in the x-y plane, therefore it scans the borehole in a circumference around it and is not azimuthally sensitive. Now to make the tool azimuthally sensitive we tilt either a transmitter or a receiver. The tilted antenna would still have the maximum sensitivity in its x-y plane but this plane is now tilted with respect to the tool x-y plane of the tool, the sensitive point with respect to the azimuth will be the point where the x-y plane of the tilted receiver coincides with the x-y plane of the tool. Therefore the receiving antenna will now have the maximum signal strength from a particular portion of the circumference around the tool rather than the strength being constant all around the circumference. This is how the propagation tools achieve azimuthal sensitivity; the orientation of the tilted coil at a particular point is given by a dedicated magnetometer.

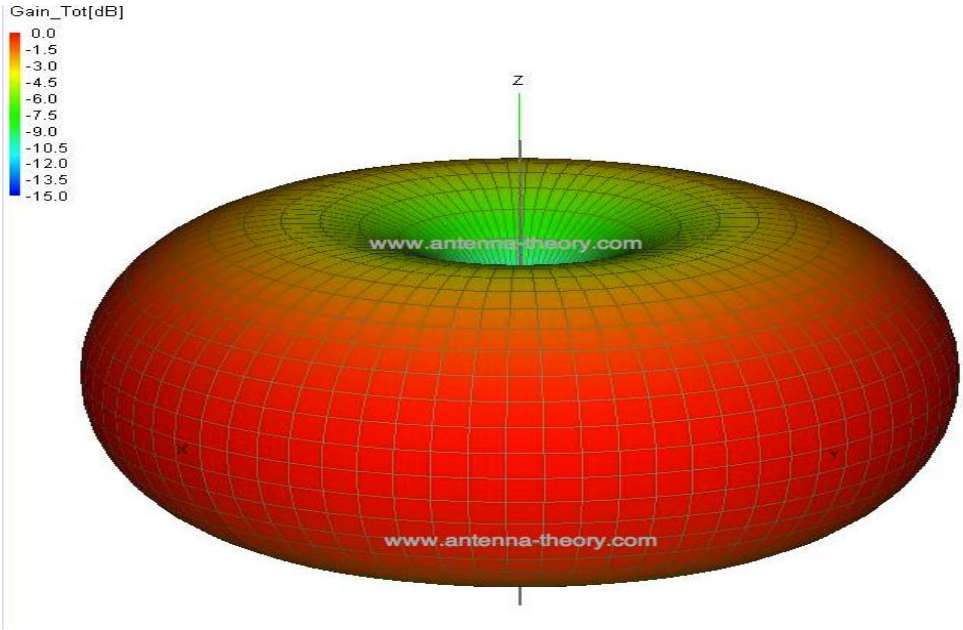

Figure C.1. 3D radiation pattern of an antenna (antennatheory.com).

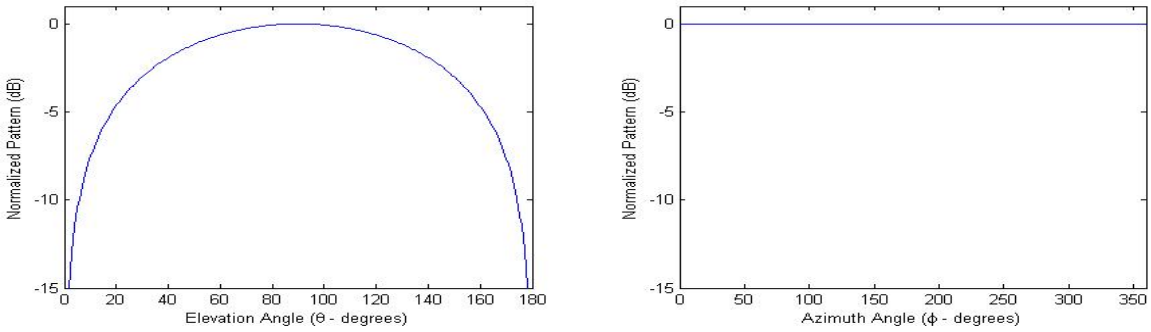

Figure C.2. 2D representation of the signal strength with respect to the polar angle and azimuth.

The first LWD directional resistivity tool, Periscope, was introduced by Schlumberger in 2005 followed by Azimuthal propagation resistivity (APR) by Baker Hughes in 2006 and Azimuthal deep resistivity (ADR) by Halliburton in 2007. These tools have almost the same working principle with different hardware designs and slightly different capabilities.

The azimuthal deep resistivity sensor array for these tools consist of certain pairs of transmitters which launch a series of electromagnetic wave trains from different spacing and frequencies: 2 MHz, 500 KHz and 125 KHz and a pair of receivers measure the phase shift and attenuation. The ADR uses only the transmitters symmetrical to the middle of the array whereas Periscope and APR use the transverse transmitters as well. These tools achieve their azimuthal sensitivity through the tilted and transverse current loop antennas. The multispacing and multifrequency measurements allow the detection of the distance to the boundaries and their orientation and thus facilitate proactive geo-steering for optimal well placement. The hardware design of each tool is shown in the following Figures C.3 through C.5 (Zhang et al, 2008).

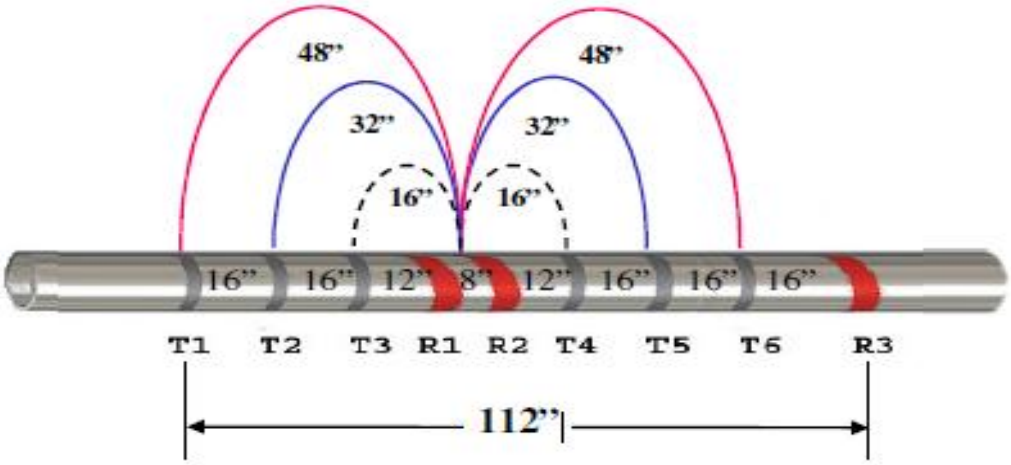

Figure C.3. Azimuthal deep reading resistivity (ADR) from Halliburton (Zhang et al, 2008).

Figure C.3 shows the multispaced coaxial transmitters, T1 through T6, and the tilted receivers, R1 through R3, arrangement for the Azimuthal Deep Resistivity tool from Halliburton. The transmitter and receivers here have a three spacing arrangement i.e. 16", 32" and 42".

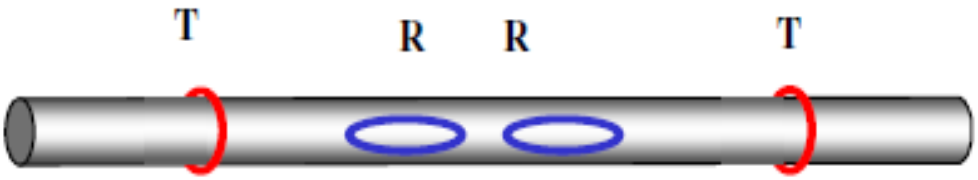

Figure C.4. Azimuthal propagation resistivity (APR) from Baker Hughes (Zhang et al, 2008).

Figure C.4 shows the transmitter and receiver arrangement for The APR tool, Baker Hughes, which comprises of two coaxial transmitters and the two transverse receivers. The APR is a complete geo-steering tool and has to be run with conventional resistivity to allow formation evaluation. The APR is a complete geo-steering tool and has to be run with conventional resistivity to allow formation evaluation.

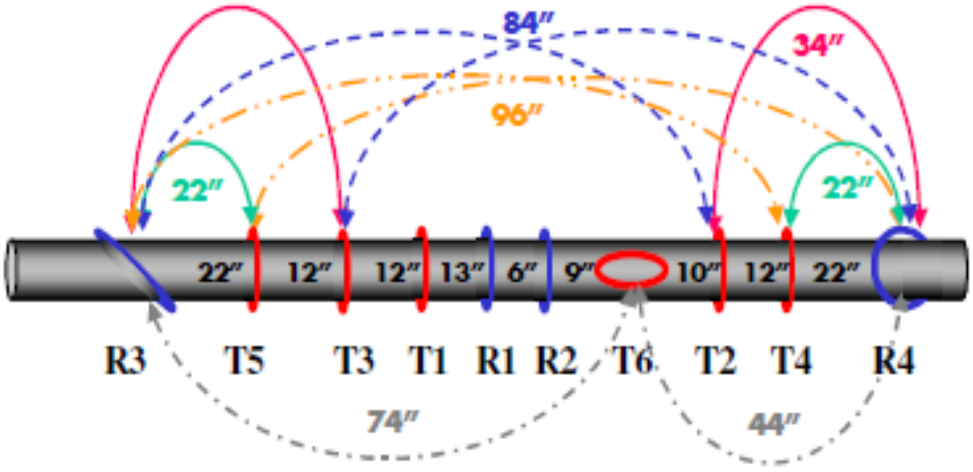

Figure C.5. Periscope from Schlumberger (Zhang et al, 2008).

Figure C.5 shows Periscope tool from Schlumbereger. The transmitter and receiver arrangement comprises of multispaced coaxial transmitters, T1 through T5, transverse transmitter, T6, and with two coaxial receivers, R1 and R2, and two inclined receivers, R3 and R4.

As can be seen in the above figures, the crossed coil pair arrangement serves as the building block for all the tools with some variations in the receiver-transmitter configuration. Table C.1 gives a comparison of the 3 tools.

	ADR	APR	PeriScope
Freq (Hz)	125k, 500k, 2M	Not published	100k, 400k, 2M
Directional arrays (in)	16", 32", 48", …..	Single spacing	22", 34", 44" 74", 84", 96"
Measured field components	zz, zx, zy	zx, zy	zz, xx, yy, zx, zy, yz, xz, xy, yx
FEWD capability	Yes	Partial	Yes
Combined conventional & directional measurements	Yes	No	Yes

Table C.1. A comparison of the capabilities of the three propagation resistivity tools. (Zhang et al, 2008)

It can be seen in the above table that the Periscope can measure all the 9 components of the tensor field. The z axis coincides with the tool's axis, for example H_{zx} is the magnetic field induced by a transmitter pointing in the z direction and detected by a receiver facing the x direction.

BIBLIOGRAPHY

Akinsanmi, O.B., Aibangbe, O., Kienitz, C. 2000. Application of Azimuthal Density While Drilling Images for Dips, Facies and Reservoir Characterization - Niger/Delta Experience. SPE European Petroleum Conference, Paris, France. SPE 65113.

Al-Mudhhi, M.A., Ma, S.M., Al-Hajari, A., Lewis, K., Berberian, G., Butt, P., Richter, P. 2005. Geo-Steering with Advanced LWD Technologies - Placement of Maximum Reservoir Contact Wells in a Thinly Layered Carbonate Reservoir. International Petroleum Technology Conference, Doha, Qatar. IPTC 10077

Al-Musharfi, N., Bansal, R., Ahmed, M., Kanj, M., Morys, M., Conrad, C., Chemali, R., Lotfy, A., Bayrakdar, M., Parker, T. 2010. Real-Time Reservoir Characterization and Geo-steering Using Advanced High Resolution LWD Resistivity Imaging. SPE Annual Technical Conference and ExhibitionFlorence, Italy. SPE 133431

Altunbay, M., Barr, D.C., Kennaird, A.F., Manning, D.K. 1994. Numerical Geology:Predicting Depositional and Diagenetic facies from wireline logs using core data. SPE Asia Pacific Oil and Gas Conference, Melbourne, Australia.

Bacon, R., Morris, S., Fernandes, W., Mahiout, S. 2010. Using High-Resolution LWD Resistivity Images For Carbonate Facies Identification and Steering. SPE 132599, SPE Annual Technical Conference and Exhibition, Florence, Italy.

Bacon, R., Kennedy, D., Hart, E., Nardi, G. 2009. Simplifying Geo-steering Interpretation and Decision Making in Complex Environments Using Deep Resistivity Images. International Petroleum Technology Conference, Doha, Qatar. IPTC 13455

Bejarano, C., Castillo, E., Germain, P., Mendoza, H., Manrique, C., Chacin, L., Pineda, G. ,Mendez, O. 2010. Challenging Complex Deltaic Reservoirs in the Orinoco Heavy-Oil Belt Aided by New-Generation Azimuthal Deep Resistivity Tools and Advanced Real-Time Geo-steering Techniques: Successful Case Study from Eastern Venezuela Basin., SPE Latin American and Caribbean Petroleum Engineering Conference, Lima, Peru. SPE 139134

Bittar, M., Chemali, R., Pitcher, J., Cook, R., Knutson, C. 2010. Real-time Proactive Optimal Well Placement Using Geosignal and Deep Images. Offshore Technology Conference, Houston, Texas, USA. OTC 20894

Bell, C., Hampson, J., Eadsforth, P., Chemali, R., Helgesen, T., Meyer, H., Peveto, C., Poppitt, A., Randall, R., Signorelli, J., Wang, T. 2006. Navigating and Imaging in Complex Geology With Azimuthal Propagation Resistivity While Drilling. SPE Annual Technical Conference and Exhibition, San Antonio, Texas, USA. SPE 102637

Bonner, S., Fredette, M., Lovelle, J., Rosthal, R. 2000. Resistivity while drilling – Images in a string.

Chemali, R., Bittar, M., Hveding, F., Wu, M., Dautel, M. 2008. Integrating Images From Multiple Depths of Investigation and Quantitative Signal Inversion in Real Time For Accurate Well Placement. International Petroleum Technology Conference, Kuala Lumpur, Malaysia. IPTC 12547

Chemali, R., Bittar, M., Hveding, F., Wu, M., Dautel, M. 2010. Improved Geo-steering by Integrating in Real Time Images From Multiple Depths of Investigation and Inversion of Azimuthal Resistivity Signals. SPE Reservoir Evaluation & Engineering journal. SPE 132439

Diaz, M., Iza, A., Rodas, J., Carrion, C., Manrique, C., Chemali, R., Pineda, G., Sandoval, J. 2009. Successful Geo-steering in Ecuador Using the Bright Spot Phenomenon From Deep Resistivity Images. Latin American and Caribbean Petroleum Engineering Conference, Cartagena de Indias, Colombia. SPE 122794

Efnik, M.S., Hamawi, M., Shamri, A. Al, Madjidi, A., Shade, C. 1999. Using New Advances in LWD technology for Geo-steering and Geologic Modeling., SPE/IADC Middle East Drilling Technology Conference, Abu Dhabi, United Arab Emirates. SPE 57537

Griffiths, R. 2009. Well placement fundamentals. Schlumberger

Glover, P. 2000. The litho density logs.

Hilgedick, S., Nygaard, R., Hellvik, S., Hoel, E., Skurtveit, E. 2012. Limitations of Log-Based in an Unconventional Conglomerate-Rich Reservoir in the Southern North Sea. 46th US Rock Mechanics/Geomechanics Symposium, Chicago, IL.

Hu, G., Bittar, M., Hou, J. 2006. Evaluation of Horizontal Wells Using LWD Propagation Resistivity and Laterolog-Type Resistivity Logs. SPE Annual Technical Conference and Exhibition, San Antonio, Texas, USA. SPE 103150

Inglis, T.A. 1987. Directional Drilling Volume 2.

Luling, M. 1991. Method for controlling directional drilling in response to horns detected by electromagnetic energy propagation resistivity measurements. US patent no. 719798.

Lyons, W.C. 1996. Standard handbook of Petroleum and Natural gas engineering Vol 1.

Market, J., Quirein, J.,Pitcher, J., Hinz, D., Buller, D., Al-Dammad, C., Spain, C., Odumosu, T. 2010. Logging While Drilling in Unconventional Shales. SPE Annual Technical Conference and Exhibition, Florence, Italy. SPE 133685

Meister, M., Pragt, J., Buysch, A., Witte, J., Nordahl, G., Hope, R. 2004. Pressure Gradient Testing With a New Formation Pressure Testing During Drilling Tool. SPE Annual Technical Conference and Exhibition, Houston, Texas. SPE 90425

Neumann, P.M., Khair, A., Aziz, A., Agrawal, V. 2007. Mobility steering helps place injectors. Offshore magazine; Drilling and completion.

Neumann, P. M., Salem, K. M., Tobert, G. P., Seifert, D. J., Dossary, S. M., Khaldi, N. A., Shokeir, R. M. 2007. Formation Pressure While Drilling Utilized for Geo-steering., SPE Saudi Arabia Section Technical Symposium, Dhahran, Saudi Arabia. SPE 110940

Teale, R. 1965. The Concept of Specific Energy in Rock Drilling, Intl. J. Rock Mech. Mining Sci. 57-73.

Olea, I.V., Shirkavand, F., Kustamsi, A., Hareland, G., Nygaard, R., Hayes, J., Teichrob, R. 2008. Correlation of Sonic log values to strength in salt. The 42nd U.S. Rock Mechanics Symposium, San Fransisco, CA.

Perez, H.H., Gupta, A.D.,Mishra, S. 2005. The Role of Electrofacies, Lithofacies and hydraulic flow units in oermeability predictions from well logs: A Comparitive analysis using classification trees. SPE reservoir evaluation & Engineering journal, Volume 8, Number 2.

Pitcher, J., Schafer, D., Botterell, P. 2009. A New Azimuthal Gamma at Bit Imaging Tool for Geo-steering Thin Reservoirs. SPE/IADC Drilling Conference and Exhibition, Amsterdam, The Netherlands. SPE 118328

Pitcher, J., Clegg, N., Burinda, C., Cook, R., Knutson, C., Scott, M., Løseth, T. 2010. Advances in Geo-steering Technology: From Simple to Complex Solutions. IADC/SPE Drilling Conference and Exhibition, New Orleans, Louisiana, USA. IADC 128155

Rabia, H. 2000. Well Engineering and construction.

Sarkar, A., Lee, J., Kasap, E. 1998. Adverse Effects of Poor Mudcake Quality: A Supercharging and Fluid Sampling Study. SPE Reservoir Evaluation & Engineering. SPE 64227

Seifert, D., Chemali, R., Bittar, M., Althoff, G., Lotfy, A. 2011. Hydrocarbon Reservoirs Where Proactive Geo-steering is Most Likely to Succeed. SPE/IADC Drilling Conference and Exhibition, Amsterdam, The Netherlands. SPE/IADC 140327

Serra, O., Abbott, H.T. 1982.The contribution of Logging data to Sedimentology and Stratigraphy. SPE Journal, Volume 22, Number 1.

Smith, L.I. 2002. A tutorial on principal component analysis.

Studer, R., Macresy, L. 2006. Improved BHA Sag Correction and Uncertainty Evaluation Brings Value to Wellbore Placement. SPE Annual Technical Conference and Exhibition, San Antonio, Texas, USA. SPE 102088

Torkildson, T., Havarstein, T., Weston, J.L., Eskseth, R. 2004. Prediction of Wellbore Accuracy when surveyed with Gyroscopic Tools. SPE Annual Technical Conference and Exhibition, Houston. SPE 90408

Zhang, Z., Gonguet, C., Rajani, V., Roeterdink, R. 2008. DIRECTIONAL LWD RESISTIVITY TOOLS AND THEIR BUSINESS IMPACTS. 49th Annual Logging Symposium, Austin, Texas.

VITA

Anuroop Pandey earned his Bachelor's degree in Petroleum Engineering from University of Petroleum and Energy Studies, Dehradun, India in the spring of 2007 and worked in the oil and gas industry as a drilling engineer for three years prior to enrolling for the Master's program in Petroleum Engineering at Missouri University of Science and Technology in the fall of 2010. He earned his Master's degree in Petroleum Engineering in December 2012.